Identification of the calmodulin-sphingosylphosphorylcholine interaction

Structural characterization and implications in signal transduction

PhD thesis

Erika Kovács

Supervisor: Károly Liliom, PhD
Institute of Enzymology, Hungarian Academy of Sciences

Biology Doctoral School of Eötvös Loránd University
Director: Prof. Anna Erdei

Doctoral Program in Structural Biochemistry
Chair: Prof. László Gráf

2010 Budapest

TABLE OF CONTENTS

1. INTRODUCTION

1.1. Lipid signaling – a historical review

Lipids, naturally occurring hydrophobic or amphiphilic molecules, fulfill three general functions in living cells: energy storage, being structural components of cellular membranes, and being important signaling molecules. Although the first two roles have long been well described, the concept of 'bioactive lipids' became well established only in the past 20 years. Since then, the theme of lipid signaling has grown to occupy center-stage in molecular and cell biology research. Lipids participate in such wide-ranging cellular processes like growth, differentiation, apoptosis, senescence, adhesion, migration, inflammation, angiogenesis and intracellular trafficking. Members of several different lipid categories, including sphingolipids, diacylglycerol, phosphatidylinositol phosphates, prostaglandins and steroid hormones, have been identified as cellular messengers, mediating specific molecular recognition processes and signal transduction pathways. In addition, some lipids function to define membrane domains (rafts), which recruit proteins from the cytosol that subsequently organize secondary signaling or effector complexes.

In the 1960s arachidonic acid was identified as the source of leukotrienes and prostaglandins, a discovery that has led to our current understanding of eicosanoid signaling, and taught us that the same signaling lipid can provoke different cellular responses, depending on the cell type. The study of the lipid components of cellular membranes, and in particular the turnover of phosphoinositides, culminated in the 1980s with the discovery that phosphatidylinositol-4,5-bisphosphate (PtdIns(4,5)P_2) could be hydrolyzed by phospholipase C (PLC) to diacylglycerol (DAG) and inositol-1,4,5-tris-phosphate (Ins(1,4,5)P3). Both products were identified as second messengers that trigger the activation of protein kinase C (PKC) and the release of Ca^{2+} from internal stores, respectively. In parallel, inositol and phosphoinositide kinases have been identified; these enzymes generate a huge repertoire of soluble inositol polyphosphates and membrane polyphosphoinositide lipids. Phosphoinositide 3-kinase (PI3K), for example, which is regulated by cell-surface receptors, promotes the formation of phosphatidylinositol-3,4,5-trisphosphate (PtdIns(3,4,5)P3), a signaling lipid that modulates cell growth, proliferation and motility. Interestingly, nature has used several possible variations of the inositol head group to create highly specific docking sites for lipid-binding proteins, effector proteins that trigger signaling cascades or enzymes that further modify these lipids (see next

chapter). Phosphoinositides have, therefore, gained importance as localization tags that are involved in the organization of membrane-bound signaling complexes [1-3].

Two groups that most recently gained attention are sphingolipids (derivatives of the sphingoid base) [4-8] and lysophospholipids (phospholipids with only one fatty acid chain) [9-11]. Ceramides and sphingosines have pro-apoptotic and antiproliferative actions; when phosphorylated by lipid kinases, however, sphingosine is converted into sphingosine-1-phosphate (S1P), which promotes cell growth and proliferation by a still poorly understood intracellular action as well as by extracellular signaling through a set of different G protein-coupled receptors (GPCRs). Another lipid that is released from cells, lysophosphatidic acid (LPA), also functions in an autocrine and paracrine manner by binding to a family of GPCRs. LPA, together with specific eicosanoids, can additionally modulate gene expression by binding to lipid-sensing transcription activators, such as the peroxisome proliferator-activated receptors (PPARs).

With this brief introduction to the most widely studied lipid mediators, I aimed to demonstrate the diversity of the lipid signaling field. For a more detailed review of the current 'hot topics' in the area please refer to the 2008 special lipid edition of Nature Reviews Molecular Cell Biology [12-17]. From now on, I will only focus on those aspects of lipid signaling that are essential for the comprehension of this thesis.

1.2. Basic concepts of lipid-protein interactions

Lipid-protein interactions drive core cellular signaling events and regulate the function of most membrane proteins. A wide variety of globular phospholipid-binding domains exist, and many have been extensively characterized (Table 1).

The interactions of these domains with the membrane surface fall into two broad classes. Some are highly specific and involve stereoselective recognition of particular lipids. The most specific cases involve domains that selectively recognize rare membrane components that are restricted in their location, time of synthesis or both. Among phospholipids, the phosphoinositides represent the best examples of acutely regulated binding targets, and all phosphoinositides except PtdIns4P and PtdIns5P have one or more well characterized specific binding domains. Figure 1 depicts the structures of the most important target-specific binding domains.

Table 1 Phospholipid-binding domains at a glance (from [12])

Domain	Typical size (amino acids)	Structure	Preferred target	Membrane insertion?	Ca^{2+} required?	Dimerization required?
C1	~50	Zn^{2+} finger	DAG, phorbol esters	Yes	No	No
PKC C2	~130	β-sandwich	PtdSer (and others)	Yes	Yes	No
PH	~125	β-sandwich	Phosphoinositides, quite diverse, some highly specific	Some reported	No	Some examples
FYVE	60-70	Zn^{2+} finger	PtdIns3P	Yes	No	Most cases
PX	~130	α+β structure	PtdIns3P (a few bind other phosphoinositides)	Yes	No	Most cases
PROPPIN	~500	β-propeller	PtdIns(3,5)P_2 (PtdIns3P also in some cases)	Unknown	No	No
Gla	~45	α-helical (requires Ca^{2+} to fold)	PtdSer	Yes	Yes	No
Annexin	~310	α-helical array	Acidic phospholipids	Unknown	Yes	No
Discoidin C2	~160	β-sandwich	PtdSer (specific)	Yes	No	No
ENTH	~150	α-helical solenoid	PtdIns(4,5)P_2 (some promiscuity)	Yes	No	No
ANTH	~280	α-helical solenoid	Phosphoinositides, relatively little specificity	No	No	Yes
BAR	~240	Extended α-helical bundle	Acidic phospholipids (via N-terminal helix)	Yes	No	Yes
F-BAR	~320	Extended α-helical bundle	Acidic phospholipids	Unknown	No	Yes
IMD	~250	Extended α-helical bundle	Acidic phospholipids, especially phosphoinositides	Unknown	No	Yes

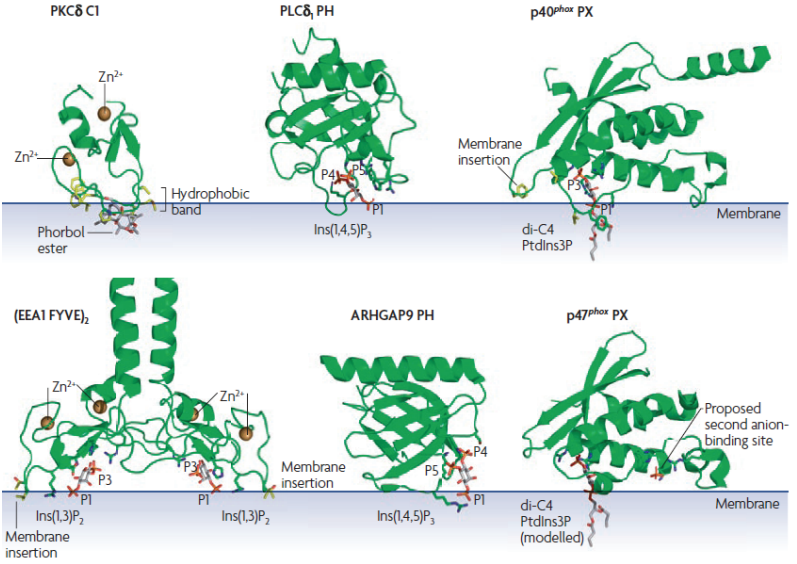

Figure 1 Structures of target-specific phospholipid-binding domains. Domains depicted are from left to right: the protein kinase Cδ (PKCδ) C1 domain (PDB code 1PTR), the phospholipase Cδ1 (PLCδ1) PH domain (PDB code 1MAI), the p40*phox* PX domain (PDB code 1H6H), the early endosome antigen-1 (EEA1)41 FYVE domain dimer (PDB code 1JOC), the ARHGAP9 PH domain (PDB code 2P0D) and the p47*phox* PX domain (PDB code 1O7K). Figure taken from [12].

Other lipid-binding domains are non-specific and involve attraction to a general physical property of the membrane, such as charge, amphiphilicity and curvature. For these membrane-binding domains, the physiological target is an abundant phospholipid that is ubiquitous in cell membranes. For example, several phospholipid-binding domains, including C2 domains and annexins, interact with phosphatidylserine, while many phosphoinositide-binding domains bind similarly to all of the polyphosphoinositides. Domains with these non-specific characteristics do not simply bind persistently to any membrane that contains phosphatidylserine or polyphosphoinositides. Rather, some of them (such as certain C2 domains and annexins) bind phospholipids only when cytosolic calcium levels are transiently elevated. Others, such as BAR and F-BAR domains, seem to interact only with highly curved regions of membranes. These mechanisms allow temporal and spatial specificity in membrane targeting without changing the nature of the headgroup itself.

These domains have taught us a lot about the mechanistic details of lipid recognition processes involved in cellular signaling. Nevertheless, those interactions that are not established by these specific lipid-binding globular domains, rather by proteins which do not hold a well-defined lipid-binding site, are yet not well described [18, 19]. These interactions are often manifested between a cluster of lipids and the protein, and cannot be characterized by a simple binding model. The change in the micellar or liposomal state (Figure 2) of the lipid under different experimental conditions often complicates evaluation of such data. The biological significance of understanding the mechanism of these interactions is outstanding, but due to technical difficulties they are rarely characterized at a structural molecular level. I hope that later on I will convince the reader that my work provides significant new insights into this emerging field.

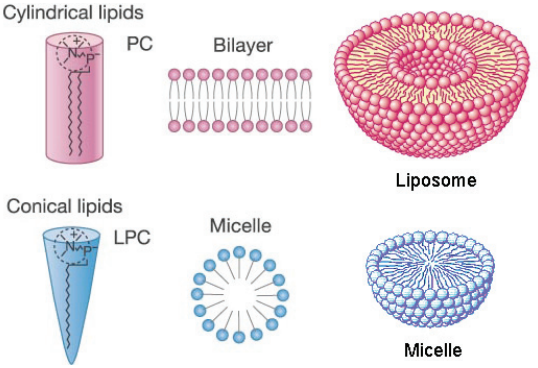

Figure 2 Clustering of lipids in an aqueous environment. Bilayer-forming phospholipids (shown in red), such as phosphatidylcholine (PC), can be approximated as rods. Micelle-forming lysophospholipids (blue), such as lysophosphatidylcholine (LPC) with only one fatty acid chain, can be regarded as cones.

1.3. Biological functions, occurrence and metabolism of sphingosylphosphorylcholine

Sphingosylphosphorylcholine (lysosphingomyelin, SPC) belongs to a group of structurally related lysophospholipids, such as sphingosine-1-phosphate (S1P), lysophosphatidylcholine (LPC) and lysophosphatidic acid (LPA) (Figure 3), which serve as potent and versatile lipid mediators in a large variety of cell types. The topic of my thesis is the characterization of a newly identified interaction between SPC and calmodulin (CaM); therefore, here I present SPC's biology in detail.

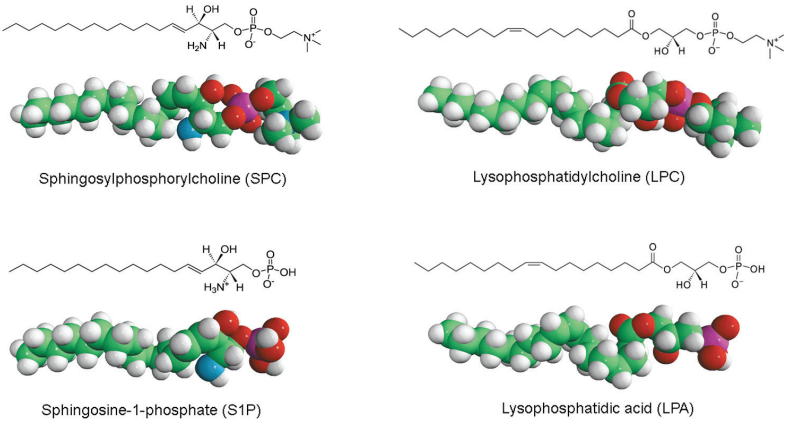

Figure 3 Lysophospholipids with important roles in cellular signaling.

In lipid signaling, two major principles can be found: cellular release or extracellular formation of a lipid species, which then activate specific plasma membrane receptors, mostly in an autocrine or paracrine manner, or stimulus-induced intracellular formation of such lipids, which then serve as intracellular mediators of the physiological reactions to the stimulus. S1P and SPC have the quaint property of being able to exert both actions (Figure 4). While the biology of S1P is extensively studied [20], less information is available regarding the mechanism of action and metabolism of SPC. For extensive reviews on SPC's biological functions see [21, 22].

SPC first attracted attention as a remarkably potent mitogen for a variety of cell types [23]. Since then, extracellularly applied SPC has been shown to cause rapid increases in intracellular Ca^{2+} concentration in a number of cell lines [24-30], to induce stress fiber formation and other cytoskeleton rearrangements [31], to activate potassium currents in atrial myocytes [32] and to modulate cell migration [33]. These findings demonstrate that SPC is a potentially important regulator of cell type specific functions in major tissues, such as the heart, blood vessels, skin, brain and the immune system. Some of these actions can be explained by low-affinity binding to S1P-receptors, while certain effects are not shared by S1P, suggesting that SPC is a lipid mediator on its own right. After the discovery of specific cell surface G-protein-coupled receptors for SPC, as ovarian cancer G-protein-coupled receptor 1 (OGR1) [34] and GPR4 [35], much attention was dedicated to its first messenger functions. However, these two papers have been

retracted, and recent studies have shown that these receptors are rather proton sensors [36], leading to debate in the field. Although the majority of publications focus on the effects of extracellularly applied SPC, the sphingolipid has intracellular messenger functions as well, mediating the release of Ca^{2+} from internal stores, described in details in the following chapter.

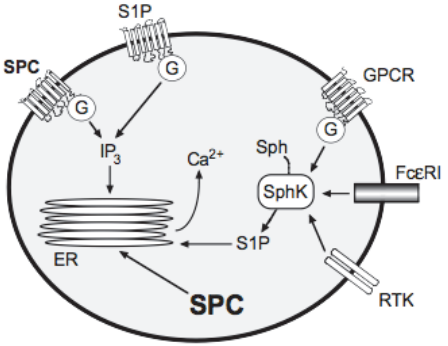

Figure 4 Extra and intracellular roles of SPC and S1P. As first messengers, SPC and S1P activate cell-surface G protein-coupled receptors in a well-described manner, triggering intracellular signaling pathways that can lead to elevation of intracellular IP_3 levels and mobilization of Ca^{2+} from the ER. As second messengers, their intracellular levels rise upon extracellular stimuli, also leading to Ca^{2+} liberation from the ER, however, in a yet unknown manner.

Albeit data on SPC metabolism is yet scarce, its presence has been demonstrated under several physiologic and pathologic conditions. SPC has been found in ascitic fluids [37]; where its levels were similar to those of S1P (~100 nM), but much lower than those of LPA (~20 μM). In ascites caused by ovarian cancer, levels of SPC were significantly higher than in non-malignant ascites, suggesting that SPC may have a pathophysiological role. Furthermore, SPC was detected in normal rabbit plasma and serum [38]. SPC levels in the serum were slightly higher than in the plasma, suggesting that SPC, like S1P and LPA, is formed during blood clotting. SPC, together with other bioactive lipids, was found to be associated with high-density lipoproteins (HDL) compared to low-density lipoproteins (LDL), and it was proposed that SPC represents one of the anti-atherogenic activities of HDL [39]. Moreover, the metabolism of SPC has been detected to be very rapid in the circulation [38] and the average concentration of the lipid in cardiac muscle has been estimated to be as high as 15.6 μM [40]. These findings strongly suggest that the sphingolipid plays an important role in the cardiovascular system.

SPC accumulates in Niemann–Pick disease, which is characterized by deficiency of acid sphingomyelinase [41]. Acid sphingomyelinase deficiency primarily leads to accumulation of sphingomyelin; the mechanism for the observed increase in SPC is presently not known. SPC levels were highly elevated in the brain, liver and spleen of Niemann–Pick disease type A patients. In type B patients, SPC was likewise elevated in liver and spleen, but normal in the brain. Therefore, a contribution of SPC to brain dysfunction, which is found in type A but not B, was postulated. In patients suffering from atopic dermatitis, the activity of sphingomyelin deacylase was enhanced, which appears to accumulate SPC and deplete sphingomyelin, so that ceramide formation by sphingomyelinase is decreased [42].

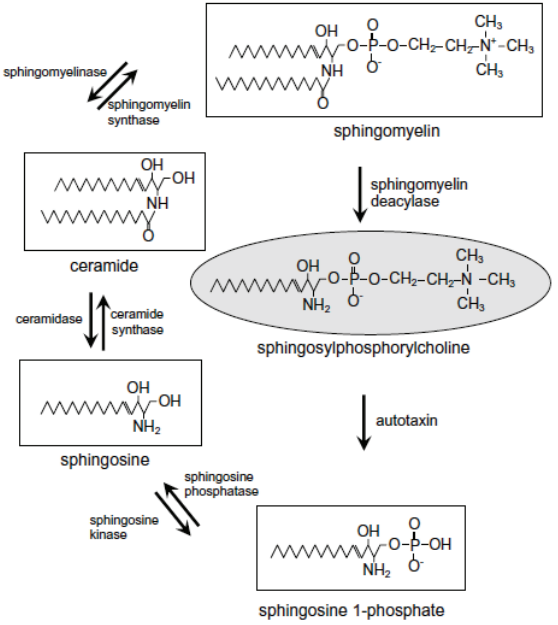

Figure 5 Potential pathways of sphingosylphosphorylcholine metabolism. Figure taken from [22].

Unfortunately, the pathways of physiological SPC production are yet unknown. Earlier work suggested the formation of SPC from sphingosine and CDP-choline [43]; however, the specific enzyme responsible for such an activity has not been identified yet. Alternatively, SPC may be formed by sphingomyelin deacylase, an enzyme that was

partially purified from the skin of atopic dermatitis patients [44]. In cardiac myocytes SPC production was significantly increased by incubation with the endothelial-derived peptide, endothelin-1 [45]. This was found to occur via breakdown of sphingomyelin, but not via sphingosine, also suggesting the involvement of sphingomyelin deacylase. The pathways of SPC degradation are even less well understood. Exogenous SPC injected *in vivo* into the blood is undetectable within a single pass through the coronary circulation suggesting that it is rapidly metabolized [38]. One possible enzyme that may be involved is autotaxin, an exoenzyme that has lysophospholipase D activity and has been implicated in regulation of tumor cell migration [46]. Nevertheless, autotaxin is a secreted enzyme, and as such, would only be able to clear extracellularly localized SPC. For an overview of SPC's supposed place in sphingolipid metabolism refer to Figure 5. It is important to note that our scant knowledge in the field can largely be attributed to the lack of a thorough analysis of SPC metabolism. Compared to the intensively studied S1P and ceramide, only weak efforts have been made to decipher SPC occurrence and metabolism in cells. I hope that the results presented in this thesis, which suggest a specific intracellular target for SPC, will encourage research in the field.

1.4. Sphingosylphosphorylcholine and Ca^{2+} signaling

As mentioned in the previous section, SPC has the unique feature of being capable to mobilize Ca^{2+} from internal stores acting both extracellularly through G protein-coupled receptors and intracellularly in a yet undefined manner [47, 48]. Although there is a certain level of confusion in the literature, it is important to differentiate between these two modes of action. SPC's effect on intact, but not in permeabilized cells, was shown to be sensitive to pertussis toxins, indicating the involvement of GPCRs. In addition, Ca^{2+} release in permeabilized cells was not stereoselective, whereas in intact cells only the naturally occurring D-*erythro*-SPC, but not L-*threo*-SPC triggered Ca^{2+} influx [49]. Ghosh *et al.* were the first to report on the intracellular Ca^{2+} release mediating ability of sphingosine derivatives [50, 51]. These studies revealed that SPC immediately liberates Ca^{2+} from permeabilized smooth muscle cells with an EC_{50} of 2.8 µM. Sphingosine exerted a similar action, but had a lag phase, implying that it first has to be enzymatically converted to S1P.

Since these first reports, two main proposals have been made on the intracellular target sites for SPC. The involvement of a novel intracellular sphingolipid-gated Ca^{2+}-

permeable channel from rat basophilic leukemia [52] and endothelial [53] cells has been suggested. The channel has been cloned and named SCaMPER, sphingolipid Ca^{2+} release mediating protein from endoplasmic reticulum [54]. However, in a subsequent study Schnurbus *et al.* demonstrated that SCaMPER is unlikely to be a Ca^{2+} channel, as it contains only one membrane-spanning region [55].

Another suggestion was that SPC regulates the activity of ryanodine receptors (RyRs), Ca^{2+} channels of the endoplasmic reticulum. These receptors were proposed to play a role in SPC-induced Ca^{2+} release from brain microsomes [56, 57] and from cardiac sarcoplasmic reticulum membranes [40]. RyRs are huge channel complexes composed of tetramers of 560 kDa monomers. Among the three isoforms RyR1 is expressed primarily in skeletal muscle, RyR2 is the dominant isoform in cardiac muscle, and RyR3 is found in a wide variety of tissues. They display a characteristic bell-shaped, biphasic dependence on cytosolic Ca^{2+} concentration with micromolar Ca^{2+}causing channel activation and elevated Ca^{2+} concentrations resulting in channel inhibition. Besides Ca^{2+}, these receptors are regulated by several small molecules and proteins (Figure 6) including the ubiquitous Ca^{2+} sensor calmodulin (CaM) [58]. Regulation of RyRs by CaM is complex, but the sensor clearly plays a role in the negative feedback of the Ca^{2+} signal, through inhibition of channel activity by Ca^{2+}CaM [59, 60]. In contrast to reports on the activation of RyRs by SPC, Uehara *et al.* demonstrated that the open probability of cardiac RyR ion channels decreases on application of SPC [61, 62]; hence, the question of SPC's intracellular mechanism of action is still open.

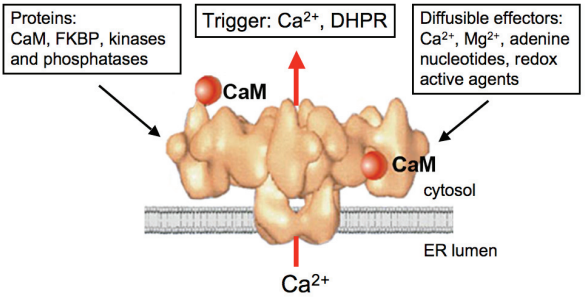

Figure 6 Regulation of RyRs. Channel opening is triggered by Ca^{2+} ions or the dihydropyridin receptor (DHPR). Prominent forms of regulation are indicated both by proteins and small molecules.

1.5. Overview of Ca^{2+} signaling

Ca^{2+} is a highly versatile second messenger regulating numerous cellular functions. Resting intracellular Ca^{2+} concentrations (~100 nM) can be elevated to low micromolar levels through several pathways to create Ca^{2+} signaling systems with different spatial and temporal properties. Importantly, the Ca^{2+} signal should not be thought of as an on or off response. Rapid, highly localized Ca^{2+} spikes regulate fast responses, whereas slower responses are controlled by repetitive global Ca^{2+} transients or intracellular Ca^{2+} waves.

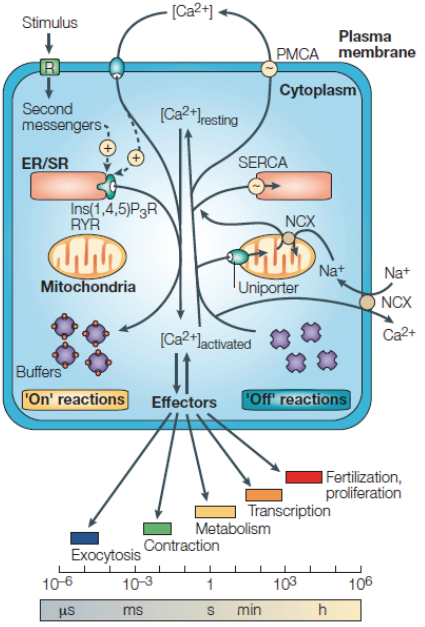

Figure 7 Calcium-signaling dynamics and homeostasis. During the 'on' reactions, stimuli induce both the entry of external Ca^{2+} and the formation of second messengers that release internal Ca^{2+} that is stored within the endoplasmic/sarcoplasmic reticulum (ER/SR). Most of this Ca^{2+} (shown as red circles) is bound to buffers, whereas a small proportion binds to the effectors that activate various cellular processes that operate over a wide temporal spectrum. During the 'off' reactions, Ca^{2+} leaves the effectors and buffers and is removed from the cell by various exchangers and pumps. The $Na^{+}/Ca2^{+}$ exchanger (NCX) and the plasma membrane Ca^{2+}-ATPase (PMCA) extrude Ca^{2+} to the outside, whereas the sarco(endo)plasmic reticulum Ca^{2+}-ATPase (SERCA) pumps Ca^{2+} back into the ER. Mitochondria also have an active function during the recovery process in that they sequester Ca^{2+} rapidly through a uniporter, and this is then released more slowly back into the cytosol to be dealt with by the SERCA and the PMCA. Cell survival is dependent on Ca^{2+} homeostasis, whereby the Ca^{2+} fluxes during the off reactions exactly match those during the on reactions. Figure imported from [63].

The Ca^{2+} signal can either be derived from the extracellular medium or from internal stores. Plasma membrane channels such as voltage operated channels and transient receptor potential channels respond to membrane depolarization, while receptor-operated channels including N-methyl-D-aspartic acid (NMDA), adenosine-triphosphate (ATP) and nicotinic acetylcholine (nACh) receptors respond to extracellular agonists. The release of Ca^{2+} from the endoplasmic reticulum (ER) or its muscle equivalent, the sarcoplasmic reticulum (SR) is mediated by Ca^{2+} itself in case of RyRs or by an expanding group of second messengers including inositol-1,4,5-triphosphate (IP_3Rs), cyclic ADP ribose (cADPR), nicotinic acid adenine dinucleotide phosphate (NAADP) and sphingolipids (see previous section).

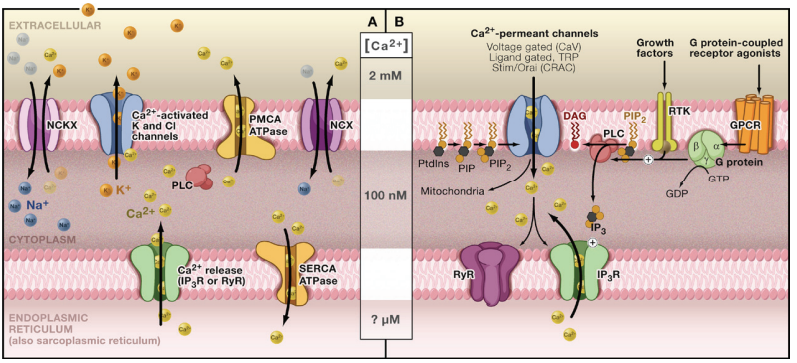

Figure 8 Maintaining and using Ca^{2+} gradients for signaling. (A) The cytoplasmic Ca^{2+} level is low in resting cells. Cytoplasmic [Ca^{2+}] is maintained at ~100 nM by extrusion via plasma membrane Ca^{2+} ATPase (PMCA) and smooth endoplasmic reticular Ca^{2+} ATPase (SERCA) transporters. The Na^+/Ca^{2+} exchanger (NCX), a major secondary regulator of [Ca^{2+}], is electrogenic, exchanging three Na^+ ions for one Ca^{2+}. Intracellular Ca^{2+} hyperpolarizes many cells by activating K^+ channels, and in some cells, Cl^- channels. This decreases CaV channel activity but increases the driving force across active Ca^{2+}-permeant channels. (B) The core of the Ca^{2+} signaling network. In excitatory Ca^{2+} signaling, plasma membrane ion channels are triggered to open by changes in voltage, or extra- or intracellular ligand binding. When open, ~1 million Ca^{2+} ions/s/channel flow down the 20,000 fold [Ca^{2+}]i gradient (ECa ~ +150 mV), maintained by elements shown in (A). Initial increases in [Ca^{2+}] trigger more release, primarily from ER via Ca^{2+}-sensitive ryanodine receptors (RyR). G protein-coupled receptor (GPCR) or receptor tyrosine kinase (RTK) mediated activation of phospholipase C (PLC) cleaves PIP_2 into inositol (1,4,5) trisphosphate (IP_3) and diacylglycerol (DAG). IP_3 is a ligand for the intracellular IP_3R channel spanning the membrane of the ER. GPCRs catalyze the exchange of guanosine diphosphate (GDP) for GTP on Gα subunits, releasing active Gα and Gβγ subunits that in turn activate PLCβ. RTKs dimerize upon ligand binding, autophosphorylate, and interact with other signaling proteins to activate PLCγ. Figure imported from [65].

In the next step of the pathway, the signal is relayed to proteins containing Ca^{2+}-binding motifs, most importantly EF-hands and C2 domains. Among them, Ca^{2+} buffers fine-tune the signal, while Ca^{2+}-sensor proteins act as effectors regulating multiple other proteins. The result of this activating process might be a wide variety of physiologic cellular responses, most notably exocytosis, contraction, metabolism, transcription, fertilization and proliferation.

Finally, to remove excess Ca^{2+} from the cytosol, the effect of channels is counteracted by pumps, the plasma membrane Ca^{2+} ATPase (PMCA) and the sarcoendoplasmic reticulum Ca^{2+} pump (SERCA) and exchangers, the Na^{+}/Ca^{2+} exchanger (NCX). Besides switching of the Ca^{2+} signal, these membrane proteins play an important role in maintaining resting Ca^{2+} levels. Various aspects of the signaling process are highlighted in Figure 7 and 8, for recent reviews see [63-65].

1.6. Calmodulin, the ubiquitous Ca^{2+} sensor

In the hub of Ca^{2+} signaling events lies calmodulin (CaM), the ubiquitous Ca^{2+} sensor of eukaryotic cells [66]. CaM is a small (148 residues), acidic (pI = 4.1), soluble, dumbbell-shaped, evolutionarily highly conserved protein.

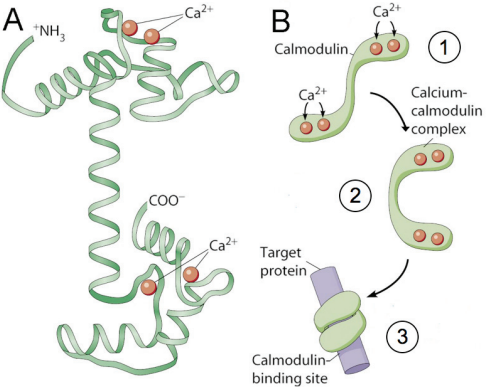

Figure 9 Basics of CaM function. (A) Structure of Ca^{2+}-saturated CaM. (B) Classical mode of CaM action. 1) CaM binds 4 Ca^{2+} ions. 2) CaM changes conformation resulting in an active complex 3) The two globular "hands" of the complex wrap around a binding site on a target protein. Figure adapted from Principles of Cell Biology, Pearson Education Inc.

The Ca^{2+} binding motifs of CaM are four EF-hand structures, which consist of an N-terminal helix (the E helix), followed by a centrally located Ca^{2+}-coordinating loop and a C-terminal helix (the F helix), resembling a thumb, index and middle fingers of a hand, hence the name EF-hand. The first two EF-hands combine to form a globular N-terminal domain that is separated by a short flexible linker from a homologous C-terminal domain consisting of the other two EF-hands (Figure 9A). CaM is the most prominent member of Ca^{2+}-sensor proteins, including the structurally similar troponin C and S100 proteins, that all undergo a conformational change upon binding to Ca^{2+}.

The mechanism of CaM function and target binding is versatile (see below), but in the most common scenario (Figure 9B) the structural rearrangements upon Ca^{2+}-binding result in the exposure of hydrophobic groups in a methionine-rich crevice of each domain, allowing CaM to interact with a wide variety of target proteins. The Ca^{2+}-sensor wraps around the CaM binding domain of target proteins, which are structurally ~20 residue-long basic amphipatic α-helices. The ensuing structural reorganization in the effector protein most often leads to its activation by release of autoinhibition. Other, less generic modes of CaM-binding have also been reported (Figure 10, [67, 68]).

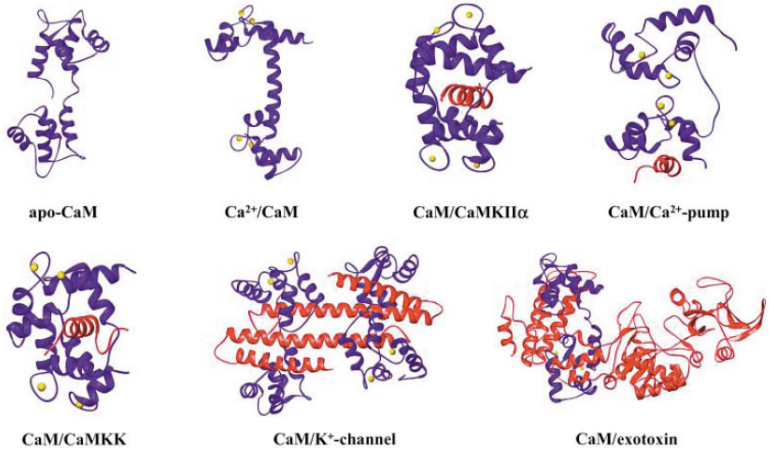

Figure 10 Ribbon presentations of CaM and CaM in complex with target peptides. CaM is colored blue, the CaM targets are red, Ca^{2+} ions are yellow. The N-terminal lobe of CaM is orientated to the top, the C-terminal lobe to the bottom of the figures. Structural data were taken from the Protein Data Bank, accession codes: apo-CaM (1CFD); Ca^{2+}/CaM (1CLL); CaM/CaMKIIa (1CM1); CaM/CaMKK (1IQ5); CaM/Ca^{2+}-pump (1CFF); CaM/K+-channel (1G4Y), CaM/anthrax exotoxin (1K93). Figure taken from [68].

The list of CaM targets is vast and constantly growing. The most extensively characterized effectors and their physiological functions are listed in Table 2.

Table 2 Prominent examples of CaM-regulated proteins.

Protein	Function	Ref.
Adenylate cyclase	cAMP generation	[69]
Phosphodiesterase	cAMP degradation	[70]
CaM kinase I	Neurotransmission, transcription regulation	[71]
CaM kinase II	Involvement in long-term potentiation, memory	[72]
CaM kinase IV	Transcription regulation	[71]
CaM kinase kinase	Regulation of CaM kinase I/IV	[71]
Myosin light chain kinase	Regulation of muscle contraction	[73]
Calcineurin	Phosphatase, essential role in transcription regulation	[74]
Plasma membrane Ca^{2+} pump	Ca^{2+} pump of the PM	[75]
Ryanodine receptor	Ca^{2+} channel of the ER	[59]
IP_3 receptor	Ca^{2+} channel of the ER	[76]

Based on their modes of regulation, CaM-dependent proteins can be categorized into six main classes (Figure 11). Class A effectors bind essentially irreversibly to CaM irrespective of Ca^{2+}, thus, the Ca^{2+}-sensor can be considered as a subunit of these proteins, for example phosphorylase kinase. Nevertheless, Ca^{2+} is required for their activation. Class B effectors bind to CaM only in the absence of Ca^{2+}. Examples include neuromodulin and neurogranin, proteins which might serve as intracellular reservoirs for CaM at resting Ca^{2+} concentrations. Class C targets form low affinity, inactive complexes with CaM at low Ca^{2+} concentrations, and engage in a high-affinity, active complex upon increase of intracellular $[Ca^{2+}]$. Smooth muscle myosin light chain kinase and calcineurin behave in this manner. Class D proteins, such as select members of the G-protein-receptor kinases and the IP_3R1, bind to CaM in the presence of Ca^{2+}, but are inhibited by the Ca^{2+}-sensor. Class E targets, such as CaM-dependent protein kinases I, II and IV, exhibit behavior considered to be more conventional and are activated by Ca^{2+}CaM. Some class E effectors are additionally regulated by another CaM regulated kinase (CaM kinase kinase), which is designated class F.

With these examples I wished to demonstrate the versatility of CaM action, in the light of which we can appreciate the potential of the CaM-SPC interaction, the topic of this thesis, to provide an utterly novel means of interfering with CaM function. Uniquely, SPC binds not only to Ca^{2+}CaM but also to the apo protein, while classical synthetic CaM

inhibitors bind only in the presence of Ca^{2+}. Removing both forms of the protein from these targets could result in yet unprecedented regulatory effects.

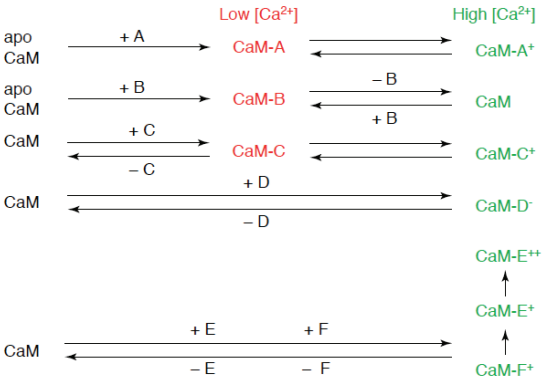

Figure 11 Ca^{2+}-dependent functions of various classes of CaM-binding proteins. Target classes A, B and C are associated with CaM or Ca^{2+}-free CaM at low (resting) intracellular free Ca^{2+} concentrations (red). When Ca^{2+} concentrations are high (green), class B dissociates from CaM, classes D, E and F associate with CaM, classes A, C, E and F are activated by CaM, and class D is inactivated by CaM. Figure taken from [66].

The intracellular abundance of CaM (0.1% of total protein) and the large array of its targets lead to the so-called ubiquitous CaM paradox [77]. How can CaM interact with specific targets in a temporally and spatially regulated manner? This question is most apparent in cases when the Ca^{2+}-sensor regulates reactions of opposing effects, such as the synthesis and degradation of cAMP by adenylate cyclase and phosphodiesterase, respectively or the phosphorylation and dephosphorylation of proteins by kinases and phosphatases. Several suggestions have been made to solve the apparent paradox, the basic concept of each being that CaM and CaM-dependent activity is highly regulated in space and time, achieved either by differential gene expression, variation in localization or post-transcriptional modification [77-79].

I wish to point out that inhibition of CaM function by SPC, described in my thesis in detail, has the potential to significantly contribute to local CaM regulation in living cells, providing another, alternative explanation for the CaM paradox. Our finding conceptually differs from previous suggestions however, as we propose that CaM activity is transiently modified by an endogenous lipid mediator. So far, apart from Ca^{2+}, no other second messenger has been shown to directly regulate CaM activity. The pharmacologic

inhibitors of CaM, such as trifluoperazine, calmidazolium and W7 [80-82], are all synthetic aromatic molecules. There are reports on natural compounds presenting anti-CaM activity [83], but these substances can only be found in certain plant species and animal venoms, and neither can be found in humans. SPC, on the other hand, has been detected under several physiological and pathological conditions in human and mammalian tissues, as discussed in previous sections.

2. AIMS

- My primary goal was to **gain information about the intracellular mechanism of action of S1P and SPC**, sphingolipids involved in Ca^{2+} signaling as putative second messengers.

- Our approach was to **identify a protein that interacts specifically with these sphingolipids**. Our candidate for an intracellular target was CaM.

- After **demonstrating that SPC is a specific inhibitor of CaM in *in vitro* enzyme assays**, my aims became more definite.

- I concentrated on the **characterization of the newly identified CaM-SPC interaction**, which potentially has important consequences in both Ca^{2+} and lipid signaling.

- My goals were to **give an in-depth structural analysis of the interaction and mechanistic insight into the binding process**.

- I aimed to **set up a detailed model that explains the basis of competitive inhibition** witnessed in enzymatic assays.

- I wanted to **reveal the functional consequences of the CaM-SPC interaction**, focusing on proteins involved in Ca^{2+} homeostasis, especially RyRs.

- The ultimate goal of deciphering the *in vivo* relevance and significance of the newly identified interaction exceeds the scope of this thesis and remains for the future.

3. MATERIALS AND METHODS

3.1. Lipids

D-*erythro*-sphingosylphosphorylcholine (SPC, cat. no. 860600), D-*erythro*-sphingosine-1-phosphate (S1P, cat. no. 860492), oleoyl-lysophosphatidylcholine (LPC, cat. no. 845875) and oleoyl-lysophosphatidic acid (LPA, cat. no. 857130) was purchased from Avanti Polar Lipids. L-*threo*-sphingosylphosphorylcholine (LT-SPC, cat. no. 1319) was from Matreya. Lipids were delivered from 10 mM methanolic stock solutions.

Please note that the 'Materials and Methods' section includes solely the information required to repeat the experiments. Rationale, explanations and comments regarding why and how these methods were applied can be found in the relevant sections of 'Results'.

3.2. Preparation of CaM from bovine brain

CaM was purified from bovine brain using isoelectric precipitation and phenyl-sepharose (Amersham Biosciences, 17-0973-05) affinity chromatography according to Gopalakrishna and Anderson [84]. Protein purity was checked by SDS-PAGE, and CaM concentration was determined by circular dichroism spectroscopy (molar residual ellipticity of 158 000 deg cm^2 at 222 nm [80]).

3.3. Intrinsic tyrosine fluorescence

Spectra were collected using a Jobin Yvon Fluoromax-3 spectrofluorimeter at 25°C in 10 mM HEPES, pH 7.4, 100 mM KCl, and 1 mM EGTA or $CaCl_2$. Bandwidths were adjusted to 5 nm, Tyr was excited at 274 nm, emission was monitored from 285 to 370 nm, and values were read at 303 nm. Protein and lipid concentrations were 1 μM and 100 μM, respectively. Buffer containing lipids was measured as a blank. After the addition of CaM, the spectrum was scanned again and corrected by subtracting the blank.

3.4. Fluorescence of dansyl-labeled CaM

CaM was dansylated by reacting 1 mg of protein with 5 fold molar excess of dansyl-chloride (Fluka, 39220) in 1 ml 10 mM HEPES, pH 7.4, 100 mM KCl, and 1 mM $CaCl_2$ for 2 hours at room temperature. Unbound fluorophores were removed by dialysis. Measurement of absorbance at 340 nm (molar extinction coefficient of 3400 $M^{-1}cm^{-1}$ [85]) gave an incorporation of ~1.1 dye units per CaM molecule. Fluorescence measurements were performed on a Jobin Yvon Fluoromax-3 spectrofluorimeter at 25°C in 10 mM HEPES, pH 7.4, 100 mM KCl, and 1 mM EGTA or $CaCl_2$. Bandwidths were set to 5 nm, dansyl was excited at 340 nm, and emission was monitored from 400 to 600 nm. Protein and lipid concentrations were 0.2 µM and 100 µM, respectively. A matching buffer scan (blank) was subtracted from each spectrum, and the maximum intensities were read. Steady state fluorescence anisotropy measurements were conducted similarly, only bandwidths were set to 10 nm and emission was monitored at 510 nm. The fluorescence intensities at vertically and horizontally aligned polarizers and analyzers were recorded. The blank I_{VV}, I_{VH}, I_{HH}, and I_{HV} values were subtracted from the CaM containing values, and anisotropy was calculated from the following equation:

$$\text{Anisotropy} = (I_{VV} - G\, I_{VH}) / (I_{VV} + 2G\, I_{VH}), \text{ where } G = I_{HV}/I_{HH}$$

3.5. ANS fluorescence

The presence of micelles was monitored using the fluorescent hydrophobic probe 8-anilinonaphtalene-1-sulfonic acid (ANS, Fluka, 10417) [86] on a Jobin Yvon Fluoromax-3 spectrofluorimeter at 25°C. ANS was excited at 388 nm, emission was monitored from 400 to 600 nm, the excitation slit was adjusted to 2 nm and the emission slit to 5 nm, and the maximum intensities were read. The fluorophore concentration was 5 µM in buffer consisting of 10 mM HEPES, pH 7.4, 100 mM KCl, and either 1 mM $CaCl_2$ or 1 mM EGTA. For determination of the CMC, two straight lines reflecting the aqueous and the micellar environments were traced, and the CMC was defined as the concentration referring to their point of intersection. For monitoring micelle integrity under conditions similar to ITC measurements, 200 µM SPC was titrated with CaM in a concentration range of 0.1-20 µM in case of apoCaM and 0.1-40 µM in case of Ca^{2+}CaM.

3.6. Calcineurin activity assay

Calcineurin (PPase-2B) was purchased from Promega (V6361), and the assay was carried out based on the protocol of the company. Dephosphorylation of the substrate p-nitrophenyl phosphate (PNPP, Sigma, 1040) was followed by monitoring the increase in absorbance at 405 nm on a Wallac Victor microplate reader. Lipids (100 μM in screening experiments and 50 μM SPC in the CaM dose response experiment) were solubilized in 50 mM Tris-HCl, pH 7.4, 0.5 mg/ml BSA, 20 mM PNPP, and 1 mM $NiCl_2$. This reaction mixture was divided into 4 separate wells on a 96 well plate and either calcineurin (0.001 unit/μl) or CaM (10 μg/ml), neither or both were added. The plate was incubated at 30°C, and the absorbance was read at 405 nm every 2 minutes for 20 minutes. Blank values (without added calcineurin) were subtracted before calculating the CaM-dependent and independent activities from fitting a linear function to the data.

3.7. X-ray crystallography

CaM and SPC were co-crystallized using the sitting drop method at room temperature. 2μl protein solution at 1 mM concentration was mixed with an equal volume of precipitant solution and 10 mM SPC solution in methanol as well as 1.5 μl 0.5% LM agarose gel. The precipitant solution was 50 mM sodium cacodylate adjusted to pH 5.5 and containing 10 mM $CaCl_2$, 10 mM $MgCl_2$, and 28% (w/v) polyethylene glycol 8000. Microseeding was carried out 24 h after setting up crystallization. The cryo solution contained 10% glycerol.

Data were collected at the ID 23-1 beamline of the European Synchrotron radiation Facility. Wavelength of the beam was 0.97620 Å and temperature was set to 100 K. Data were processed using Mosflm [87] and scaled using the SCALA program [88]. The crystals are isostructural with structures of CaM complexed with various small molecules (TFP, arylalkylamine).

The structure was solved by molecular replacement using the program MOLREP [89] of the Collaborative Computational Project 4 [90]. The N- and C-terminal CaM domains of PDB entry 1LIN were used as search models. Refinement was carried out with the REFMAC5 program, using TLS refinement and restrained maximum likelihood refinement [91]. One TLS domain was defined for both CaM domains and one for the SPC molecules. Hydrogen atoms were generated in the riding positions. Model building was carried out using the Coot program [92].

The final model contains CaM residues 3–78 and 80–146, with 12 disordered side chains and 3 side chains in alternate positions, as well as 4 calcium ions, 4 SPC molecule fragments, and 79 water molecules. The stereochemistry of the structure was assessed with PROCHECK [93], 94.4% and 5.6% of the CaM residues are in the most favored and additional allowed regions of the Ramachandran plot, respectively. Data collection and refinement statistics are shown in Table 3. The atomic coordinates and structure factors were deposited in the PDB with accession code 3IF7.

Table 3 Data collection and refinement statistics for the Ca^{2+}CaM / SPC complex

	Ca^{2+}CaM / SPC
Data collection	
Space group	P 3_221
Cell dimensions	
a, *b*, *c* (Å)	39.67, 39.67, 170.34
α, β, γ (°)	90, 90, 120
Resolution (Å)	29.393-1.60 (1.60-1.69) *
R_{merge} **	0.105 (0.446)
$I / \sigma I$	12.3 (4.1)
Completeness (%)	100.0 (100.0)
Redundancy	8.6 (7.9)
Refinement	
Resolution (Å)	29.09-1.60 (1.64-1.60)
No. reflections	20426 (1554)
R_{work} / R_{free}	0.195/0.238 (0.200/0.252)
No. atoms	
Protein	1096
Ligand/ion	80 SPC / 4 Ca^{2+}
Water	79
B-factors (Å^2)	
Protein	26.664
Ligand/ion	48.393 / 18.778
Water	34.547
R.m.s. deviations	
Bond lengths (Å)	0.025
Bond angles (°)	2.085

*Values in parentheses are for highest-resolution shell. **A high resolution and a low resolution data set were collected from the same crystal and were merged.

3.8. Isothermal titration calorimetry

Thermodynamics of the interaction of Ca^{2+}CaM and apoCaM with SPC was examined using a VP-ITC instrument (MicroCal, Piscataway, NJ, USA). 5-10 μL aliquots of the protein at a concentration of 300 or 75 μM in a buffer containing 10 mM HEPES, pH 7.4, 100 mM KCl and either 5 mM $CaCl_2$ or 1 mM EGTA, was injected into the ITC cell containing 200 μM SPC in the same buffer at 25°C. A time interval of ten minutes was applied between injections. The analysis of titration curves and the energetics calculations were done using the Origin software provided by MicroCal.

3.9. Dynamic light scattering

Size distributions of SPC-CaM solutions were assessed by an ALV goniometer with a Melles Griot diode-pumped solid-state laser at 457.5 nm wavelength (type: 58 BLD 301). The intensity of the scattered light was measured at 90° at room temperature. The autocorrelation function was calculated using an IBM PC-based data acquisition system developed in the Institute of Biophysics and Radiation Biology, Semmelweis University. The most probable particle distribution was estimated using the maximum entropy method that produces normalized distribution [94]. The hydrodynamic radii of the particles were calculated based on the Einstein-Stokes equation. Size distributions calculated in this manner bear a standard error of less than 5%. Micelle size distribution is essentially independent of total SPC concentration [95], we therefore optimized SPC concentrations for the best signal-to-noise ratios.

3.10. Stopped-flow

All measurements were carried out in a buffer comprising 10 mM HEPES, pH 7.4, 100 mM KCl and 1 mM $CaCl_2$ at 25 °C. Fluorescence time courses were recorded using an SX-20 (Applied Photophysics, UK) stopped-flow apparatus having 2 ms dead-time. Dansyl fluorescence was excited at 340 nm and emission was selected with a 455 nm long-pass filter. Time courses were analyzed using the curve fitting software provided with the stopped-flow apparatus or by Origin 7 (OriginLab Corp., Northampton, MA). At least 5 individual curves were collected and averaged for each data point. Each experiment was repeated 2-5 times. Error bars represent the sample standard deviation of the average

of data points obtained from different experiments. In most amplitude vs. concentration graphs no error bars are present due to the fact that signal amplitudes of different curves collected at different detector gains are not in the same range. In these cases, amplitudes of the actually shown set of curves are presented. Amplitude titration curves are fitted with the following quadratic equation (derived in the Supplement of [96]) to extract dissociation constants:

$$y = s + A*\left((c + x + K) - \sqrt{(c + x + K)^2 - 4*c*x} \right) / 2*c$$

s = y at x = 0, A = amplitude, c = concentration of the constant component, K = dissociation constant. Errors reported on the fitted parameters comprise not only the fitting error, but the standard deviation of the individual data points as well. Kinetic simulation was performed using the Gepasi software [97] and the kinetic parameters given in Table 6.

3.11. Equilibrium fluorescence peptide-binding assays

Peptides representing CaM-binding domains were from several sources. Melittin was purchased from Sigma (M 2272). The CaM-binding domain of the skeletal muscle Ca^{2+} release channel (RyR1) [98] and two putative CaM-binding domains from the type 1 IP_3 receptor (IP_3R1) [99, 100] were synthesized by Bio-Science Trading Ltd. The CaM-binding domain of the plasma membrane Ca^{2+} ATPase (PMCA) [101] was a kind gift of Dr. Ágnes Enyedi (National Blood Center, Department of Molecular Cell Biology). For the exact sequence of peptides used in the study refer to Table 4.

Table 4 Sequence of peptides used in the study.

CaM-binding peptide	Sequence	Ref.
Melittin	GIGAVLKVLTTGLPALISWIKRKRQQ	[102]
RyR1 peptide (3614-3643)	KSKKAVWHKLLSKQRRRAVVACFRMTPLYN	[98]
IP_3R1 peptide1 (1564-1585)	KSHNIVQKTALNWRLSARNAAR	[100]
IP_3R1 peptide2 (106-128)	ENRKLLGTVIQYGNVIQLLHLKS	[99]
PMCA peptide (2-21)	LRRGQILWFRGLNRIQTQI	[101]

Fluorescence of dansyl-labeled CaM and of the Trp residue of the RyR peptide was monitored on a Jobin Yvon Fluoromax-3 spectrofluorimeter at 25 °C in 10 mM HEPES, pH 7.4, 100 mM KCl and 1 mM $CaCl_2$. Bandwidths were set to 5 nm, dansyl was

excited at 340 nm, and emission was monitored from 400 to 600 nm. Dansyl-CaM titration with melittin was carried out at 0.2 μM dansyl-CaM and the resulting curve was fitted with the above quadratic equation. When screening with lipids SPC, S1P, LPC, LPA and LT-SPC, dansyl-CaM, RyR peptide, and lipid concentrations were 0.2, 0.5 and 100 μM, respectively. When measuring dose-response for SPC, dansyl-CaM and RyR peptide concentrations were 0.2 and 0.5 μM, respectively, and SPC concentration was varied between 10 and 100 μM. In the complimentary set of experiments, the Trp residue of the RyR peptide was excited at 295 nm, and spectra were recorded from 310 to 400 nm. RyR peptide and CaM (unlabeled) concentrations were both 1 μM. In screening experiments, lipid concentrations were 100 μM, while measuring the dose-response, SPC concentration was varied between 10 and 100 μM. Experiments with dansyl-labeled apoCaM were carried out similarly to measurements with Ca^{2+}-saturated CaM, only in buffer containing 1 mM EGTA instead of 1 mM $CaCl_2$. Measurements with peptides derived from the IP_3R1 and the PMCA were conducted as in the case of the RyR peptide. Mixed micelles were prepared by mixing the methanolic stock solutions of the two lipids, and then adding them to the appropriate assay buffer. Each spectrum was corrected for corresponding lipid, protein, peptide and buffer effects by subtracting a matching buffer scan.

3.12. Single-channel recordings

Heavy SR vesicles were isolated from rabbit hind limb and back muscle as previously described [103]. In the -CaM experiments, endogenous CaM was removed by incubating SR vesicles for 30 min at 24 °C with 1 μM myosin light chain kinase-derived CaM binding peptide in the presence of 100 μM Ca^{2+} followed by centrifugation through a layer of 15% sucrose to remove complexed CaM and the peptide [59]. For purification, SR vesicles were solubilized in CHAPS, purified by sucrose density gradient centrifugation, and reconstituted into phosphatidylcholine liposomes [104].

Single channel measurements were carried out as previously described [103] in planar lipid bilayers containing phosphatidylethanolamine, phosphatidylserine, and phosphatidylcholine in the ratio of 5:3:2 (25 mg of total phospholipid/ml of *n*-decane). The side of the bilayer to which the proteoliposomes containing the purified RyR1s were added was defined as the cis (cytoplasmic) side. The trans (SR lumenal) side of the bilayer was defined as ground. Measurements were made with symmetrical 0.25 M KCl, 20 mM

K-HEPES, pH 7.4, with 22 μM free Ca^{2+} in the cis chamber. The cis solution was varied according to experimental conditions. For +CaM samples, proteoliposomes were preincubated with 1 μM CaM at room temperature for 30 min, and measurements were done in the presence of 100 nM CaM in the cis chamber. Data were acquired using test potentials of ±35 mV and were sampled at 10 kHz and filtered at 2 kHz. Channel open probabilities (*Po*) were determined from at least 2 min of recordings for each condition.

3.13. [^{3}H]ryanodine binding assays

SR vesicles were incubated with 2.5 nM [^{3}H]ryanodine for 20 h at room temperature in 0.3 M sucrose, 0.15 M KCl, 20 mM K-Pipes, pH 7.0, 50x diluted protease inhibitor cocktail (Sigma), 0.1 mg/ml BSA, either 5 mM reduced (GSH) or oxidized (GSSG) glutathione and 50 μM free Ca^{2+} (150 μM $CaCl_2$, 100 μM EGTA). Nonspecific binding was determined using heat-inactivated SR vesicles. Aliquots of the samples were diluted with 10 volumes of ice-cold water and placed on Whatman GF/B filters soaked with 2% polyethyleneimine. Filters were washed with three 5-ml volumes of ice-cold 0.1 M KCl, 1 mM K-Pipes, pH 7.0. Radioactivity remaining with the filters was determined by liquid scintillation counting to obtain bound [^{3}H]ryanodine.

3.14. [^{35}S]CaM binding assays

CaM was metabolically labeled with ^{35}S and purified according to Balshaw *et al.* [59]. SR vesicles were incubated at room temperature for 2 h with 84 nM [^{35}S]CaM in 0.3 M sucrose, 0.15 M KCl, 20 mM K-Pipes, pH 7.0, 50x diluted protease inhibitor cocktail (Sigma), 0.1 mg/ml BSA, 5 mM GSH and 100 μM free Ca^{2+} (200 μM $CaCl_2$, 100 μM EGTA). Equilibrium [^{35}S]CaM binding was assayed by centrifugation in a Beckman Airfuge for 30 min at 90,000 *g*. Nonspecific binding was determined by measuring [^{35}S]CaM binding to heat-inactivated SR vesicles. Bound [^{35}S]CaM was determined by scintillation counting after solubilization of pellets in Tris-HCl buffer, pH 8.5, containing 2% SDS.

3.15. Ca^{2+}-release measurements on bovine brain microsomes

Cerebral microsomes were isolated from bovine brain by differential centrifugation based on the procedure of Volpe *et al.* [105]. Measurements of Ca^{2+} release were performed fluorimetrically using Fluo-3 (Molecular Probes, F3715) as a Ca^{2+} sensor on a Jobin Yvon Fluoromax-3 spectrofluorimeter. Microsomes at a concentration of 0.5 mg/ml were preloaded with Ca^{2+} present in 10 mM HEPES, pH 7.2, 100 mM KCl, 5 mM KH_2PO_4, 1 mM MgATP, 5 mM phosphocreatine (Sigma, P7936), 20 µg/ml creatine phosphokinase (Sigma, C3755) and 2 µM Fluo-3 at 37 °C for 20 min. The excitation slit was adjusted to 1 nm, the emission slit to 5 nm, Fluo-3 was excited at 506 nm, and emission was monitored at 526 nm at 37 °C. Ca^{2+} efflux was initiated by the addition of either 0.1-100 µM ryanodine (Calbiochem, 559276), 5 mM caffeine (Sigma, C0750), 100 µM SPC, LPC, LPA or 2 µM Ca^{2+} ionophore A23187 (Sigma, C7522). Each compound was tested for possible artificial signals arising from their effect on Fluo-3 fluorescence by adding them to an assay mixture that did not contain microsomes.

3.16. Membrane permeability assay using radioactive Ca^{2+}

Proteinless liposomes were prepared from brain total lipid extract purchased from Avanti Polar Lipids (131101). Lipids were added from a 30 mM chloroform stock solution, dried in glass vials, and resuspended to a final concentration of 1 mM in 10 mM HEPES, pH 7.4, 100 mM KCl, 1 mM $CaCl_2$ and 5 µCi/ml (approximately 6 µM) $^{45}Ca^{2+}$ (American Radiolabeled Chemicals, ARX 0102) by sonication. Liposomes were washed twice with 2 volumes of buffer free of $CaCl_2$ and $^{45}Ca^{2+}$ by centrifugation at 16,000 *g* for 10 min. Liposomes were resuspended, and either 2 µM A23187 Ca^{2+} ionophore (Sigma, C7522), 0.2% saponin, 100 SPC, LPC or LPA were added to trigger Ca^{2+} release. After 10 min, liposomes were centrifuged again, and radioactivity in both the pellets and the supernatants were measured by scintillation counting.

3.17. Membrane permeability assay using [^{14}C]glucose

Skeletal SR vesicles were incubated for 4 h at 0 °C in a large volume (1 mg of protein/ml) of incubation medium (0.3 M sucrose, 150 mM KCl, 20 mM K-Pipes, pH 7.0, 50x diluted

protease inhibitor cocktail (Sigma), 0.1 mg/ml BSA, 10 mM glucose, 2 mM $MgCl_2$), sedimented by centrifugation for 30 min at 35,000 rpm in a Beckman 42.1 rotor, and resuspended in a small volume (20 mg of protein/ml) of incubation medium. Vesicles were incubated overnight at 4 °C in the presence of 0.1 mCi/ml [^{14}C]glucose. The vesicles were then diluted 100-fold into an unlabeled release medium supplemented with the appropriate lysophospholipid. Efflux of [^{14}C]glucose was terminated by placing aliquots (0.2 ml) on 0.45 μm HAWP Millipore filters followed by rapid rinsing with unlabeled release medium. The radioactivity retained on the filters was determined by scintillation counting.

4. RESULTS

4.1. Identification of SPC as a CaM inhibitor

4.1.1. Fluorescence binding assays indicate a selective interaction between SPC and both apo and Ca^{2+}CaM

As the simplest binding assay to examine whether S1P or SPC interacts with CaM, changes caused by the addition of these sphingolipids in the intrinsic Tyr fluorescence of the protein were analyzed (Figure 12).

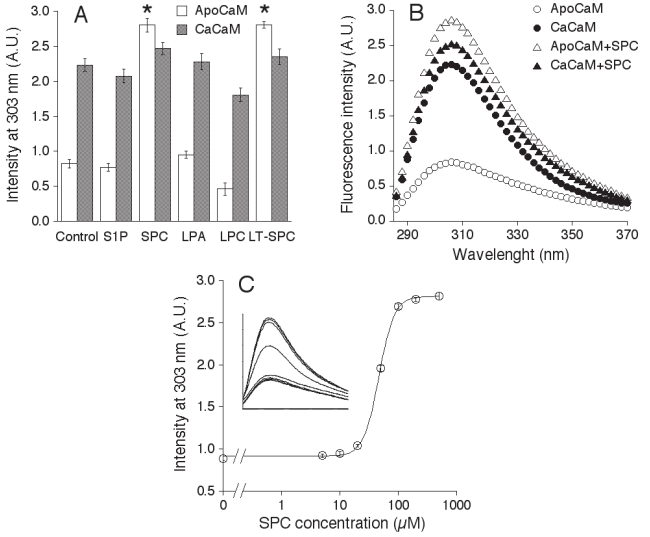

Figure 12 Effect of SPC on the intrinsic Tyr fluorescence of CaM. (A) Effect of lysophospholipids on apo (white bars) and Ca^{2+}-bound (grey bars) CaM. Protein and lipid concentrations were 1 μM and 100 μM, respectively. Results are means ± S.E.M. for at least three independent experiments. SPC and LT-SPC treated apoCaM values show significant differences (*P<0.01) with regard to the apoCaM control, based on Student's t test. (B) The average spectra for SPC. 1 μM apoCaM (○), 1 μM Ca^{2+}CaM (●), 1 μM apoCaM with 100 μM SPC (△), and 1 μM Ca^{2+}CaM with 100 μM SPC (▲). (C) Titration of apoCaM with SPC. Protein concentration was 1 μM and SPC concentration was varied from 5 to 500 μM. See inset for the individual spectra. Data points represent three independent determinations (Mean ± S.E.M.). Fitting a sigmoid function to the data resulted in an apparent K_D of 46.9 ± 0.8 μM and a Hill-coefficient of 3.3 ± 0.2.

CaM has two Tyr residues at positions 99 and 138 in the two C-terminal EF-hand motifs. Ca^{2+} binding caused an approximately 2.5-fold increase in fluorescence intensity, consistent with previous data [106, 107]. Effects of S1P and SPC, and of the related glycerolipid mediators LPA and LPC, were inspected at a concentration of 100 μM on both apo and Ca^{2+}-saturated CaM. Among these lipids, SPC elicited selective effects, causing significant changes in the intrinsic Tyr fluorescence of the apoprotein (Figure 12A). To address the stereoselectivity of SPC's action, I also explored the impact of the synthetic L-*threo* stereoisomer, and found that L-*threo*-SPC modified the intrinsic Tyr fluorescence of CaM in the same manner as D-*erythro*-SPC. It is important to note that the naturally occurring stereoisomer is D-*erythro*-SPC, which I have abbreviated to SPC throughout this report. As can be seen from Figure 12B, SPC raised the fluorescence intensity of apoCaM approximately 3 fold, resulting in a similar spectrum to that of the Ca^{2+}-saturated protein. The binding of SPC could be described by a saturation curve resulting in an apparent K_D of 46.9 ± 0.8 μM and a Hill-coefficient of 3.3 ± 0.2 (Figure 12C).

A change in the fluorescence of dansyl-labeled CaM is another good indicator of ligand binding to the protein (Figure 13). Besides recording the fluorescence spectra, the steady state anisotropy of the fluorophore, which is sensitive to the radius of giration of the molecule carrying the label, was also measured. The same set of lipids were tested, and results were consistent with that of Tyr fluorescence. SPC and LT-SPC brought forth significant changes in the intensity and anisotropy of both the Ca^{2+}-free and Ca^{2+}-bound protein (Figure 13A). The precise anisotropy values could not be determined in case of S1P (see high errors), because this sphingolipid greatly elevated the baseline, which I could not correct appropriately. Regarding the spectra (Figure 13B), Ca^{2+} binding caused an approximately 1.5 fold elevation in the fluorescence intensity, which was accompanied by an approximately 20 nm blue shift, in good agreement with former data [108, 109]. As in the case of Tyr fluorescence, SPC enhanced the intensity of apo and, to a smaller extent, Ca^{2+}CaM, resulting in a similar spectrum, regardless of the presence or absence of Ca^{2+}. The SPC-bound spectra were again closer to that of the Ca^{2+}-saturated protein, but differed from it in the intensity and in the wavelength of the maximum intensity as well. Binding of SPC to apoCaM followed saturation kinetics resulting in an apparent K_D of 21.7 ± 1.3 μM and a Hill-coefficient of 1.8 ± 0.2 (Figure 13C).

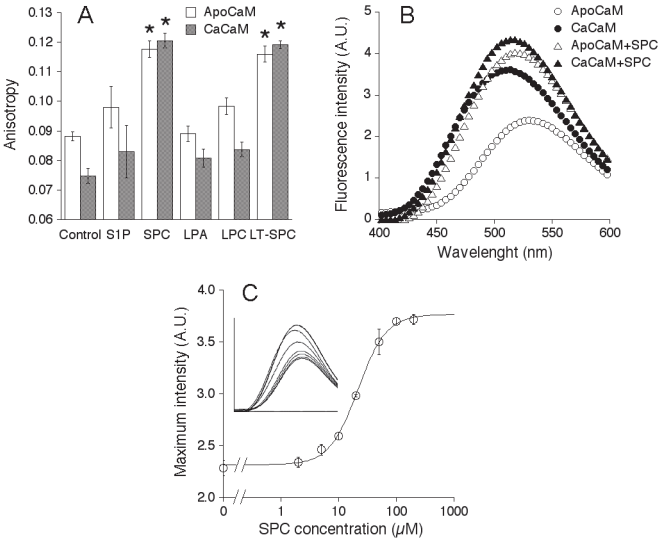

Figure 13 Effect of SPC on the fluorescence of dansyl-labeled CaM. (A) Effect of lysophospholipids on the steady state anisotropy of apo (white bars) and Ca^{2+}-saturated (grey bars) dansyl-labeled CaM. Protein and lipid concentrations were 0.2 μM and 100 μM, respectively. Results are means ± S.E.M. for at least three independent experiments. The addition of SPC and LT-SPC caused significant differences (*P≤0.01) in the anisotropy of both the apo and the Ca^{2+}-bound protein, with regard to the corresponding controls. (B) The average spectra for SPC. 0.2 μM apoCaM (○), 0.2 μM Ca^{2+}CaM (●), 0.2 μM apoCaM with 100 μM SPC (△), and 0.2 μM Ca^{2+}CaM with 100 μM SPC (▲). (C) Titration of apoCaM with SPC. Protein concentration was 0.2 μM and SPC concentration was varied from 2 to 200 μM. See inset for the individual spectra. Data points represent three independent determinations (Mean ± S.E.M.). Fitting a sigmoid function to the data resulted in an apparent K_D of 21.7 ± 1.3 μM and a Hill-coefficient of 1.8 ± 0.2.

We demonstrated that SPC binds selectively to CaM using surface plasmon resonance as well. Furthermore, the sphingolipid does not exert detergent-like effects, it binds as a real ligand, as I showed using circular dichroism spectroscopy. These results are not presented here, for details refer to [110]. Since my thesis is based on the results of four publications, I felt that the amount of data presented in them is too extensive to be part of one report without losing coherency. Therefore, I omitted those experiments, which I felt redundant and superfluous to convey the main line of thought, and I only refer to them where appropriate.

4.1.2. SPC micelles are required for efficient binding to CaM

Since lysophospholipids form micelles in aqueous solutions, the question arises as to whether we are seeing a monomeric lipid – protein or a micelle – protein interaction. To provide an answer, I measured the critical micelle concentration (CMC) of SPC under our experimental conditions. The fluorescent hydrophobic probe ANS exerts increased fluorescence in a hydrophobic environment, and as such, is well suited to detect the formation of micelles in a solution [86]. Using this method, the CMC of SPC was determined to be 33 ± 2 μM (Figure 14), and did not depend on the presence of Ca^{2+}. The fact that this value is in the same range as the apparent K_D values obtained from titrating apoCaM with SPC (46.9 ± 0.8 μM when monitoring intrinsic Tyr fluorescence and 21.7 ± 1.3 μM when monitoring the fluorescence of the dansyl-labeled protein, Figures 12C and 13C), and the intensive apparent positive cooperativity of the titration curve suggested to us that there is a strong interaction between CaM and SPC micelles, whereas SPC monomers do not bind efficiently to the protein. Therefore, the dissociation constants estimated from titrating with the lipid only provide information about micelle formation and do not characterize the strength of the interaction. For determination of the true dissociation constant and other binding parameters of the CaM-SPC interaction see Chapter 4.2.

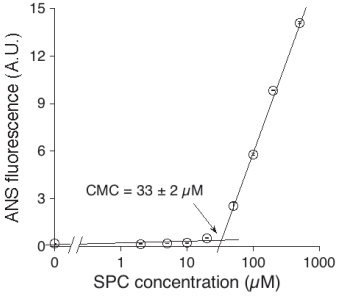

Figure 14 Determination of the critical micelle concentration of SPC. The CMC of SPC was determined using the fluorescent hydrophobic probe ANS. Two straight lines reflecting the aqueous and the micellar environment were traced, and the CMC was defined as the concentration referring to their point of intersection, yielding a CMC of 33 ± 2 μM for SPC. Mean and standard error values were calculated from three independent experiments.

To rule out the possibility that the specificity of the observed effects arises from the different CMC values of the lipids tested, i.e. only SPC forms micelles at the concentration at which our experiments were carried out, the CMC of S1P, LPA, LPC, and LT-SPC was determined as well (data not shown). I found that the CMC values of each lie in the 20-50 μM concentration range, thus, each tested lipid forms micelles at a concentration of 100 μM, at which the screening experiments were conducted.

4.1.3. SPC inhibits CaM function in *in vitro* enzyme activity assays

To assess the functional effects of the CaM-SPC interaction, calcineurin, also known as Ca^{2+}CaM-dependent protein phosphatase 2B, was chosen as a target enzyme. Calcineurin is a heterodimer of a 61 kDa catalytic and CaM-binding subunit, calcineurin A and a 19 kDa Ca^{2+}-binding regulatory subunit, calcineurin B, which is an EF-hand protein very similar to CaM (for a review on calcineurin see [74]). The enzyme reaction can be easily followed by monitoring the increase in absorbance at 405 nm, caused by the dephosphorylation of the substrate p-nitrophenyl phosphate (PNPP).

As can be seen in Figure 15A, CaM increased the activity of calcineurin approximately 2.5-fold. This activating ability was substantially inhibited in case of SPC and LT-SPC, while it was not significantly affected in case of S1P, LPA, and LPC. For clarity, fold activation by CaM is shown, because the lysophospholipids slightly influenced (S1P increased, whereas SPC, LPC, and LT-SPC decreased) the basal activity of calcineurin.

The concentration dependent inhibition of both the CaM-dependent and independent calcineurin activity by SPC is shown in Figure 15B. The IC_{50} was estimated to be 27.4 ± 2.6 μM with a cooperativity coefficient of 2.3 ± 0.4 in case of the CaM-dependent, and 29.8 ± 3.5 μM with a cooperativity coefficient of 1.7 ± 0.2 in case of the basal activity. Since interaction between the two subunits, calcineurin A and CaM-like calcineurin B, is essential for activity [74], I hypothesize that the decrease in basal activity is a consequence of the fact that SPC disrupts the complex of these two subunits similarly to CaM-target interactions (refer to chapter 4.3). To prove that the inhibition of the CaM-dependent calcineurin activity is a result of CaM inhibition, calcineurin was titrated with CaM both in the presence and absence of 50 μM SPC (Figure 15C). The fact that excess CaM can retain calcineurin activation in the presence of SPC, and that SPC causes a right shift of the saturation curve, is indicative of a competitive mechanism. The thousand-fold

difference of the EC_{50} values (2.5 ± 0.4 nM for CaM alone versus 2.9 ± 0.2 μM in the presence of 50 μM SPC) also reveals strong CaM inhibition by SPC.

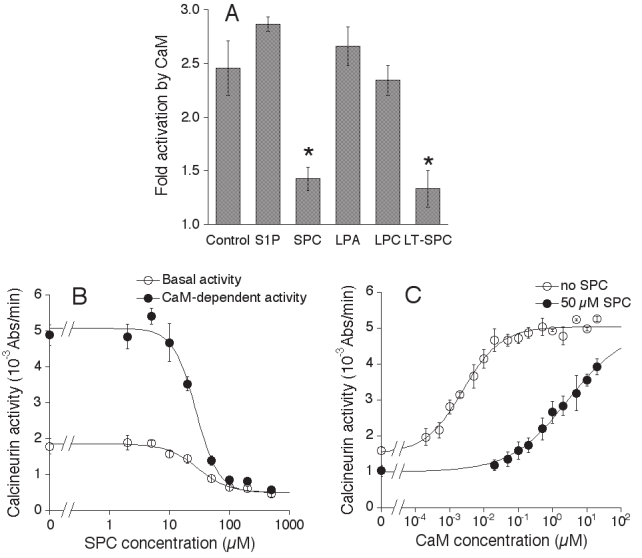

Figure 15 Effect of SPC on the calcineurin activating ability of CaM. Calcineurin activity was measured by monitoring the increase in absorbance at 405 nm due to the dephosphorylation of the substrate PNPP (20 mM). Calcineurin and CaM concentrations were 0.001 unit/μl, and 10 μg/ml, respectively. Data points represent mean ± S.E.M of at least four independent measurements. (A) Effect of lysophospholipids (100 μM) on the calcineurin activating ability of CaM. Student's t-test revealed significant differences (*P<0.05) for SPC and LT-SPC with regard to control. (B) Concentration dependent inhibition of the Ca^{2+}-CaM-dependent (●) and independent (○) activity of calcineurin by SPC. Fitting a displacement function to the data yielded an IC_{50} value of 27.4 ± 2.6 μM with a cooperativity coefficient of 2.3 ± 0.4 in case of the Ca^{2+}-CaM-dependent, and an IC_{50} value of 29.8 ± 3.5 μM with a cooperativity coefficient of 1.7 ± 0.2 in case of the basal activity. (C) Dose response curves for the activation of calcineurin by CaM in the presence (●) and absence (○) of 50 μM SPC. Fitting a dose response function to the data yielded an EC_{50} value of 2.5 ± 0.4 nM in case of CaM alone, and an EC_{50} value of 2.9 ± 0.2 μM in the presence of 50 μM SPC.

I have also shown that SPC inhibits the phosphodiesterase (PDE1) activating ability of CaM, these results are presented in [110].

4.2. Structural characterization of the CaM-SPC interaction

4.2.1. Crystal structure of the Ca^{2+}CaM/SPC complex

After the identification of a specific interaction between CaM and SPC, I continued research in two main directions. I focused on unraveling the putative functional consequences of the interaction and also on giving an in-depth structural and mechanistic characterization of the binding process. The latter one was a highly exciting challenge, since the fact that SPC binds in a micellar form raised several intriguing questions and necessitated special experimental treatment. During the course of our structural studies, we have determined the crystal structure of the Ca^{2+}CaM/SPC complex, which I consider a huge achievement since lipid-protein interactions are rarely characterized at this level. Most of the results I present from here on derive from experimental techniques that require special expertise. Therefore, they are not solely my own accomplishments, I have attained them in collaboration with experts of a given field. In these cases, I clearly state at the beginning of each chapter what my contribution was to the given project. X-ray crystallography was carried out in collaboration with Veronika Harmat (ELTE, Laboratory of Structural Chemistry and Biology). I have participated in each part of the structure determination, including crystallization, data collection at ESRF, Grenoble, model refinement and writing the appropriate sections of the manuscript [111]. Of course, Veronika is responsible for the substantive work, I mostly learned and participated actively in simple tasks.

The crystal structure of the Ca^{2+}CaM/SPC complex was refined to 1.6 Å resolution (Figures 16A and B). The protein is well defined by electron density, except for the central linker region and the ends of the protein chain known to be highly flexible and often disordered in CaM structures [80, 112-114]. The protein is in a collapsed conformation with a binding channel of mainly hydrophobic character formed between its two domains. The hydrophobic pockets known to be adaptable to the bound ligand are open.

Four SPC molecules could be identified in the calculated electron density maps (Figure 16C). Their most rigid parts are the long extended alkyl chains bound in nearly parallel positions. The binding channel between the two CaM domains is filled by these four chains. The alkyl chains of the sphingosyl moiety spread outside the binding channel (cca. 17 Å long) and the overhangs are disordered. The phosphocholine moieties could be built in electron density maps fully for two SPC molecules and partially for the third one, however, they show significantly lower electron density than the alkyl chains.

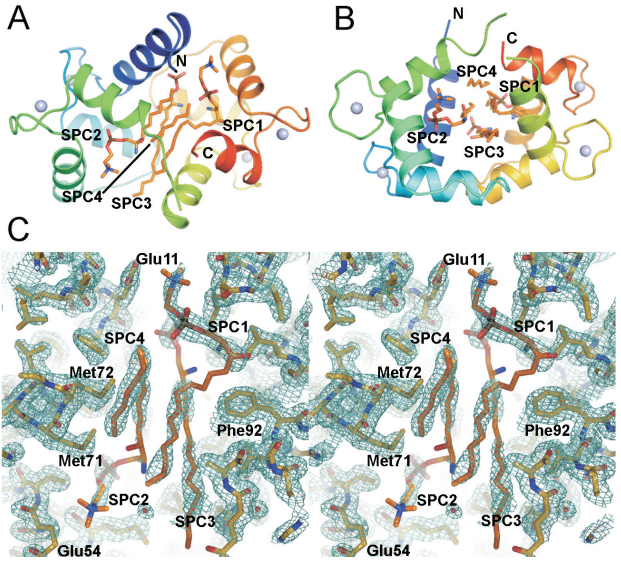

Figure 16 Overall structure of the Ca^{2+}CaM/SPC complex. (A,B) Cartoon representation of CaM with the four SPC molecules. Side view (A) shows SPC1 and SPC2 bound in quasy-symmetry related positions occupying the hydrophobic pockets of CaM. Top view (B) shows the four SPC molecules bound in nearly parallel orientations. (C) Stereo view of the electron density map contoured at 1.0 σ level in the SPC binding region. Note that segments of the SPC molecules outside the hydrophobic binding region are disordered. The figure was prepared using Pymol (DeLano Sci.).

Two of the SPC molecules are bent near their phosphate moieties and fill the hydrophobic pockets of CaM, while their positively charged choline groups are pointing towards the acidic regions of CaM forming electrostatic interactions. The strongest electrostatic interactions of these charged choline groups are established with Glu11 and Glu127 (2.9-3 Å) as well as with Glu54 and Glu123 (5.4 Å). The low occupancy of the phosphocholine moieties suggests that they are partially disordered in the crystal and possibly flexible in solution. This results in a non-directed binding of the phosphocholine head group and in a possible mobility of the SPC molecule along its axis within the binding channel.

Most importantly, the overall conformation of CaM is well-defined in our crystal structure and resembles its complexes with the small molecules trifluoperazine [82] and the arylalkylamine derivative AAA [80] and many of its peptide complexes, e.g. [112, 113] (Figure 17). Accordingly, residues involved in SPC binding could be also mapped to

the small molecule inhibitor and target peptide binding sites (Supplementary Information in [111]). In the Ca^{2+}CaM/SPC complex, CaM is in a collapsed overall conformation with SPC molecules bound between the two CaM domains. The fact that the lipid occupies the same binding pocket as the target peptides of CaM explains competitive inhibition witnessed in the calcineurin functional assay (Figure 15) and in peptide binding assays (Figure 25).

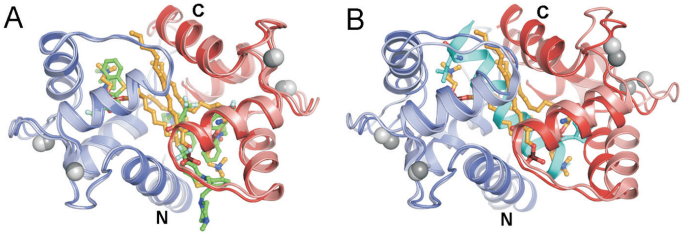

Figure 17 The conformation of Ca^{2+}CaM in the Ca^{2+}CaM/SPC structure is collapsed, similarly to Ca^{2+}CaM complexes with small molecules and most of its target peptides. The structures show overlapping binding sites of the ligands. (A) Structural alignment with the Ca^{2+}CaM/4TFP complex (pdb accession code 1LIN). N- and C-terminal CaM domains of the Ca^{2+}CaM/SPC complex are colored blue and red, respectively. The compared structure is shown in lighter colors. Carbon atoms of the SPC and TFP molecules are shown in orange and green, respectively. (B) Structural alignment with the Ca^{2+}CaM/myosin light chain kinase target peptide complex (pdb accession code 2K0F). The target peptide is in cyan, with its residues anchoring in the hydrophobic pockets of CaM shown as sticks. The figure was prepared using Pymol (DeLano Sci.).

4.2.2. Isothermal titration calorimetry provides clues for a two-step binding model

To thermodynamically characterize the CaM-SPC interaction, isothermal titration calorimetry (ITC) measurements were conducted in collaboration with József Kardos (ELTE, Department of Biochemistry). We carried out experiments together, he evaluated data, while I wrote the corresponding sections of the manuscript [111]. As previously mentioned, because binding occurs between the protein and sphingolipid micelles, characterization of the interaction requires special treatment. Hence, instead of applying the conventional ITC experimental setup of ligand injection, we injected the protein into the cell containing 200 µM SPC. By keeping the SPC concentration constant, well above its CMC, we avoided the heat effects caused by the change in the micellar state of the lipid.

Calorimetric traces were obtained both in the presence and absence of Ca^{2+} (Figure 18). Parameters obtained from the fitting process are presented in Table 5. ΔH, ΔS, and K_D values correspond to the binding of one CaM molecule to one apparent binding site. Both titrations generated two clearly distinguishable binding processes. The binding of apoCaM to SPC was very similar to Ca^{2+}CaM binding to the lipid, only it took place in a narrower concentration range, that is, with different stoichiometry (see inset in Figure 18). In case of apoCaM, we observed an additional endothermic heat reaction, which gradually decreased during the whole experiment and overlapped with the two binding reactions (Supplementary Information in [111]). We interpreted this process as micelle rearrangement, the effect of which could be removed by subtraction for the whole concentration range, yielding an undistorted double binding curve for data evaluation. Parameters given for the first process of the Ca^{2+}CaM titration should be taken as approximative values (Table 5), because the beginning of the reaction could not be resolved. In general, the observed stoichiometry-range for the CaM-SPC interaction is similar to what we and others have found previously for other lipid-protein interactions [115, 116].

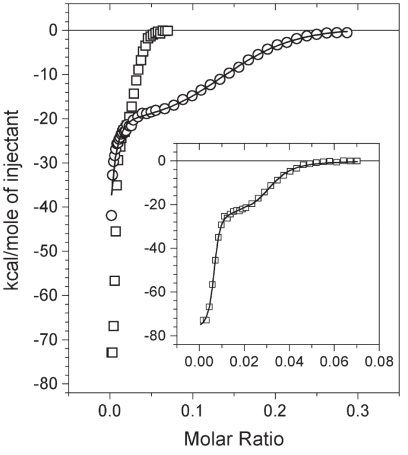

Figure 18 Calorimetric traces of titrating 200 µM SPC with Ca^{2+}CaM (○) or apoCaM (□). Inset depicts the titration with apoCaM on a more appropriate scale. Solid lines show the fit by a two-site binding model provided by the Origin for ITC software, yielding parameters listed in Table 4.

The stoichiometry of the two binding processes enabled us to envisage the following scenarios. The first, stronger binding, for which the fitting process yielded a stoichiometry of 100-200 SPC monomers / protein and a K_D of 61 ± 10 nM for Ca^{2+}CaM, and a stoichiometry of 164 ± 5 SPC monomers / protein and a K_D of 2.4 ± 0.4 nM for apoCaM, may be interpreted as the binding of the protein to available surfaces on micelles. The second binding process is weaker, yielding a stoichiometry of 7 ± 0.15 SPC monomers / protein and a K_D of 2.1 ± 0.2 μM for Ca^{2+}CaM and a stoichiometry of 40 ± 1 SPC monomers / protein and a K_D of 0.22 ± 0.03 μM for apoCaM, and could result from additional protein molecules binding to the micelles. However, this scenario is quite unlikely in the case of Ca^{2+}CaM, where the estimated number of SPC monomers per protein molecule is 7 at the end of the second ITC phase. This would mean that approximately 30 CaM molecules bind to one micelle, which is hardly possible considering that the size of the protein and the micelle are comparable (see dynamic light scattering results for evidence). More likely, the binding of further CaMs could result in the disintegration of micelles by the protein. Ca^{2+}CaM could then isomerize in a collapsed conformation wrapped around only a few SPC monomers, as we see in our crystal structure. ApoCaM, on the other hand, follows a reaction with the stoichiometry of approximately 40 SPC monomers / protein. This stoichiometry would allow the binding of several apoCaM molecules to one micelle or alternatively, the disintegration of micelles into smaller "parts" stabilized by the protein.

Table 5 Thermodynamic parameters of the CaM – SPC interaction obtained from ITC measurements

	First process				Second process			
	n_1[a]	K_{D1} (nM)	ΔH_1 (kcal·mol^{-1})	$-T\Delta S_1$[c] (kcal·mol^{-1})	n_2	K_{D2} (μM)	ΔH_2 (kcal·mol^{-1})	$-T\Delta S_2$ (kcal·mol^{-1})
Ca^{2+}CaM	100-200[b]	61±10	-56±1	+46	7±0.15	2.1±0.2	-22.9±0.5	+15
ApoCaM	164±5	2.4±0.4	-77±1	+65	40±1	0.22±0.03	-24.7±0.6	+15.5

[a] n_1 and n_2 are the numbers of SPC molecules bound by one CaM molecule for the given binding process. ΔH, ΔS, and K_D are values corresponding to the binding of one CaM molecule to one apparent binding site. The reliability of the fittings are shown by the error values. Each experiment was repeated three times. The deviation between the individual measurements was found to be less than 5%.

[b] The fitting provided acceptable results in this n_1 range, K_{D1} and ΔH_1 values are calculated for n_1 = 200.

[c] $-T\Delta S = R \cdot T \cdot \ln K_D - \Delta H$

Considering the enthalpy and entropy values (Table 5), we can conclude that both reactions are entropically largely unfavorable. A study of Brokx *et al.* on target peptide binding by CaM revealed that binding can be either entropically or enthalpically driven, but even in the second case, it is only slightly unfavorable entropically with the highest -$T\Delta S$ value of approximately +5 kcal/mol [117]. In contrast, our titrations yielded -$T\Delta S$ values of +46 and +65 kcal/mol for the first reaction and +15 and +15.5 kcal/mol for the second reaction, in case of Ca^{2+}CaM and apoCaM, respectively. Accordingly, our ΔH values are larger compared to the results of Brokx *et al.* who obtained ΔH values between approximately -15 and +15 kcal/mol in contrast to our -56 ± 1 and -77 ± 1 kcal/mol for the first reaction and -22.9 ± 0.5 and -24.7 ± 0.6 kcal/mol for the second reaction for Ca^{2+}CaM and apoCaM, respectively. On the other hand, ΔG (around -10 kcal/mol) and K_D values (in the nanomolar range) are similar for interactions of CaM with target peptides and SPC. The large differences in the thermodynamic properties between SPC – CaM and single ligand – CaM interactions could be explained by the different nature of the two interactions. In our experiments, the initial state of SPC is micellar, not monomeric, and instead of one ligand, a CaM molecule embraces several SPC molecules upon binding.

4.2.3. Dynamic light scattering affirms that CaM first binds to SPC micelles, which are then disintegrated by the protein

To ascertain the size distribution profile of SPC – CaM mixtures of varying stoichiometries, dynamic light scattering (DLS) measurements were carried out in collaboration with Károly Módos (SOTE, Institute of Biophysics and Radiation Biology). We carried out experiments together, he evaluated data, while I wrote the corresponding sections of the manuscript [111]. It is worth noting that the intensity dimension of the DLS data (Figure 19) is not informative, since it is greatly influenced by the larger contaminating particles in the solution that vary from sample to sample. To compare the size distributions of the species present, curves were normalized to their area. The R_h values of the peaks correspond to the average hydrodynamic radii of the particles, and are therefore the relevant values characterizing the size of a given particle.

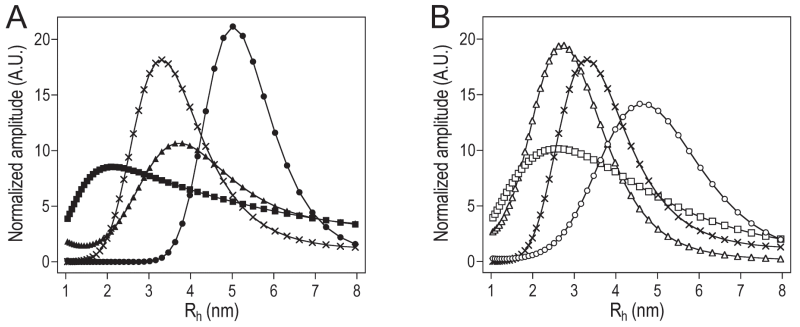

Figure 19 Dynamic light scattering profiles of different CaM-SPC solutions in case of Ca^{2+}CaM (A) and apoCaM (B). Symbols represent 500 μM SPC (×), 40 μM Ca^{2+}CaM (▲), 40 μM apoCaM (△), 200 μM SPC with 8 μM Ca^{2+}CaM (●), 200 μM SPC with 3 μM apoCaM (○) (plateau of the first ITC phase), 200 μM SPC with 40 μM Ca^{2+}CaM (■) and 200 μM SPC with 12 μM apoCaM (□) (plateau of the second ITC phase). Note that curves are normalized to their area and their amplitudes are not informative. R_h values corresponding to the peaks describe the average size distribution of the population.

Samples of 40 μM Ca^{2+}CaM and 40 μM apoCaM both gave homogenous size distributions of 3.3 nm and 2.6 nm hydrodynamic radii, respectively, in accordance with preceding reports [118]. A sample of pure SPC micelles revealed that micelles have an average hydrodynamic radius of 3.1 nm. In mixtures of 200 μM SPC with 8 μM Ca^{2+}CaM or 3 μM apoCaM (concentrations near the end of the first ITC phase), an increase in particle size could be observed compared to SPC-free Ca^{2+}CaM and apoCaM (Figure 19). 200 μM SPC with 8 μM Ca^{2+}CaM yielded particles with an average hydrodynamic radius of 5 nm, while 200 μM SPC with 3 μM apoCaM yielded particles with an average hydrodynamic radius of 4.5 nm. At concentrations corresponding to the end of the second ITC phase, 200 μM SPC with 40 μM Ca^{2+}CaM or 12 μM apoCaM, the size distribution profile decreased substantially in agreement with the hypothesis that the large protein – micelle particles are disintegrating. The size distribution became less homogenous, a small amount of the large complexes could still be observed. In case of Ca^{2+}CaM the resulting particles are significantly smaller than Ca^{2+}CaM alone, which indicates that the protein adopts a more compact conformation. Together with the 7 SPC monomers per protein stoichiometry estimated from the ITC fitting, this suggests that the ensuing Ca^{2+}CaM / SPC complex is in the typical collapsed conformation seen in Ca^{2+}CaM / inhibitor and Ca^{2+}CaM / target peptide complexes.

4.2.4. ANS fluorescence reveals the disruption of SPC micelles by CaM

To further verify the proposed model, I monitored micelle integrity during titration with CaM. Under conditions identical to that of ITC experiments, we followed the fluorescence of the hydrophobic probe, ANS. As the intensity of ANS fluorescence increases greatly when incorporated into lipid micelles [86], it is well suited to certify the presence of micelles in a solution. The change in ANS fluorescence in the presence of 200 μM SPC upon incremental addition of Ca^{2+}CaM or apoCaM is depicted in Figure 20. It is clearly demonstrated that increasing protein concentration disrupts micelles, moreover, their disruption occurs in the same range of molar ratios (0.02-0.2 for Ca^{2+}CaM and 0.01-0.05 for apoCaM) as the second phase of the ITC measurements. This observation along with the results of the DLS measurements strongly argues for the explanation that the second phase witnessed in ITC experiments is a micelle disintegration process.

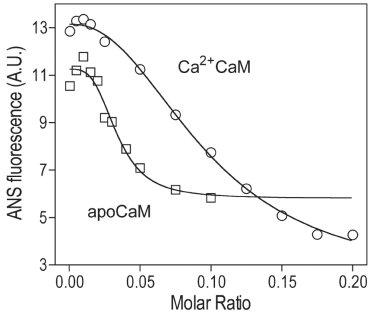

Figure 20 Monitoring micelle integrity with ANS fluorescence. 200 μM SPC was titrated with Ca^{2+}CaM (○) or apoCaM (□) similarly to ITC measurements only monitoring the fluorescence of ANS instead of released heat. Disruption of micelles occurrs in the same range of molar ratios as the second phase of ITC measurements.

4.2.5. Kinetic properties of the two-step binding process

Since several kinetic features of the binding process are presented in the following section (Chapter 4.3.), I chose not to show kinetic results obtained under conditions similar to ITC measurements in detail. For these, please refer to [111]. Most importantly, determined dissociation constants and stoichiometries are close to the ones calculated from ITC experiments, suggesting that we observe the same events in both experimental setups.

Comparing Figure 21 with Figure 18, it appears even more strikingly that the same processes are observed utilizing two utterly different techniques.

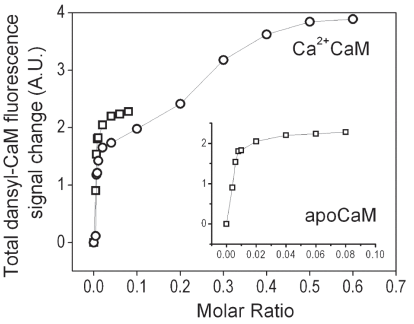

Figure 21 Fluorescence data from stopped-flow measurements calculated in molar ratios. 50 µM SPC was mixed with increasing concentrations of apo (□) or Ca^{2+} (○) CaM.

4.3. SPC inhibits CaM function in a competitive manner

4.3.1. Kinetic characterization of Ca^{2+}CaM binding to target peptides

As a next step, moving in the direction of functionality, but still continuing the mechanistic approach, I wished to understand how exactly SPC inhibits CaM function. For addressing this question transient kinetic stopped-flow measurements proved especially useful, which are largely the merit of Judit Tóth (Institute of Enzymology). We carried out experiments together, while data evaluation, performing kinetic simulations and writing the corresponding sections of the manuscript were done by her alone. Although this is the part of my thesis, which I contributed to least, I present these results in detail, because they are essential to the message I wish to convey, and represent a bridge between our structural and functional studies.

As the simplest model of CaM-target interactions, we turned to the CaM-melittin complex, which is widely used to study the interaction between CaM and the effector proteins it regulates [102]. The details of the CaM-melittin binding mechanism, nevertheless, have not been revealed before to the degree we needed to study a composite system with both putative CaM binding partners − SPC and melittin − present. Previous kinetic studies focused on the mutual effect of Ca^{2+} and target peptide binding to CaM [119, 120] and did not aim at characterizing the CaM – peptide interaction at saturating

Ca^{2+} concentration. Therefore, we performed melittin binding experiments both by equilibrium and transient kinetic methods using the fluorescence of dansyl-CaM. Dansyl labeling was performed in conditions to produce a 1:1 homogeneous labeling to avoid artifacts in the transient kinetics experiments.

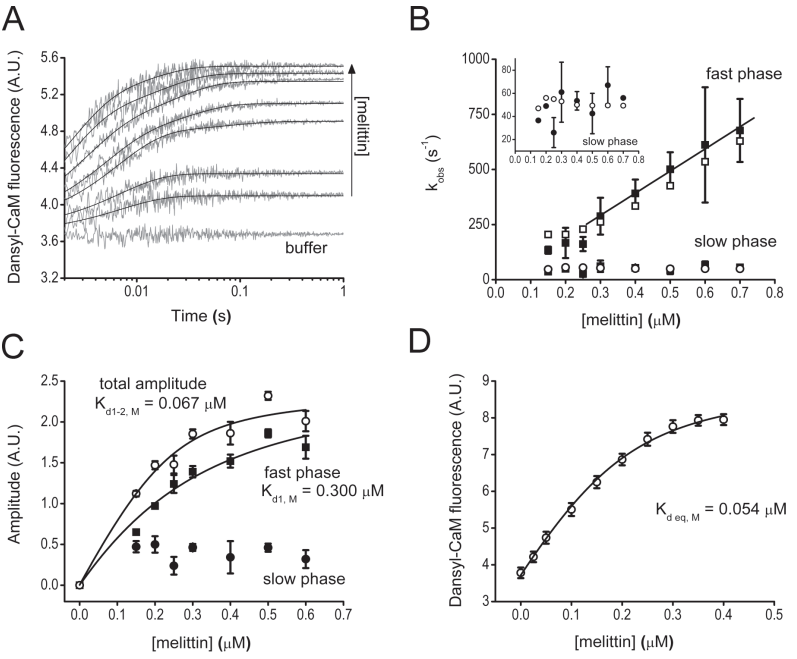

Figure 22 Binding of Ca^{2+}-saturated dansyl-CaM to the model peptide melittin. (A) Fluorescence time courses on the reaction of 0.1 μM (final concentration) dansyl-CaM with buffer or with 0.15-0.6 μM melittin. Stopped-flow traces are shown in grey, black lines through the data represent the best double exponential fits to the curves. The x-axis is shown from t = 0.002 s (the dead-time of the stopped-flow apparatus), exponential fits converge to the fluorescence intensity level of the „buffer" curve. (B) Melittin concentration dependence of the observed binding rate constants from exponential fits to the stopped-flow traces (fast phase (■) and slow phase (●)) or from kinetic simulation of the same time-courses (fast phase (□) and slow phase (○)). A linear fit to the pseudo-first order part of the curve yielded $k_{+1, M}$ = 1004 ± 366 $\mu M^{-1}s^{-1}$. The rate constants of the slow phase (inset, ●) did not exhibit concentration dependence and had a first-order $k_{2obs, M}$ = 49 ± 13 s^{-1}. (C) Amplitude titration extracted from the exponential fits to the stopped-flow traces. The quadratic fit (smooth line through the data) to the concentration-dependent fast phase (■) comprising 88% of the total amplitude at the highest measured concentration yielded an apparent K_d of 0.3 ± 0.15 μM. The amplitude of the slow phase (●) exhibited a tendency to decrease with concentration. Fitting the total amplitude data (○) yielded a K_d of 0.067 ± 0.044 μM. (D) Equilibrium fluorescence titration of 0.2 μM dansyl-CaM with melittin. The K_d from the quadratic fit is 0.054 ± 0.016 μM.

Time courses of fluorescence change after mixing dansyl-CaM with melittin are biphasic (Figure 22A) indicating at least two biochemical transitions both characterized by the expected fluorescence increase [108, 109] upon binding. Time courses were analyzed by double exponential fitting. The concentration dependence of the observed rate constants of the two phases (Figure 22B) suggests that the fast phase is a second-order reaction followed by a slow first-order reaction reflecting some conformational reorganization of the CaM-melittin complex ($k_{2obs,\ M}$ = 49 ± 13 s^{-1}, Table 6). The association rate constant of the second-order reaction was determined from the linear phase of the k_{obs} vs. concentration curve, in which range the pseudo first-order approximation applies ($k_{+1,\ M}$ = 1004 ± 366 $\mu M^{-1}s^{-1}$, Table 6). The dissociation rate constant could not be reliably extracted from the linear fit because of the large uncertainty of the y-intercept. We could extract the dissociation constant of the first process of the binding from the concentration dependence of the fast phase amplitude (Figure 22C, $K_{d1,\ M}$ = 0.3 ± 0.15 µM, Table 6). The total amplitude describing the entire binding process is analogous to equilibrium binding data and yielded $K_{d1\text{-}2,\ M}$ = 0.067 ± 0.044 µM. Consistently, equilibrium fluorescence titration of dansyl-CaM with melittin in a fluorimeter yielded $K_{d\ eq,\ M}$ = 0.054 ± 0.016 µM (Figure 22D, Table 6) close to the previous $K_{d1\text{-}2,\ M}$ value within error. Taking Equations 1 and 2 (derived in the Supplement of [96]) and $K_{d1\text{-}2,\ M}$ into consideration, we calculated all remaining parameters of the two-step binding process summarized in Scheme 1.

$$k_{2obs,M} = k_{+2,M} + k_{-2,M} \qquad \text{Eq. 1}$$

$$K_{eq,M} = \frac{K_{d1,M}}{1 + K_{2,M}} \qquad \text{Eq. 2}$$

Using the kinetic parameters in Scheme 1, we ran numerical simulations for the time courses shown in Figure 22A to test the validity of our model. To model the experimentally observed time courses, we assumed that the two high fluorescence states have similar intensities and thus the observed fluorescence reflects the sum of the concentrations of the two populations (* and ** in Scheme 1). The simulated time courses were subjected to the same analysis procedures as the experimental data. As a result, k_{obs} values showed good agreement with the experimentally obtained ones (Figure 22B) indicating that the established CaM-ME binding model is consistent with our experimental data.

$$dCaM + ME \underset{k_{-1,M}=301s^{-1}}{\overset{k_{+1,M}=1004\mu M^{-1}s^{-1}}{\rightleftharpoons}} dCaM.ME* \underset{k_{-2,M}=11s^{-1}}{\overset{k_{+2,M}=38s^{-1}}{\rightleftharpoons}} dCaM.ME**$$

$K_{d1,M}=0.3\mu M$ $K_{2,M}=3.5\mu M$

SCHEME 1

4.3.2. Kinetic evidence for a competitive mechanism by which SPC interferes with Ca^{2+}CaM-target interactions

We wished to characterize the kinetics of the interaction between dansyl-CaM and SPC as we did for the CaM-peptide interaction. Fluorescence time courses upon mixing dansyl-CaM with various concentrations of SPC proved to be extremely fast and yielded only small fluorescence changes. Even at the lowest SPC concentration the course of fluorescence change was lost in the 2 ms dead-time of the stopped-flow apparatus and is therefore not shown. We can only put a lower estimate on the association rate constant ($k_{+1,\,S} > 40\ \mu M^{-1}s^{-1}$, Table 6). As a result of these SPC-binding experiments we conclude that Ca^{2+}CaM binding to SPC is fast and saturated above the CMC which is relevant for designing the competition experiments.

Table 6 Measured kinetic and thermodynamic parameters of the interaction of Ca^{2+}CaM with melittin or with SPC.

Experiment	Parameter	Value	Dimension	Figure
CaM-ME binding	$k_{+1,\,M}$	1004 ± 366	$\mu M^{-1}s^{-1}$	22B
	$k_{-2,\,M} + k_{+2,\,M}$	49 ±13	s^{-1}	22B
	$K_{d1,\,M}$	0.3 ± 0.15	μM	22C
	$K_{d1\text{-}2,\,M}$	0.067 ± 0.044	μM	22C
	$K_{d\ eq,\,M}$	0.054 ± 0.016	μM	22D
CaM-SPC binding	$k_{+1,\,S}$	> 40	$\mu M^{-1}s^{-1}$	-
SPC micelle formation	CMC	33 ± 2	μM	14
SPC chase	$K_{d1\text{-}2,\,SC}$	32 ± 0.7	μM	23B
	$K_{d1,\,SC}$	51 ± 3	μM	23B
	$k_{+1,\,SC}$	2.4 ± 0.2	$\mu M^{-1}s^{-1}$	23C
	$k_{1\ sat,\,SC}$	348 ± 30	s^{-1}	23C
	$k_{2obs,\,SC}$	14 ± 6	s^{-1}	23C
	$k_{3obs,\,SC}$	0.9 ± 0.3	s^{-1}	23C
ME chase	$K_{d1\text{-}2,\,MC}$	1.0 ± 0.3	μM	24B
	$k_{1\ sat,\,MC}$	59 ± 13	s^{-1}	24C
	$K_{1app,\,MC}$	5.4 ± 3.4	μM	24C
	$k_{2obs,\,MC}$	4-8	s^{-1}	24C

Explanation of the indexes: M, parameter obtained for CaM – melittin binding; S, parameter obtained for CaM – SPC binding; C, parameter obtained in a chasing experiment; +/- signs and numbers indicate specific reaction steps as shown in Scheme 1.

We reacted pre-mixed dansyl-CaM − melittin complexes with various concentrations of SPC to investigate whether these two ligands compete with each other for the same CaM target site. Luckily, formation of the two different dansyl-CaM complexes display opposite fluorescence changes and thus transformation of one complex to the other is expected to be accompanied by a large signal change (CaM.ME** → CaM.SPC).

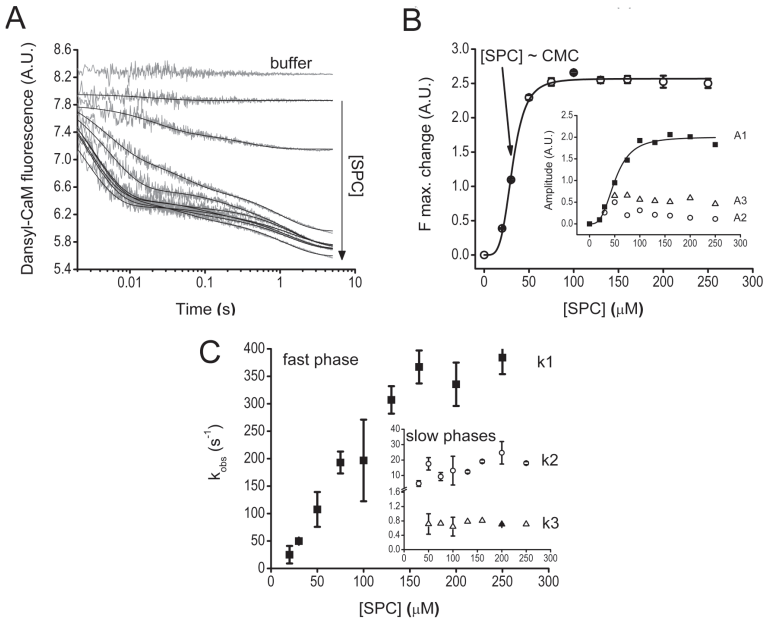

Figure 23 Kinetics of the interaction of SPC with the Ca^{2+}-saturated dansyl-CaM – melittin complex. (A) Time courses of melittin dissociation from dansyl-CaM after mixing an equilibrated sample of 0.4 μM dansyl-CaM and 0.8 μM melittin with 0-500 μM SPC (pre-mix concentrations). The first trace was best fitted with single, the second with double and further curves with triple exponentials represented by the smooth lines through the data. (B) Concentration dependence of the amplitudes (inset, A_1 (■), A_2 (○), A_3 (△)) and maximal fluorescence changes derived from the exponential fits to the stopped-flow traces shown in panel A. Maximal fluorescence change was calculated from the y_{max} value of the exponential fits. A Hill equation having n = 4 ± 0.4 and a half-maximal signal change at [SPC] = 32 ± 0.7 μM, close to the previously determined CMC for SPC, provided the best fit to the curve. Similar fit to the amplitude of the fast phase yielded n = 3 ± 0.5 and $A_{1max}/2$ = 51 ± 3 μM. At saturation, the three observed kinetic phases A_1, A_2 and A_3 take a 78%, 4%, 18% share of the total amplitude, respectively. (C) SPC concentration dependence of the observed rate constants of the fast (main panel, ■) and slow (inset, k_2 (○), k_3 (△)) phases. The fast phase data showed linear concentration dependence and reached saturation at about 150 μM SPC with $k_{1\ sat,\ SC}$ = 348 ± 30 s^{-1}. The two slower phases did not depend on SPC concentration in the measured range and varied in the range of $k_{2obs,\ SC}$ = 14 ± 6 s^{-1} and $k_{3obs,\ SC}$ = 0.9 ± 0.3 s^{-1}.

The large fluorescence decrease upon mixing indicated that SPC replaced the previously bound melittin on dansyl-CaM (Figure 23A). Time courses could be fitted with one (1st data point), two (2nd data point) or three exponentials. The slower kinetic phases have smaller amplitudes, which may explain why they go unseen when the total amplitude is relatively small (first data points). The first, concentration dependent, fast phase corresponds to SPC binding to dansyl-CaM and is characterized by a cooperative amplitude saturation curve (Figure 23B), which probably reflects micelle formation (parameters in Table 6). As previously observed, above the CMC the fluorescence change becomes saturated. The k_{obs} of the fast phase saturates at about 350 s^{-1} (Figure 23C, $k_{1sat, SC}$ in Table 6), close to the value of the rate constant estimated for CaM-melittin dissociation ($k_{-1, M}$ = 301 s^{-1}, Scheme 1). The first-order rate constant observed for the second phase ($k_{2obs, SC}$ = 14 ± 6 s^{-1}) is also almost equal to $k_{-2, M}$ (11 s^{-1}, Scheme 1) in the melittin binding mechanism. These observations imply that SPC binding to CaM is limited by the dissociation of melittin. The initially melittin-saturated dansyl-CaM − melittin complex (mostly populates the dCaM.ME** state in Scheme 1) must go through the kinetic steps characterized by $k_{-2,M}$ and $k_{-1,M}$ before SPC can associate with CaM. The apparent SPC-CaM association ($k_{+1,SC}$ = 2.4 ± 0.2 $\mu M^{-1}s^{-1}$) is not as fast as in the case of SPC binding to pure dansyl-CaM because melittin re-binding occurs and the observed rates are set as a function of the concentration ratios and kinetic parameters of the two ligands. A third kinetic phase with a slow observed rate constant of $k_{3obs, SC}$ = 0.9 ± 0.3 s^{-1} and an 18% relative amplitude appears at [SPC] > CMC possibly due to a conformational change in the dansyl-CaM − micelle complex.

We also carried out the reverse chasing experiment in which dansyl-CaM saturated with SPC was mixed with various concentrations of melittin (Figure 24). We again expected large fluorescence changes, fluorescence increase this time, as SPC exchanges to melittin on dansyl-CaM (CaM.SPC → CaM.ME**). Time courses followed double exponentials (Figure 24A) and the fluorescence change exhibited hyperbolic saturation with an apparent dissociation constant of 1 μM (Figure 24B, $K_{d1-2, MC}$ = 1.0 ± 0.3 μM, Table 6). The observed rate constants of both phases were dependent on melittin concentration in the measured concentration range (Figure 24C). The fast phase exhibited a saturating character and could be fitted with a hyperbole that saturates at $k_{1\ sat, MC}$ = 59 ± 13 s^{-1}. This rate constant likely originates from the one observed for the second process in melittin binding which is in the same range within error ($k_{+2, M} + k_{-2, M}$ = 49 ± 13 s^{-1}). At

infinite melittin concentration, the initial binding of melittin (characterized by $k_{+1,\ M}$ * [CaM]) will be fast and saturated, thus, the entire binding process will be limited by the second, slower kinetic step. The apparent half maximal saturation of the fast phase ($K_{1app,\ MC}$ = 5.4 ± 3.4 μM) is the result of an interplay between the three reversible processes (CaM + ME ⇌ CaM.ME* ⇌ CaM.ME**, CaM + SPC ⇌ CaM.SPC), and it appears to be close to the equilibrium constant calculated for the second CaM – melittin binding step.

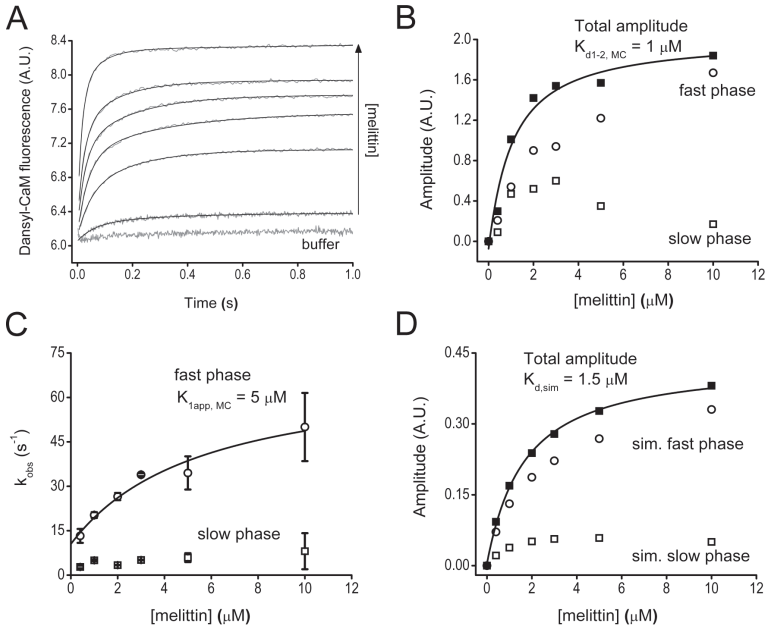

Figure 24 Dissociation of the Ca^{2+}-saturated dansyl-CaM − SPC complex by melittin. (A) Time courses of the chasing experiment. Equilibrated 0.4 μM dansyl-CaM and 100 μM SPC was mixed with 0-20 μM melittin (pre-mix concentrations). Smooth lines represent double exponential fits to the data. (B) Concentration dependence of the amplitudes (fast phase (○), slow phase (□) and total amplitude (■)) derived from exponential fits to the stopped-flow traces. The best quadratic fit to the total amplitude curve yielded an apparent $K_{d1-2,\ MC}$ of 1 ± 0.3 μM. (C) Concentration dependence of the observed rate constants of the fast (○) and slow (□) phases. The fast phase was best fitted with a quadratic equation having an y-intercept at 10 ± 4 s^{-1}, a rate constant of 59 ± 13 s^{-1} at saturation and an apparent K_d = 5.4 ± 3.4 μM. The slow phase exhibited a weak dependence on melittin concentration and the k_{obs} varied between 4-8 s^{-1}. (D) Analysis of simulated time courses. Kinetic parameters used for the simulation are shown in Table 6. Concentration dependence of the amplitudes of exponential fits to the simulated curves (fast phase (○), slow phase (□) and total amplitude (■)). The best quadratic fit to the total amplitude curve yielded an apparent K_d of 1.5 ± 0.12 μM.

The slow phase (4-8 s^{-1}) represents the smaller portion of the total amplitude. On the basis of our parallel binding model, it should originate from the dissociation of the CaM – micelle complex (consistently with the relatively small signal change observed upon the CaM – SPC interaction) and is expected to reach saturation ($k_{obs\ sat} = k_{-1,\ S}$). Since micelle binding to CaM was too fast to be measured, these observed rate constants are the only accessible parameters to indicate that $k_{-1,\ S}$ is relatively slow.

We formulated a relation between the thermodynamic parameters of CaM binding to either SPC or melittin and the apparent K_d-s of the chasing experiments (Equation 3; for details, see the Supplement of [96]).

$$K_{d,app} = \frac{K_C * L}{K_L} + K_C \qquad \text{Eq. 3}$$

Where C represents the chaser, L represents the prebound ligand, and K_L and K_C indicate the dissociation constants for the ligand and the chaser. Substituting the previously determined values for K_C (~ 60 nM, Figures 22C-D, $K_{d1\text{-}2,\ M}$ and $K_{d\ eq,\ M}$ in Table 6), $K_{d,app}$ (1 µM, Figure 24B and $K_{d1\text{-}2,\ MC}$ in Table 6) and L (50 µM) into Eq. 3, we calculate the experimentally inaccessible parameter, K_L to be 3 µM (in SPC monomer concentration). This corresponds to 3/n µM in SPC micelle concentration, where n is the number of monomers per micelle. From results presented in Chapter 4.2, we estimate the molecular ratio to be 100-200 monomers per micelle, which would imply that the K_d for the dansyl-CaM − micelle complex is 0.015-0.03 µM.

We performed kinetic simulations to test if our kinetic model is plausible taking an average size of 150 monomers/micelle into account. We used the herein defined kinetic parameters and relative fluorescence levels of 2 and 0.8 for the dansyl-CaM − melittin and dansyl-CaM − micelle complexes, respectively, compared to free dansyl-CaM. By simulating the experiment shown in Figure 24A, we obtained double exponential curves similar to the measured ones. The amplitude analysis of the simulated curves (Figure 24D) resulted in an apparent K_d of 1.5 ± 0.12 µM, close to the experimentally determined 1 µM. Simulated k_{obs} values were also in the range of the measured ones. As a summary of our results on the SPC-melittin competition experiments we suggest a model shown in Figure 35 in the Discussion section.

4.4. Putative functional consequences of the CaM-SPC interaction

4.4.1. SPC dissociates the complex between Ca^{2+}-saturated CaM and the CaM-binding domain of RyR1

To investigate the possible functional consequences of CaM inhibition by SPC, I examined the impact of SPC on interactions between CaM and CaM-binding domains of proteins involved in Ca^{2+} homeostasis, since the best described function of SPC as a putative second messenger is the liberation of Ca^{2+} from intracellular stores [50, 51]. As SPC has been suggested to be involved in activation of ryanodine receptors (RyRs) [40, 56], I started working with the CaM-binding domain (amino acids 3614-3643) of the skeletal muscle Ca^{2+} release channel (RyR1) [98]. By monitoring the fluorescence of both the dansyl-labeled protein and the Trp of the RyR1 peptide, I was able to examine their interaction from the aspect of both CaM and the Ca^{2+} channel. As both fluorescence signals undergo large changes upon complexation, they provide a convenient method to distinguish whether a third compound dissociates the complex or not.

The fluorescence intensity of dansyl-labeled Ca^{2+}-saturated CaM increases approximately 2-fold accompanied by an approximately 30 nm blue-shift upon binding to its target peptide on the RyR. After the addition of saturating amounts of SPC to the peptide − CaM complex, the spectrum resembles the SPC-bound form of dansyl-labeled CaM, implying that the peptide was replaced by SPC on CaM (Figure 25A). We have demonstrated that this complex-dissociating effect of SPC is selective compared to structurally and functionally related lysophospholipids S1P, LPC and LPA, whereas L-*threo*-SPC is also potent (Figure 25C). SPC's action can be described with an EC_{50} value of 19.4 ± 1.4 μM and a cooperativity coefficient of 2.6 ± 0.4 (Figure 25E).

In the complementary experiment, when monitoring the Trp fluorescence of the RyR peptide, the acquired results correspond exactly to the ones obtained using dansyl-CaM fluorescence as a reporter. Binding of Ca^{2+}-saturated CaM brought forth an approximately 2.5-fold increase in Trp fluorescence intensity and an approximately 20 nm blueshift. The addition of SPC resulted in a spectrum similar to the spectrum of the free RyR peptide (Figure 25B). This effect was again specific (Figure 25D), and gave an EC_{50} value of 19.3 ± 3.4 μM and a cooperativity coefficient of 2.2 ± 0.8 (Figure 25F), very similar to the ones obtained from dansyl-CaM fluorescence.

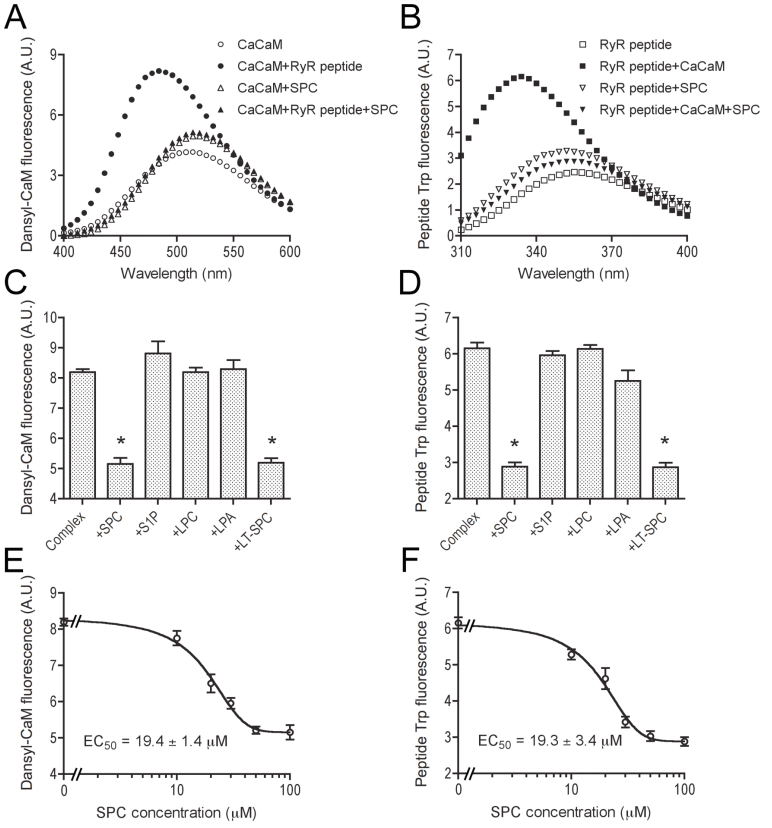

Figure 25 Dissociation of the complex between Ca^{2+}CaM and the CaM-binding domain of RyR1 by SPC, revealed by the fluorescence of dansyl-labeled CaM and the Trp of the RyR peptide. (A) Spectra of 0.2 μM Ca^{2+}-saturated dansyl-CaM (○), 0.2 μM Ca^{2+}-saturated dansyl-CaM with 0.5 μM RyR peptide (●), 0.2 μM Ca^{2+}-saturated dansyl-CaM in the presence of 100 μM SPC (△) and 0.2 μM Ca^{2+}-saturated dansyl-CaM in the presence of 0.5 μM RyR peptide and 100 μM SPC (▲). (B) Spectra of 1 μM RyR peptide (□), 1 μM RyR peptide with 1 μM Ca^{2+}CaM (■), 1 μM RyR peptide in the presence of 100 μM SPC (▽) and 1 μM RyR peptide in the presence of 1 μM Ca^{2+}CaM and 100 μM SPC (▼). Spectra in panels A and B are averaged from three independent measurements. (C) Effect of related lysophospholipids on the interaction between Ca^{2+}CaM and the CaM-binding domain of RyR1. Bars depict the fluorescence intensity of 0.2 μM Ca^{2+}-saturated dansyl-CaM in the presence of 0.5 μM RyR peptide and 100 μM lipids. (D) The same as in panel C, but measuring the Trp fluorescence of the RyR peptide. Bars depict the fluorescence intensity of 1 μM RyR peptide in the presence of 1 μM Ca^{2+}CaM and 100 μM lipids. Mean and standard error values in panels C and D were calculated from three independent experiments. The addition of SPC and LT-SPC brought forth a significant decrease in intensity ($p<0.05$, see asterisks), based on Student's t-test. (E) Concentration dependence of the complex dissociating ability of SPC. Ca^{2+}-saturated dansyl-CaM and RyR peptide concentrations were 0.2

μM and 0.5 μM, respectively. (F) The same as in panel E, but measuring the Trp fluorescence of the RyR peptide. RyR peptide and Ca^{2+}CaM concentrations were both 1 μM. Data points in panels E and F represent the mean and standard error values of three independent determinations. Fitting a sigmoidal dose-response function yielded an EC_{50} value of 19.4 ± 1.4 μM with a cooperativity coefficient of 2.6 ± 0.4 in case of dansyl-CaM, and an EC_{50} value of 19.3 ± 3.4 μM with a cooperativity coefficient of 2.2 ± 0.8 in case of Trp fluorescence of the peptide.

4.4.2. SPC dissociates the complex between apoCaM and the CaM-binding domain of RyR1

Calcium binding to CaM leads to an N-terminal shift in its binding site on the RyR, hence this region of the channel possesses the unique feature of containing a distinct binding site for both apo and Ca^{2+}-saturated CaM [98]. As mentioned in the Introduction, traditional CaM inhibitors only interact with Ca^{2+}-saturated CaM, while SPC binds to both forms of the protein. Thus, I investigated the effect of SPC on the apoCaM – RyR peptide interaction. Though the complex formation between apoCaM and the RyR peptide yielded significantly smaller changes in fluorescence than in the case of Ca^{2+}-saturated CaM, the complex dissociating ability of SPC could still be demonstrated. The spectra of dansyl-labeled apoCaM revealed that if saturating amounts of SPC are present, the protein is predominantly bound to the sphingolipid (Figure 26).

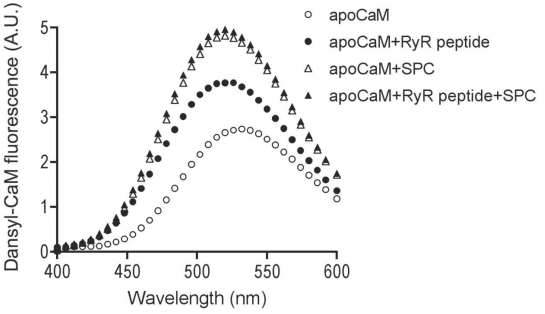

Figure 26 Dissociation of the complex between apoCaM and the CaM-binding domain of RyR1 by SPC. Spectra of 0.2 μM dansyl-labeled apoCaM (○), 0.2 μM dansyl-labeled apoCaM with 0.5 μM RyR peptide (●), 0.2 μM dansyl-labeled apoCaM in the presence of 100 μM SPC (△) and 0.2 μM dansyl-labeled apoCaM in the presence of 0.5 μM RyR peptide and 100 μM SPC (▲). Spectra are averaged from three independent measurements.

4.4.3. SPC dissociates the complex between Ca^{2+}-saturated CaM and the CaM-binding domain of several proteins involved in Ca^{2+} homeostasis

The effect of SPC on the interaction of CaM with further CaM-binding proteins involved in Ca^{2+} homeostasis was also explored. Besides the RyR1 peptide, two peptides corresponding to residues 1564-1585 and 106-128 of the type 1 IP_3 receptor (IP_3R1) and a peptide corresponding to residues 2-21 of the human erythrocyte plasma membrane Ca^{2+}-ATPase (PMCA) was examined. For details on these peptides refer to Table 4. I found that SPC disrupted the complex between each of these peptides and Ca^{2+}-saturated CaM, as the fluorescence of the dansyl-labeled protein in the presence of both the peptide and SPC resembled the SPC-bound form (Figure 27). Other lysophospholipids such as S1P, LPC and LPA did not significantly affect the fluorescence of the CaM-target complex.

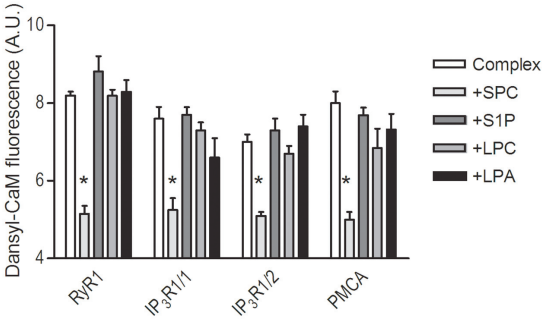

Figure 27 SPC-induced dissociation of complexes between Ca^{2+}CaM and peptides derived from proteins involved in Ca^{2+} homeostasis. Bars depict the fluorescence intensity of 0.2 μM Ca^{2+}-saturated dansyl-CaM with peptides from RyR1, IP_3R1 and PMCA (see Table 4 for details) at a concentration of 0.5 μM, in the absence (white bars) and in the presence (grey bars) of 100 μM SPC, S1P, LPC and LPA, respectively. Mean and standard error values were calculated from three independent experiments, and the asterisks represent significant decrease ($p<0.05$), based on Student's t-test.

4.4.4. SPC exerts its effects in mixed micelles, more relevant to *in vivo* conditions

To assess whether SPC can displace CaM from its targets under conditions more resembling the *in vivo* situation, experiments with mixed micelles were carried out. In these experiments, varying amounts of SPC were incorporated into micelles consisting of lipids that did not have any significant effect on the CaM – target peptide system, such as S1P, LPC and LPA. Figure 28A clearly demonstrates that SPC dissociates the CaM –

peptide complex in the presence of other lipids just as potently as pure SPC. To comprehend the effect of "dilution" caused by other lipids, I measured the dose-response of complex dissociation in case of SPC/LPC mixed micelles keeping the SPC content at a constant 20% (Figure 28B). Comparing these results with the dose-response for pure SPC revealed that the fluorescence of dansyl-CaM changes less steeply in the case of mixed micelles. A possible explanation for this phenomenon might be that at lower concentrations additional lipids aid the effect of SPC's action by forming micelles at lower SPC concentrations. While at higher concentrations, the presence of other lipids seems to have a minor negative diluting effect on SPC's ability to interfere with CaM function. These observations point to the potential of SPC to displace CaM under *in vivo* conditions near membrane surfaces enriched in the signaling sphingolipid.

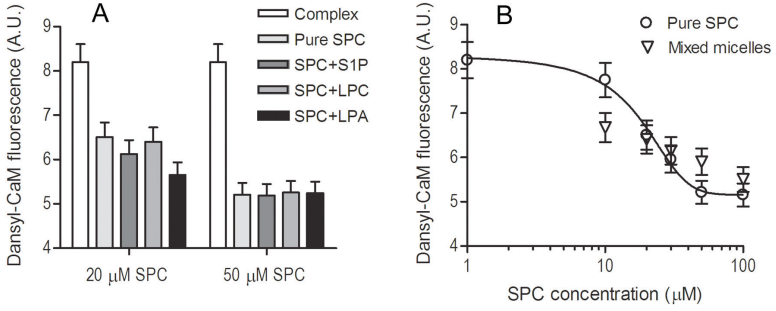

Figure 28 Effect of SPC on the Ca^{2+}-saturated CaM – RyR1 peptide complex in mixed micelles. (A) Bars depict the fluorescence intensity of 0.2 μM Ca^{2+}-saturated dansyl-CaM with 0.5 μM RyR1 peptide in the absence (white bars) and in the presence of pure SPC (lightest grey bar) or mixed micelles of varying amounts of SPC incorporated into either S1P, LPC or LPA micelles, respectively (darker grey bars). Total lipid concentration was held constant at 100 μM, and mixed micelles contained either 20 or 50 μM SPC. Error bars depict an average experimental error of 5 %. (B) Concentration dependence of the complex dissociating ability of 20 % SPC containing LPC micelles (▽) compared to pure SPC (○) taken from Figure 25E. Ca^{2+}-saturated dansyl-CaM and RyR peptide concentrations were 0.2 μM and 0.5 μM, respectively. In contrast to panel A, the total lipid concentration varied, and the SPC content was held constant at 20 %. Data points represent the mean and standard error values of three independent measurements.

4.5. SPC regulates RyRs through both CaM-dependent and -independent mechanisms

4.5.1. Monomeric SPC induces long channel closings of purified RyR1 independently of CaM

To explore the effect of SPC on the intact RyR, I visited the laboratory of Dr. Gerhard Meissner at the University of North Carolina, Chapel Hill in the framework of an EMBO Short-term Fellowship. The following experiments were conducted in his laboratory, RyR preparations were provided by Daniel Pasek, single channel recordings were carried out by Le Xu, and all other work was done by me, including preparation of the manuscript [121].

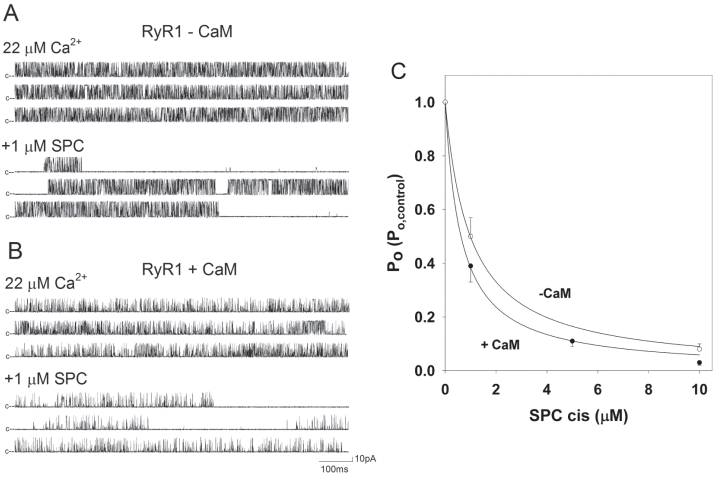

Figure 29 Effects of SPC on single channel activities of purified RyR1 in absence and presence of CaM. (A) Single channel currents were recorded at +35 mV before (top 3 traces) and after the addition of 1 μM SPC cis (bottom 3 traces) in symmetrical 0.25 M KCl in presence of 22 μM free Ca^{2+} cis and absence of CaM. The closed states are indicated by c--. (B) As in (A) in presence of 100 nM CaM. Proteoliposomes were incubated with 1 μM CaM for 30 min before the addition to the cis chamber of the lipid bilayer system, and channels were recorded in presence of 100 nM CaM in the cis chamber. (C) Dependence of purified RyR1 channel activity on SPC concentration in absence and presence of CaM. Relative open channel probability ($P_o/P_{o,control}$) was obtained from single channel recordings similar to those shown in panels A and B. Solid lines were obtained according to the equation $P_o = P_{o,control}\ (1 + [SPC]/K_i)^{-1}$, where K_i is the inhibition constant and P_o and $P_{o,control}$ are single channel open probabilities in presence and absence of SPC. Inhibition constants in the absence (n=6) and presence (n=10) of 1μM CaM were 1.3 ± 0.3 μM and 0.7 ± 0.2 μM, respectively.

The effects of SPC on the skeletal muscle ryanodine receptor (RyR1) both in the presence and absence of CaM were studied with the method of single channel recordings in planar lipid bilayers. Proteoliposomes containing purified RyR1 were fused with the lipid bilayer and the resulting channel activities were recorded. Figure 29A shows a representative single channel recording in the absence (upper panel) and after the addition of 1 μM SPC (lower panel) to the cis chamber with 22 μM free Ca^{2+} in the cis chamber. Addition of SPC decreased single channel open probability (P_o) from 0.51 to 0.16. The lipid induced long channel closings without noticeably altering the duration of open events. In Figure 29B, the effects of the lipid on RyR1 were measured in the presence of 100 nM CaM in the cis chamber. To assure CaM binding to RyR1, proteoliposomes were preincubated with 1 μM CaM for 30 min. Addition of 1 μM SPC reduced P_o from 0.15 to 0.05 by inducing long channel closings, similarly to those observed in the absence of CaM. The open probability of the channel was decreased by SPC with an IC_{50} of 1.3 ± 0.3 μM and 0.7 ± 0.2 μM in the absence and presence of 1 μM CaM, respectively (Figure 29C).

Table 7 Effect of SPC on purified RyR1 channel parameters in the absence and presence of CaM

Channel parameter	Additions to cis bilayer chamber			
	22 μM Ca^{2+}		22 μM Ca^{2+} and 1 μM CaM	
	–1 μM SPC	+1 μM SPC	–1 μM SPC	+1 μM SPC
No. of events	19,874 ± 7337	9767 ± 1884	20,544 ± 4074	10,392 ±2633*
P_o	0.52 ± 0.16	0.24 ± 0.10	0.39 ± 0.12	0.18 ± 0.09*
A_{o1}	0.87 ± 0.12	0.81 ± 0.18	0.91 ± 0.08	0.94 ± 0.05
A_{o2}	0.13 ± 0.12	0.19 ± 0.18	0.09 ± 0.08	0.06 ± 0.05
τ_{o1} (ms)	0.56 ± 0.53	0.24 ± 0.19	0.26 ± 0.22	0.16 ± 0.12
τ_{o2} (ms)	2.93 ± 2.22	5.09 ± 3.32	1.48 ± 0.85	3.12 ± 2.10
A_{c1}	0.98 ± 0.01	0.994 ± 0.003	0.85 ± 0.09	0.96 ±0.03
A_{c2}	0.02 ± 0.01	0.006 ± 0.003	0.15 ± 0.09	0.04 ± 0.03
τ_{c1} (ms)	0.05 ± 0.02	1.07 ± 0.68	0.77 ± 0.47	2.81 ± 1.66
τ_{c2} (ms)	3.21 ± 2.09	452 ± 140*	16.53 ± 6.21	619 ± 242*

Channel parameters were obtained from 2 min continuous recordings as described in Experimental Procedures. P_o refers to open channel probability. Dwell-time data were fitted by the maximum likelihood method to the probability density function: $f(t) = \sum A_i\ (1/\tau_i)\ \exp\ (-t/\tau_i)$, where A_i and τ_i are the relative areas of the distributions and time constants of the *i*th state, respectively [123]. Both the open and closed time histograms could be fitted by the sum of two exponentials.
*Values significantly different from the –SPC control ($P < 0.05$; n = 4 and 6 in case of –CaM and +CaM samples, respectively).

Analysis of single channel recordings showed that, both in the absence and presence of CaM, the open and closed times of Ca^{2+}-activated channels could be fitted by the sum of two exponentials (data not shown), in agreement with a previous report [122]. SPC significantly increased the lifetimes of the second closed state (an increase from 3.21 ± 2.09 ms to 452 ± 140 ms and from 16.53 ± 6.21 ms to 619 ± 242 ms in the absence and presence of 1 μM CaM, respectively, Table 7).

4.5.2. Micellar SPC affects [^{3}H]ryanodine binding in a CaM-dependent and -independent manner

According to our previous results, in order to see an effect on the Ca^{2+} sensor, SPC would have to be applied at concentrations near its CMC. We could not study the effects of micellar SPC in single channel measurements, because the lipid bilayer broke at SPC concentrations above 10 μM. To explore the effect of SPC on RyR activity at concentrations expected to disrupt the CaM-RyR interaction, [^{3}H]ryanodine binding assays were conducted. This ligand binding assay is a good indicator of channel activity, since the plant alkaloid ryanodine has been shown to bind with higher affinity to the open than the closed channel state [124].

Measurements with skeletal SR vesicles at 50 μM free Ca^{2+}, under both reducing (5 mM GSH) and oxidizing (5 mM GSSG) conditions were carried out. Ca^{2+} concentration was optimized to saturate CaM, but not to inhibit RyR activity directly [59]. An oxidizing environment is expected to yield higher ryanodine but lower CaM binding, while CaM is expected to be inhibitory under both conditions [59]. In the absence of CaM, SPC inhibited [^{3}H]ryanodine binding with an apparent IC_{50} of 26.1 ± 0.8 μM (Figure 30A) and 25.5 ± 4.0 μM (Figure 30C) under reducing and oxidizing conditions, respectively. These values are approximately 20-fold higher than the ones obtained in the single channel measurements and may have been caused by the different SPC to membrane lipid ratios in the two techniques. The effect of SPC was selective compared to structurally similar lysophospholipid mediators such as LPC and LPA, but a minor inhibitory effect could also be observed in case of S1P (Figures 30B and D).

In the presence of CaM, on the other hand, SPC did not significantly alter [^{3}H]ryanodine binding. A possible explanation for this finding is that SPC exerts two opposing effects on the Ca^{2+}CaM-bound RyR. Displacement of inhibitory Ca^{2+}CaM from RyR1 has an activating effect, whereas direct interaction with RyR1 is inhibitory, negating

the effects of SPC. [^{35}S]CaM binding studies (see below) and the fact that S1P (which does not interact with CaM) further decreased [^{3}H]ryanodine binding in the presence of CaM (Figure 30D), favour this explanation.

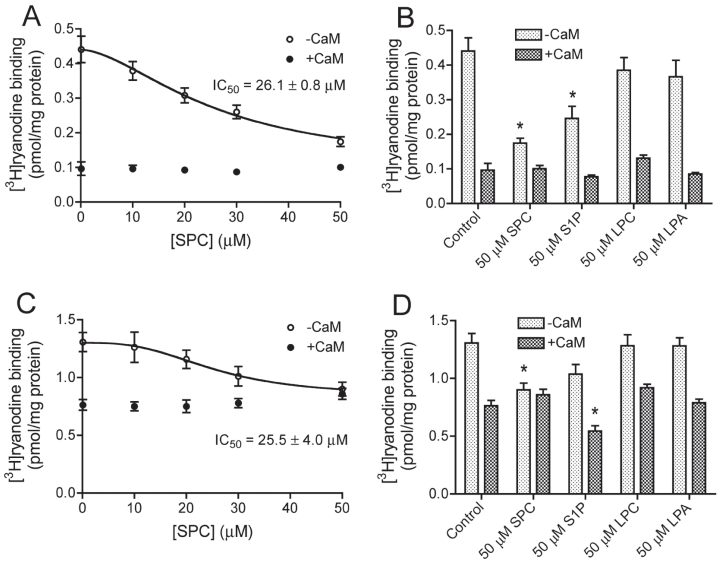

Figure 30 Effect of SPC on [^{3}H]ryanodine binding to skeletal SR vesicles. Free Ca^{2+} concentration was set to 50 µM and either 5 mM GSH (A,B) or 5 mM GSSG (C,D) was added. Open circles and light bars depict [^{3}H]ryanodine binding in the absence of CaM, while closed circles and dark bars depict [^{3}H]ryanodine binding in the presence of 0.1 µM (A,B) and 1 µM (C,D) CaM. In the absence of CaM, the dose-response for SPC yielded an apparent IC_{50} of 26.1 ± 0.8 µM and 25.5 ± 4.0 µM and a Hill-slope of -1.7 ± 0.04 and -2.9 ± 0.2 under reducing (A) and oxidizing (C) conditions, respectively. Data points depict mean ± S.E. (n=3), a sigmoidal dose-response curve with variable slope was fitted to the data, and asterisks denote significant differences at $p<0.05$ compared to control, based on Student's t-tests.

4.5.3. SPC displaces CaM from skeletal muscle SR vesicles

[^{35}S]CaM binding assays revealed that SPC displaces Ca^{2+}-saturated CaM from skeletal SR vesicles enriched in RyR1 with an IC_{50} of 14.2 ± 0.8 µM (Figure 31A). This value compares well with the results of peptide binding assays (IC_{50} = 19.4 ± 1.4 µM, Figure 25). S1P and LPA were ineffective, while LPC also decreased [^{35}S]CaM binding to SR

vesicles (Figure 31B). This effect is probably an artefact as LPC also decreased nonspecific binding, and it was without action in peptide binding experiments (Figure 25).

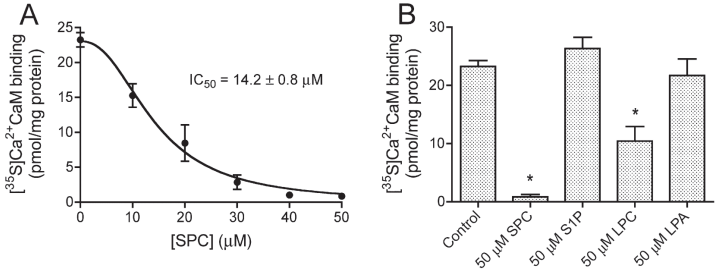

Figure 31 Displacement of [^{35}S]CaM from RyR1 by SPC. (A) SPC dissociates Ca^{2+}-saturated [^{35}S]CaM from skeletal SR vesicles rich in RyR1 with an IC_{50} of 14.2 ± 0.8 µM and a Hill-slope of 2.3 ± 0.7. Data points depict mean ± S.E. (n=3), a sigmoidal dose-response curve with variable slope was fitted to the data. (B) Among the tested lysophospholipids, SPC and LPC significantly decrease [^{35}S]CaM binding to skeletal SR vesicles. Data points depict mean ± S.E. (n=3), asterisks denote significant differences at $p<0.05$ compared to control, based on Student's t-tests. Note that the effect of LPC is probably an artefact as LPC also decreased nonspecific binding, and it was without action in peptide binding assays (Figure 25).

4.5.4. SPC, LPC and LPA release Ca^{2+} from bovine brain microsomes, while ryanodine and caffeine do not

Our data reveal that SPC directly inhibits RyR1. Thus, the question arose, could Ca^{2+} mobilization by SPC from brain microsomes be attributed to RyR activation as suggested by Dettbarn *et al.* [56]? Hence, I studied RyR activity similarly as these authors had, isolating microsomes from bovine brain cerebrum by differential centrifugation, loading these with Ca^{2+} in the presence of an ATP-regenerating system, and measuring Ca^{2+} release using a fluorescent Ca^{2+} indicator.

I have found that while SPC, LPC and LPA at a concentration of 100 µM each mobilized Ca^{2+}, classical channel activators such as 1 µM ryanodine and 5 mM caffeine only showed minor effects (Figure 32). S1P could not be tested because of solubility difficulties, since for microsomes to remain intact, only gentle suspension could be applied, which hindered solubilization of this hydrophobic sphingolipid. Since ryanodine is known to act as an activator at lower concentrations and as an inhibitor at higher concentrations, I applied ryanodine in the concentration range of 100 nM to 100 µM, to rule out the possibility that I am trying to trigger Ca^{2+} release with an inefficient amount of

ryanodine, but significant Ca^{2+} efflux could not be observed at any concentration. The possibility that the membranes lacked functioning proteins can be excluded, since the loading of microsomes was an ATP-dependent process. These results suggest that the SPC-evoked Ca^{2+} response of cerebral microsomes could not be solely attributed to RyR activation, the majority of the effect was caused by some other mechanism.

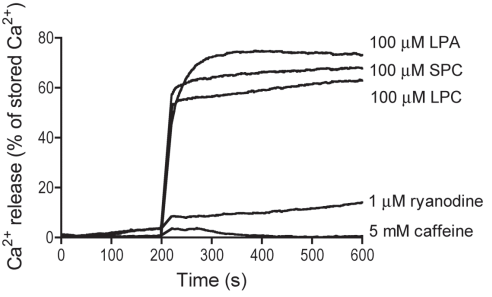

Figure 32 Ca^{2+} release measurements on bovine brain microsomes using a Fluo-3 Ca^{2+} indicator. 0.5 mg/ml microsomes were loaded with Ca^{2+}, and release was triggered by the addition of either 1 μM ryanodine, 5 mM caffeine, 100 μM SPC, LPC or LPA. The amount of liberated Ca^{2+} was calculated as the percentage of Ca^{2+} released upon the addition of 2 μM Ca^{2+} ionophore A23187. Each trace is a representative of at least three independent measurements.

4.5.5. SPC does not break the permeability barrier of membrane preparations

To rule out the possibility that SPC's action on SR vesicle and microsomal preparations is an artefact due to membrane permeabilization, I examined this issue using two independent methods. First, I explored the effect of SPC on proteinless liposomes using a sedimentation assay. Since these vesicles do not contain ion channels, the release of the radioactive Ca^{2+} entrapped during their formation, could only be the consequence of disrupting the integrity of the lipid bilayer. I found that neither 100 μM SPC, LPC or LPA liberated significant amounts of Ca^{2+} from liposomes, while 2 μM Ca^{2+} ionophore A23187 and 0.2% saponin detergent released the majority of stored Ca^{2+} (Figure 33A). In the other experimental setup, SR vesicles were loaded with [^{14}C]glucose, and release was determined after dilution in an unlabeled medium. These measurements also reassured me that the lysophospholipids do not disrupt the permeability barrier at the concentrations used in our measurements (Figure 33B).

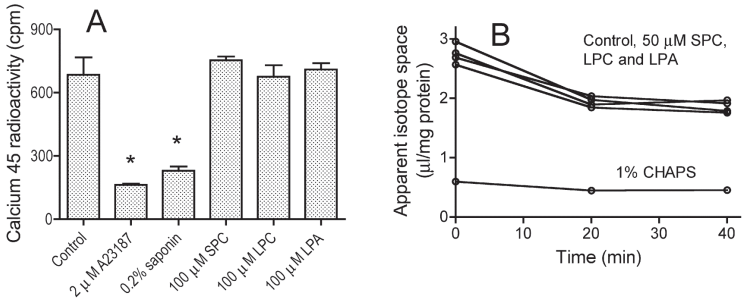

Figure 33 Membrane permeability assays. (A) Measurement of $^{45}Ca^{2+}$ release from proteinless liposomes. Liposomes were formed from 1 mM brain total lipid extract (Avanti Polar Lipids, 131101) in buffer containing 1 mM $CaCl_2$ spiked with 5 μCi/ml Calcium 45 radionuclide. Liposomes were washed twice, and after the addition of either 2 μM Ca^{2+} ionophore A23187, 0.2% saponin, 100 μM SPC, LPC or LPA, release of Ca^{2+} was determined by measuring radioactivity in both the pellets and the supernatants. Remaining radioactivity in pellets is shown, data points depict mean ± S.E. (n=3), asterisks denote significant differences at $p<0.05$ compared to control, based on Student's t-tests. (B) Measurement of [^{14}C]glucose efflux from skeletal SR vesicles. Vesicles were loaded with [^{14}C]glucose and retained radioactivity was measured after dilution into unlabeled release medium.

5. DISCUSSION

5.1. Identification of an interaction with potentially important consequences in Ca^{2+} and lipid signaling

Sphingosylphosphorylcholine (SPC) and sphingosine-1-phosphate (S1P) have emerged in the past 20 years as important mediators of cellular signaling. Perhaps the most exciting feature of their biology is that they can act as first and second messengers as well. Although their action on plasma membrane G protein-coupled receptors is extensively studied and quite well elaborated, not much is known about their intracellular site and mechanism of action. Initially, my supervisor, Károly Liliom postulated that these sphingolipids might interact with calmodulin (CaM). Indeed, several published data point to the reasonability of this idea: 1) CaM binds to its target proteins and to its aromatic inhibitors through hydrophobic interactions [125], 2) sphingosine has been shown to be an inhibitor of several CaM-dependent enzymes [126-128], 3) sphingosine kinase binds to and is regulated by CaM [129, 130] and 4) S1P and SPC can mobilize Ca^{2+} from internal stores [50, 51].

In the beginning, my goal was to screen S1P, SPC and structurally similar glycerolipids lysophosphatidic acid (LPA) and lysophosphatidylcholine (LPC) for a specific interaction with CaM. I carried out classical biochemical binding assays using purified proteins and lipids, and *in vitro* enzymatic assays to assess the functional consequences of the interaction. This approach was rather new in sphingolipid signaling, since most publications in the field present data obtained from live cell experiments, the results of which are often hard to reconcile to interactions of individual partners. Presumably this is the reason why the intracellular target sites of S1P and SPC are still unidentified, and why the field lags behind GPCR research, which is relatively easily explored by cell biological methods. In my opinion, to identify the intracellular target proteins through which these lipids exert their actions as second messengers, and to characterize their interaction without the disturbing effects of other cellular components, an approach using purified proteins is more efficient.

My first set of experiments revealed several important aspects of the CaM-SPC interaction. Intrinsic Tyr (Figure 12) and dansyl-labeled protein (Figure 13) fluorescence demonstrated that SPC binds selectively to CaM compared to S1P, LPC and LPA. Importantly, selectivity has also been demonstrated compared to membrane-composing

lipids such as sphingomyelin, phosphatidylcholine, phosphatidylethanolamine, phosphatidylserine and phosphatidylinositol (data not shown). Surprisingly, SPC bound both in the presence and absence of Ca^{2+}, unlike classical aromatic CaM inhibitors such as trifluoperazine, calmidazolium and W-7, which only bind to Ca^{2+}-saturated CaM [82, 131]. This finding has several interesting structural and functional implications, which I focused on in my later work.

Titration of CaM with SPC resulted in a saturation curve showing strong cooperativity and an apparent K_D of 46.9 ± 0.8 μM and 21.7 ± 1.3 μM, in case if intrinsic Tyr and dansyl fluorescence, respectively. These values lie close to the critical micelle concentration (CMC) of the lipid (33 ± 2 μM, Figure 14). These data strongly suggest that micelles are necessary for binding, thus, the high SPC concentration is only required for the development of the appropriate *in vitro* conditions for the interaction, i.e. that the sphingolipid should be clustered. Once SPC clusters exist, binding occurs, resulting in a strong interaction between SPC and CaM, characterized by a submicromolar dissociation constant. This mode of binding also raises interesting issues regarding the mechanism of binding, addressed later on (Chapter 5.2.).

I demonstrated that the binding of SPC to CaM has functional effects as well, since SPC inhibited the Ca^{2+}-CaM-dependent activity of two target enzymes, calcineurin (Figure 15) and phosphodiesterase. Dose response for calcineurin activation by CaM in the absence and presence of SPC provided the first clue for competitive inhibition and also indicated a strong binding of SPC to CaM. The fact that the synthetic stereoisomer L-*threo*-SPC was also active in both the binding and the functional assays implies that CaM might indeed be the mediator of SPC's intracellular actions, since previous studies have shown that the effects of extracellularly applied SPC are stereospecific, while those of intracellularly applied are not [49, 132].

SPC's selective inhibitory action on CaM unambiguously has important implications in cellular signaling. First, it proposes that CaM might be an intracellular receptor for SPC, making CaM, the hub of Ca^{2+} signaling, the first putative intracellular target of the sphingolipid. Second, it raises the possibility for a novel endogenous regulation of CaM, making SPC the only known small molecule of mammalian cells capable of modifying CaM's activity besides Ca^{2+} ions.

5.2. Development of a stoichiometry-dependent lipid-protein binding model

My first set of experiments clearly indicated that the CaM-SPC interaction is worth further, more precise analysis. To unravel the structural and mechanistic details of the binding process, we (Veronika Harmat, József Kardos, Módos Károly, Tóth Judit and myself) utilized several independent biochemical and biophysical methods that allow evaluation of distinct features of the lipid-protein interaction. Based on our results we propose a complex and consistent model of CaM binding to SPC both in the presence and absence of Ca^{2+}.

As Ca^{2+}CaM is the functionally more important and better-characterized species, I present a detailed model on the Ca^{2+}CaM – SPC interaction (Figure 34). Both ITC (Figure 18) and stopped-flow (Figure 21) measurements revealed a strong binding of Ca^{2+}CaM to SPC (K_D of 60 nM and 20 nM, respectively) with a stoichiometry suggesting that the protein binds to micelles (values of 100-200 and 114 SPC/Ca^{2+}CaM, respectively). DLS measurements (Figure 19) verified this concept as the size of this species was determined to be significantly larger than SPC micelles or CaM alone. The driving force of this interaction is probably an electrostatic attraction between the positively charged choline groups of SPC and the negatively charged residues of CaM. This notion is aided by the fact that SPC micelles are supposedly perceived as positively charged spheres with their hydrophobic carbon chains buried inside, and also that this phase was shown to be entirely enthalpically driven in ITC experiments (Table 5).

ITC (Figure 18) and stopped-flow (Figure 21) measurements also demonstrated that a second process takes place during binding of Ca^{2+}CaM to SPC micelles, which is observable when micelles become limiting. This second process results in a complex with an estimated stoichiometry of 3-7 SPC monomers/protein. As our crystal structure of the Ca^{2+}CaM/SPC complex (Figure 16) revealed that Ca^{2+}CaM can adopt a collapsed conformation wrapped around a few SPC molecules (4 in our structure), we hypothesized that the species resulting from the second process is identical to the one we see in the crystal structure. This concept was supported by DLS experiments (Figure 19) since the size of this species was significantly smaller than micelles or the protein alone. Furthermore, fluorescence measurements with ANS (Figure 20) clearly demonstrated that micelles are disrupted during the second process. This species strikingly resembles the collapsed conformation of CaM, which the protein adopts upon binding to target peptides or synthetic inhibitors (Figure 17). Intriguingly, the peptide binding site of CaM is now

occupied by several lipid molecules. Since the exact positions of the SPC headgroups were ambiguous to some extent in the crystal structure, hydrophobic interactions between the aliphatic chain of the lipid and the hydrophobic residues of the protein are more likely to contribute to the stabilization of this complex.

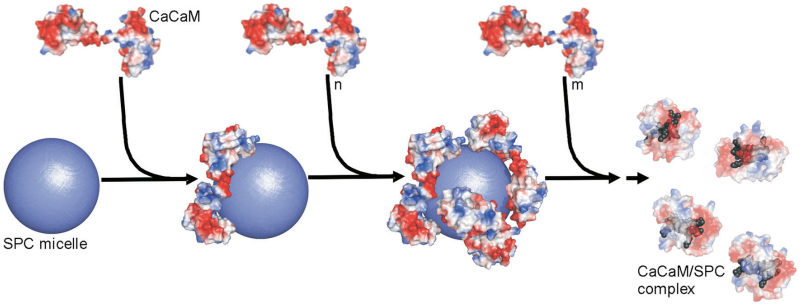

Figure 34 Stoichiometry-dependent binding model for the Ca^{2+}CaM – SPC interaction. The SPC micelle is represented as a sphere with a radius of 30 Å. Molecular surfaces are colored according to surface charge distribution (red: negative, blue: positive). First process (step 1 and 2): Ca^{2+}CaM molecules bind to the positively charged micelle. Electrostatic interaction with the acidic CaM regions is important in this phase. Second process (step 3): Saturation of the micelle surface with protein molecules will eventually result in the disintegration of the micelle and Ca^{2+}CaM adopting a collapsed conformation (transparent view) embracing several SPC monomers (grey). In this phase hydrophobic interactions play an important role in complex formation. The exact mechanism by which the protein disintegrates the micelle is unknown, as depicted by the dashed arrow. Crystal structures of Ca^{2+}CaM (PDB structure 1UP5) and Ca^{2+}CaM/SPC (PDB structure 3IF7) were used for modeling the complexes. Note that while the Ca^{2+}CaM – SPC micelle complex is only a model, the structure of the resulting Ca^{2+}CaM/SPC complex has been determined by X-ray crystallography. The figure was prepared using Pymol (DeLano Sci.).

We envision that the surface of SPC micelles are coated by CaM, until there is not enough free space for the negatively charged protein to bind to the positive surface provided by the choline headgroups of SPC without sterically hindering each other (Figure 34). As micelles are dynamic structures, we propose that they fluctuate during the competition of CaM molecules for their positive surface, which leads to the appearance of the collapsed protein conformation engulfing several lipid monomers. CaM molecules embracing several SPC monomers continuously leave the micelle-protein complex, thus gradually resulting in disintegration of the micelle. It is important to emphasize that this scenario only pictures one possible way the two species (CaM bound to micelles and the collapsed conformation) might arise, other possibilities also exist. What we have demonstrated unambiguously is the stoichiometry-dependent appearence of the two

species, both of which are inhibitory. The lipid shields the target peptide binding sites in both CaM conformations resulting in an inhibitory effect in enzyme activity (Figure 15) and peptide-binding assays (Figure 25).

The binding of apoCaM resembles that of Ca^{2+}CaM, as it can be described by similar two processes, but with a difference in the complex arising in the second phase. The apoCaM-SPC complex can be characterized by a stoichiometry of approximately 40 SPC monomers / protein and is larger than the one appearing in the presence of Ca^{2+}. Presumably, this phenomenon can be explained by the fact that apoCaM is unable to adopt a collapsed conformation with a hydrophobic binding channel surrounded by acidic residues as Ca^{2+}CaM can. As mentioned earlier, the fact that SPC can bind to apoCaM is a unique feature among CaM antagonists. This special behavior might be explained by the fact that the binding of the protein to the micelle is almost entirely driven by electrostatic forces, as the hydrophobic chains of the lipid are buried within the micelle. Hence, the open hydrophobic patches of the protein are not required in the initial stage of binding. In contrast, traditional aromatic inhibitors bind as monomers, offering mostly the possibility of hydrophobic interactions with CaM.

It is important to note that the precise affinity and stoichiometry values determined here characterize the protein-micelle system and should not be directly applied to cellular conditions. What our model reveals about the *in vivo* lipid-protein interaction is the following: 1) CaM interacts with SPC clusters at high (nanomolar) affinity; 2) once the SPC-CaM complex forms, it can adopt different conformations depending on several factors, most likely on the curvature and size of the lipid cluster and the local abundance of CaM. For a more particular consideration of the physiological relevance and the *in vivo* plausibility of the interaction see Chapter 5.6.

5.3. Kinetic description of CaM inhibition by SPC

After we understood the details of how SPC binds to CaM, I thought it highly important to reveal how exactly this affects target recognition by CaM. To decipher the mechanism of this novel regulation of CaM by SPC, we (Judit Tóth and myself) turned to the simplest model system for CaM-target interactions, and studied the impact of SPC on the interaction between CaM and its target peptides using fluorescence methods.

Having recognized that relevant kinetics data are missing on the mechanism of CaM binding to its target peptides, we first aimed to characterize the CaM-melittin

interaction at saturating Ca^{2+} concentrations (Figure 22). Details of the model we established are shown in Scheme 1 and in Figure 35, and its main features are 1) rapid, reversible binding of the peptide to CaM accompanied by a fluorescence increase of the dansyl label, 2) slower, reversible conformational change with further apparent fluorescence increase. The overall process is shifted to the right implying that the predominant conformation is the compact dCaM.ME** species. Our two-step sequential binding model agrees with literature data proposing that an initial binding of target proteins occurs on the N-terminal domain of CaM followed by the formation of the compact structure shown in Figure 35 [120].

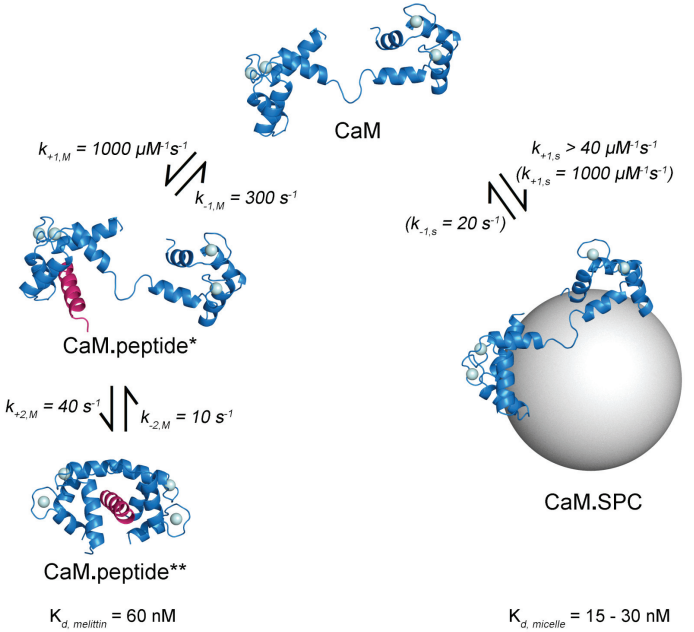

Figure 35 Shematic representation of the model by which SPC competes for CaM with target peptides. PDB IDs 1CLL and 1CDM were used to prepare the structures representing CaM and the CaM.peptide** complex, respectively. The CaM (blue) and the peptide (magenta) molecules are shown as cartoons. Bound Ca^{2+} ions are shown as light blue spheres. The CaM.peptide* and the CaM.SPC species are purely hypothetical, and are depicted by the Ca^{2+}-saturated CaM structure 1CLL bound to the peptide or the micelle. The SPC micelle is depicted as a grey sphere with a diameter comparable to the width of a lipid bilayer. Rate constants shown in brackets are estimated values and were used for global simulation. The figure was prepared using PyMol (DeLano Sci.).

We demonstrated that SPC competes for CaM with the model CaM-binding domain melittin, using ligand chasing experiments for both ligands (Figures 23-24). The kinetic parameters we obtained in the SPC chasing assay (Figure 23) clearly indicated that SPC competes with melittin for the same binding site. SPC could only bind to CaM upon melittin dissociation as its binding rate constant was limited by the dissociation rate constant of the CaM-melittin complex (Table 6). No sign of a trimeric complex comprising all three interacting partners have been observed. The previous observation that SPC binds to CaM as a micelle, not as a monomer, was reinforced in the stopped-flow measurements as well.

The reverse chasing experiment, in which melittin served as a competitor of the pre-bound SPC (Figure 24), also indicated the concentration dependent replacement of the pre-bound ligand for melittin on CaM. In addition, this experiment yielded information relevant to the size of the SPC micelle that interacts with CaM. Using the relation described in Eq. 3 and kinetic simulations, we can estimate that an SPC micelle is composed of about 150 monomers.

Please note that all stopped-flow experiments were carried out with protein-lipid ratios allowing only CaM binding to micelles, but not the generation of the collapsed protein conformation. Therefore, under these experimental conditions only binding to micelles was investigated, and as such, only the micelle-bound form is depicted in Figure 35.

5.4. CaM as the intracellular receptor for SPC?

With experiments discussed in Chapters 5.1-5.3, we laid down the structural and mechanistic basis of CaM inhibition by SPC. I reckoned that the most important following step is to reveal what the functional consequences of such a novel regulation could be in the context of a cellular environment. My approach was to make a connection between the literature on SPC's actions as a second messenger and CaM. This proved to be a relatively easy task, since the most well-described intracellular effect of SPC is mobilization of Ca^{2+} [50, 51], and CaM has been shown to play a role in the negative feedback of the Ca^{2+} signal [58, 75, 76]. My hypothesis was that SPC elevates intracellular Ca^{2+} levels by interfering with this negative feedback.

Several published data suggested that SPC is involved in the regulation of ryanodine receptors (RyRs) [40, 56, 61], hence, I started working on the CaM-binding

domain of the skeletal muscle Ca^{2+} release channel (RyR1). Moreover, Ca^{2+} binding to CaM leads to an N-terminal shift in its binding site on RyR1 [98], thus, this CaM-binding domain binds CaM constitutively regardless of Ca^{2+}, providing a convenient tool to study the effect of SPC on the apoCaM-target interaction as well. I clearly demonstrated that SPC dissociates the complex between Ca^{2+}-saturated CaM and the CaM-binding domain of RyR1 (Figure 25). This effect was selective compared to structurally related signaling lipids such as S1P, LPC and LPA, and occured with an EC_{50} of approximately 20 μM. This is in the similar low micromolar range as the observed Ca^{2+} mobilizing action of SPC in former reports [40, 49, 50, 56]. Furthermore, it has also been shown that L-*threo*-SPC, a synthetic stereoisomer, liberated Ca^{2+} only if administered intracellullarly, while was ineffective extracellularly [49, 132]. The fact that in my measurements L-*threo*-SPC gave similar results as the naturally occuring D-*erythro*-SPC, also implies that the effect we observe and the findings by these authors may share a common underlying mechanism.

I also showed that SPC dissociates the complex between apoCaM and the CaM-binding domain of RyR1 (Figure 26). This finding suggests an entirely novel endogenous regulation for RyRs and other proteins that constitutively bind CaM regardless of Ca^{2+}, or are regulated by CaM in any other unconventional way (Figure 11). SPC is the first compound having the potential to completely free these proteins from the Ca^{2+} sensor.

Regarding other proteins involved in Ca^{2+} homeostasis, Ca^{2+}CaM has been shown to inhibit the two most abundant Ca^{2+} channels, RyRs and IP_3Rs [58], and to activate the plasma membrane Ca^{2+} pump (PMCA) [133]. Once again, according to my hypothesis, if SPC interferes with any of these interactions, that would activate the Ca^{2+} channels and inhibit the Ca^{2+} pumps, eventually leading to the elevation of intracellullar Ca^{2+} levels. I demostrated that SPC disrupts the complex between CaM and the CaM-binding domain of RyR1, IP_3R1 and PMCA (Figure 27). I excluded Ca^{2+} pumps of the endoplasmic reticulum (SERCAs) from my study because they are not directly regulated by CaM. Experiments carried out with micelles containing other lipids besides SPC (Figure 28) confirmed that SPC can displace CaM from its targets even when incorporated into a mixed lipid environment. This finding argues for the plausibility of the same phenomenon to occur under *in vivo* conditions near a membrane surface enriched in SPC (for a more thorough discussion refer to Chapter 5.6.). Therefore, my findings provide a putative explanation for the Ca^{2+} mobilizing activity of SPC. Of course the interactions the sphingolipid can actually modify *in vivo* are probably selected by their cellular

localization, and the concept needs to be tested on intact proteins (see Chapter 5.5.) and cellular systems.

5.5. Regulation of RyRs by SPC – a short detour

Following the previous line of thought, but moving on to intact proteins, I started working with RyRs. My attempts to purify active receptors were rather unsuccessful, and I realized that working with these huge channel complexes requires expertise, which we lacked in our laboratory. To overcome this problem, I contacted Dr. Gerhard Meissner at the University of North Carolina, who has been conducting exactly those types of experiments, studying RyR regulation by CaM, that I wished to repeat, but focusing on the effect of SPC. He was enthusiastic about the project and invited me in his laboratory, which I joined as an EMBO Short-term Fellow for two months.

As presented in the Introduction (Chapter 1.4.), literature on regulation of RyRs by SPC is quite contradictory. One group of investigators reported an activation of these receptors by the sphingolipid [40, 56], while another one observed channel inhibition [61, 62]. Neither group examined the role of CaM in this process, and I expected to see that SPC, by dissociating CaM from the RyR1, relieves negative feedback inhibition of Ca^{2+}CaM, leading to channel opening.

I showed that SPC indeed displaces CaM from the intact channel (Figure 31). The functional consequences of CaM dissociation were explored in single channel measurements and a ligand ([^{3}H]ryanodine) binding assay. Single channel recordings on purified RyR1 (Figure 29) revealed that SPC at concentrations well below its CMC decreases the open channel probability of RyRs, and induces the appearance of long-lived closed states. These data are in good agreement with former reports that low concentrations of SPC decrease the open probability of the cardiac ryanodine receptor (RyR2), and RyR2 inhibition is characterized by the appearance of long-lived closed channel states [61, 62]. As expected, this inhibitory effect was independent of CaM, since we were only able to study the effects of monomeric SPC in single channel measurements, because SPC concentrations greater than 10 μM resulted in disruption of the sensitive reconstituted bilayer.

To overcome this limitation, [^{3}H]ryanodine binding experiments were carried out (Figure 30), which confirmed inhibition of receptor activity in the absence of CaM. However, if Ca^{2+}CaM was present, this inhibition could not be observed. This phenomenon could be explained by assuming that two antagonistic molecular events are

occurring at the same time: 1) a direct inhibition of channel activity by the sphingolipid, as suggested by single channel recordings and 2) displacement of inhibitory Ca^{2+}CaM by SPC, as suggested by [^{35}S]CaM binding assays.

Taken together, our data are consistent with the findings of Uehara *et al.* [61, 62] in that SPC directly inhibits RyRs. Our current results are also consistent with our former data suggesting that SPC can dissociate the complex between RyRs and CaM, and we have found that the presence of CaM can modify the direct inhibitory effect of SPC on the channel. However, under our experimental conditions, channel activation was never observed, whereas an involvement of ryanodine receptors in SPC-induced Ca^{2+} release from brain microsomes has been reported [56]. One possibility was that brain expresses all three mammalian RyR isoforms [134] and therefore type 3 RyR was responsible for the activating effects. Under similar experimental conditions, we found that while 100 μM SPC, LPC and LPA each released a large amount of Ca^{2+} from brain microsomes, classical channel activators that act on all three RyR isoforms such as 1 μM ryanodine and 5 mM caffeine only had minor effects (Figure 32). Interestingly, Dettbarn *et al.* were also incapable of triggering Ca^{2+} release by ryanodine or caffeine. Their major argument for SPC's action on RyRs was that ruthenium red, an inhibitor of the RyRs, inhibited SPC-elicited Ca^{2+} release. However, in two subsequent studies, SPC-induced Ca^{2+} release was much less sensitive to ruthenium red inhibition [40, 57]. Taken together, the sphingolipid's mechanism of action on cerebral microsomes remains elusive, but a significant contribution of RyRs to the phenomenon can most likely be excluded.

In conclusion, we have shown that SPC regulates RyR1 in a diverse manner. Below the CMC, SPC directly inhibits the skeletal muscle Ca^{2+} release channel, while above the CMC, besides a direct action on the channel, the sphingolipid also displaces inhibitory Ca^{2+}CaM from the RyR1, further modifying channel activity. However, net activation of the channel never occurs, so SPC's effect on the RyR cannot explain how the sphingolipid liberates Ca^{2+} from the endoplasmic reticulum. Although this question remains open, we have at least clarified the role of SPC in RyR regulation.

All available information in the literature clearly pointed to RyRs as the link between CaM and SPC-elicited Ca^{2+}-release. Unfortunately, it turned out that some of these data are not well established, and instead of activating these receptors, SPC directly inhibits channel opening. Nevertheless, we should keep in mind that even though RyRs proved to be a bad choice of study, CaM inhibition by SPC can still be the key to the

sphingolipid's second messenger function, exerting its effects on some other Ca^{2+} channel or pump.

5.6. Considerations on the physiological relevance of the CaM-SPC interaction

During my PhD studies I presented my work at several scientific forums, and it was always greeted with much enthusiasm, but one controversial issue always emerged. What is the physiological relevance of our findings if micelles are required for binding? To avoid possible misunderstandings, I decided to dedicate a chapter to my arguments on this subject. Of course, I do not think that an *in vivo* interaction would occur between a protein and micelles, as micelles do not exist in living cells. I opine that a membrane surface enriched in SPC might serve as an *in vivo* equivalent for the SPC surface presented by micelles *in vitro*. My detailed reasoning is as follows.

It is very important to distinguish between our *in vitro* experimental conditions and the situation in a cellular environment. We use micelles as the simplest alternative to *model* a clustered SPC environment. We worked with high SPC and CaM concentrations to 1) obtain stable micelles and 2) to obtain large heat effects, DLS signals, crystals etc. *In vivo*, such elevated concentrations of either interacting partner are unnecessary, only a clustered form of SPC is required, already given in a membrane environment. Our simplified artificial micelle system was very useful to reveal the molecular events of binding and to extract precise K_d and stoichiometry values. Nevertheless, we should always keep in mind that the binding parameters obtained this manner cannot always be applied directly to the cellular conditions. For example, the first binding process, when SPC binds to intact micelles yielded a stoichiometry of ~100-200 SPC molecule/CaM. This large number arises from the fact that a micelle consists of ~100-200 monomers. Thus, if the interacting partner is smaller, for example a membrane surface containing 10-20 SPC molecules, the stoichiometry value would be accordingly lower.

Therefore, the exact affinity and stoichiometry values characterize the *in vitro* protein-micelle system and should not be directly applied to the *in vivo* situation. Yet, this study provides important conclusions about the physiologic lipid-protein interaction as well. These are the following: 1) CaM interacts with SPC clusters at high (nanomolar) affinity; 2) once the SPC-CaM complex forms, it can adopt different conformations

depending on several factors, most likely on the curvature and size of the lipid cluster and the local abundance of CaM.

We have demonstrated that the interaction can manifest itself in both mixed lipid (liposomes [110], mixed micelles (Figure 28 and [96])) and protein (measurements on cerebral microsomes [111]) environments, which findings argue for the plausibility of the same phenomenon to occur under *in vivo* conditions near a membrane surface enriched in SPC. Of course, the ultimate goal would be to provide *in vivo* evidence for the CaM-SPC interaction. Unfortunately, little is known about the metabolic pathway that generates SPC (refer to section 1.3), which hinders our ability to design and conduct relevant experiments. Simply treating cells with SPC would be largely ineffective, as the membrane permeability of SPC is very restricted. Regarding the estimated cellular concentrations of SPC, albeit information is yet scarce, its presence has been demonstrated under several physiologic and pathologic conditions. SPC accumulates in Niemann–Pick disease [41] and atopic dermatitis [42], and Betto *et al.* [40] measured the overall SPC concentration in cardiac muscle to be approximately 15.6 μM, which is very promising. A lot of future work in Károly Liliom's laboratory will be focused on finding the SPC producing enzyme, which in my opinion would be absolutely necessary to study the CaM-SPC interaction *in vivo*.

5.7. Major conclusions and significance of the findings

In this report I demonstrate that the putative second messenger SPC, binds to the ubiquitous Ca^{2+} sensor CaM selectively compared to related lysophospholipid mediators such as S1P, LPC and LPA. The interaction has functional effects, as the sphingolipid inhibits the CaM-dependent activity of target enzymes calcineurin and phosphodiesterase. Unlike classical aromatic CaM antagonists, SPC is a natural compound and binds regardless of the presence of Ca^{2+}. Furthermore, I present a crystal structure of the Ca^{2+}CaM/SPC complex, and a stoichiometry-dependent lipid-protein binding model. At low protein-to-lipid ratios CaM binds to intact micelles, whereas at high protein-to-lipid ratios micelles are disintegrated by the protein, eventuating in a compact globular conformation of Ca^{2+}CaM. I provide kinetic evidence for a competitive inhibitory mechanism and show that SPC disrupts the complex between CaM and the CaM-binding domain of several proteins involved in Ca^{2+} homeostasis, suggesting a mechanism by

which SPC can evoke a Ca^{2+} response and exert its second messenger functions. In the end, I clarify the controversial role of SPC in RyR regulation and the role of CaM in it.

I believe that results presented in this thesis are new and significant findings for three main reasons. First, the identification of SPC as a CaM inhibitor is the first specific suggestion of the sphingolipid's intracellular target site, and provides a link between the sphingolipid and Ca^{2+} signaling. Second, inhibition of CaM action by SPC proposes an utterly new type of endogenous regulation for the Ca^{2+} sensor. So far, no other second messenger has been suggested to regulate CaM function, apart from Ca^{2+} ions. Moreover, SPC can bind to both the Ca^{2+}-bound and free forms of the protein, offering multiple non-conventional ways of modulating CaM activity. Finally, the two-step binding model presented here describes a novel and peculiar biochemical mechanism, which might be applicable to other lipid-protein interactions as well, and reveals how versatile such interactions can be.

6. SUMMARY

Sphingosine 1 phosphate (S1P) and sphingosylphosphorylcholine (SPC) are important mediators of cell signaling, possessing the unique feature to act as first and second messengers as well. Although their activation of cell surface G protein-coupled receptors has been studied extensively, their intracellular sites of action are yet to be identified. We hypothesized that these sphingolipids might bind to calmodulin (CaM), the ubiquitous intracellular Ca^{2+} sensor of eukaryotes.

In my thesis I demonstrate that 1) SPC binds to both apo- and Ca^{2+}-bound CaM selectively, when compared with the related lysophospholipid mediators S1P, LPA (lysophosphatidic acid) and LPC (lysophosphatidylcholine). Binding has serious functional consequences, as SPC inhibits the Ca^{2+}CaM-dependent activity of target enzymes calcineurin and phosphodiesterase. 2) I present a 1.6 Å resolution crystal structure of the CaM-SPC complex, in which the sphingolipid occupies the conventional hydrophobic binding site on CaM. Based on thermodynamic and kinetic studies I describe a peculiar stoichiometry-dependent binding process: at low or high protein-to-lipid ratio CaM binds lipid micelles or a few lipid molecules in a compact globular conformation, respectively. 3) I give mechanistic insight into CaM inhibition by SPC based on fluorescence stopped-flow studies, and present experimental evidence that both species compete for the same target site on CaM. 4) I show that SPC disrupts the complex of CaM and the CaM-binding domain of RyR1, IP_3R1 and the PMCA. Interfering with these interactions, and inhibiting the negative feedback CaM has on Ca^{2+} signaling, could lead to intracellular Ca^{2+} mobilization, providing a means by which the sphingolipid exerts its second messenger functions. 5) Finally, utilizing single channel measurements and radioactive binding assays, I demonstrate that SPC regulates the intact ryanodine receptor (RyR) by both CaM-dependent and -independent mechanisms.

I believe that these findings are a major contribution to both the Ca^{2+} and the lipid signaling field. We propose that CaM might be the intracellular target site for SPC and also raise the possibility of a novel endogenous regulation of the well known Ca^{2+} sensor. Furthermore, our detailed structural and mechanistic characterization of the CaM-SPC complex might provide insight into other lipid-protein interactions as well, an emerging field with outstanding importance.

7. ÖSSZEFOGLALÁS

A szfingozin-1-foszfát (S1P) és a szfingozilfoszforilkolin (SPC) lipid mediátorok összetett szerepet töltenek be a jelátvitelben, különleges tulajdonságuk, hogy ugyanazok a molekulák elsődleges és másodlagos hírvivők is lehetnek. Míg sejtfelszíni G-fehérje kapcsolt receptoraik azonosítottak és jól jellemzettek, addig nem sokat tudunk intracelluláris célfehérjéikről. Szakirodalmi adatok alapján feltételeztük, hogy ezek a lipidek kölcsönhatnak a kalmodulinnal (CaM), a legáltalánosabb intracelluláris kalcium szenzorral.

A jelen dolgozatban ismertetem eredményeim, mi szerint 1) az SPC szelektíven kötődik mind az apo mind a Ca^{2+}-mal telített CaM-hoz, míg a szerkezetileg hasonló lizofoszfolipidek mint az S1P, LPC (lizofoszfatidilkolin) és LPA (lizofoszfatidsav) nem. A kölcsönhatásnak komoly funkcionális következményei vannak, hiszen az SPC specifikusan gátolja mind a foszfodiészteráz mind a kalcineurin célenzimek CaM-függő aktivitását. 2) Bemutatom a CaM-SPC komplex 1.6 Å felbontású röntgenszerkezetét, amelyben a fehérje a CaM-célpeptid komplexekre jellemző zárt konformációt veszi fel, és négy sphingolipid molekula foglalja el a fehérje hidrofób kötőcsatornáját. Ismertetek egy termodinamikai és kinetikai mérések alapján felállított olyan újszerű lipid-fehérje kötődési modellt, amelyben a CaM alacsony fehérje-lipid aránynál a micellákhoz kötődik, míg magas fehérje-lipid aránynál magába zár néhány SPC molekulát. 3) Tranziens kinetikai bizonyítékkal szolgálok arra nézve, hogy a peptid és a szfingolipid ugyanazért a kötőhelyért verseng a CaM-on. 4) Bemutatom, hogy az SPC disszociáltatja a CaM és számos Ca^{2+} homeosztázisban szerepet játszó fehérje (IP_3R, RyR, PMCA) CaM-kötő doménje közötti komplexet, amely magyarázatul szolgálhat az SPC sejten belüli Ca^{2+} mobilizáló hatására. 5) Végül ismertetem ryanodine receptorokon (RyR) kapott eredményeimet, melyek alapján a szfingolipid mind CaM-függő mind CaM-független módon szabályozza a Ca^{2+} csatornát.

Hiszem, hogy az itt bemutatott eredmények jelentősen hozzájárulnak mind a Ca^{2+} mind a lipid jelátvitel témakörében felgyülemlett ismeretekhez. Felvetjük a lehetőségét a CaM egy biológiailag releváns, újszerű szabályozásának, és javaslatot teszünk az SPC első intracelluláris receptorára. Továbbá felállítottunk egy olyan kétlépcsős, szerkezeti-biofizikai lipid-fehérje kötődési modellt, mely feltételezhetően más kölcsönhatásokra is alkalmazható lesz majd.

8. ACKNOWLEDGEMENTS

I wish to thank my supervisor, Károly Liliom, for the great project, for generous financial support and for teaching me how to be an independent researcher. He was always open to my ideas and let me carry out the experiments I envisaged. He encouraged me to participate in many scientific meetings and collaborations, of which I benefited greatly.

I am very grateful to my collaborators, without whom several experimental techniques could not have been carried out nor evaluated. Specifically, I thank Veronika Harmat for X-ray crystallography, József Kardos for ITC, Károly Módos for DLS and Judit Tóth for stopped-flow. Their superb expertise was essential for unraveling the binding mechanism of CaM to SPC.

I would especially like to express my gratitude to Judit Tóth, one of the most talented young scientists I know. Not only did I learn a great deal from her professionally, she was always willing to help me in personal matters related to my scientific career.

I would like to thank Dr. Gerhard Meissner, at the University of North Carolina, for accepting me in his laboratory as an EMBO short-term scholar. He was enthusiastic and helpful about our collaboration from the start. I also thank Le Xu for conducting single channel measurements and Daniel Pasek for providing the SR vesicle preparations.

I am most grateful to my parents who fully supported me, and to my father for being the scientist who will always serve for me as a role model.

Finally, I would like to thank Dániel Süveges for sharing my enthusiasm in science, and constantly reminding me to appreciate the beauties of even such small wonders as the bubbles emerging from bacterial media.

9. PUBLICATION LIST

Publications related to the subject of the present thesis:

Kovacs E, Xu L, Pasek D, Liliom K, Meissner G. Regulation of ryanodine receptors by sphingosylphosphorylcholine: involvement of both calmodulin-dependent and -independent mechanisms. Submitted to *FEBS J.*

Kovacs E, Harmat V, Toth J, Vertessy BG, Modos K, Kardos J, Liliom K. Structure and mechanism of calmodulin binding to a signaling sphingolipid reveal new aspects of lipid-protein interactions. *FASEB J.* 2010 Jun 14. [Epub ahead of print]

Kovacs E, Toth J, Vertessy BG, Liliom K. Dissociation of calmodulin – target peptide complexes by the lipid mediator sphingosylphosphorylcholine: implications in calcium signaling. *J Biol Chem*. 2010; 285(3): 1799-808.

Kovacs E, Liliom K. Sphingosylphosphorylcholine as a novel calmodulin inhibitor. *Biochem J.* 2008; 410(2):427-37.

Other publications:

Kovacs E, Tompa P, Liliom K, Kalmar L. Dual coding in alternative reading frames correlates with intrinsic protein disorder. *PNAS.* 2010;107(12):5429-34.

Pal-Gabor H, Gombos L, Micsonai A, Kovacs E, Petrik E, Kovacs J, Graf L, Fidy J, Naiki H, Goto Y, Liliom K, and Kardos J. Mechanism of lysophosphatidic acid-induced amyloid fibril formation of beta-2 microglobulin in vitro under physiological conditions. *Biochemistry*. 2009; 48(24): 5689-99.

Conference proceedings:

Kovacs E, Harmat V, Toth J, Vertessy BG, Modos K, Kardos J, Liliom K. Structure and mechanism of calmodulin binding to a signaling sphingolipid reveal new aspects of lipid-protein interactions. Selected oral presentation. 10th FEBS Young Scientist Forum and 35th FEBS Congress, 2010, Gothenburg, Sweden.

Kovacs E, Harmat V, Toth J, Vertessy BG, Modos K, Kardos J, Liliom K. New aspects of lipid-protein interactions revealed by calmodulin binding to the lipid mediator sphingosylphosphorylcholine. Poster presentation. Biophysical Society 54th Annual Meeting, 2010, San Francisco, California.

Toth J, Kovacs E, Vertessy BG, Liliom K. A kalmodulin effektor komplexeinek kölcsönhatása szfingolipid micellákkal: a Ca^{2+}-jelátvitel új aspektusai. Toth J szóbeli előadása. A Magyar Biokémiai Egyesület Vándorgyűlése, 2009, Budapest.

Kiss B, Kovacs E, Liliom K, Nyitray L. Az S100A4 metasztázis-asszociált fehérje protein-lipid kölcsönhatásainak szerkezet-funkció vizsgálata. Kiss B poszter előadása. A Magyar Biokémiai Egyesület Vándorgyűlése, 2009, Budapest.

Kovacs E, Liliom K. Regulation of ryanodine receptors by signaling sphingolipids: calmodulin is the missing link? Selected oral presentation. FEBS Workshop "Lipids as regulators of cell function", 2008, Spetses, Greece.

Kovacs E, Liliom K. Calmodulin is a potential intracellular receptor for the lipid mediator sphingosylphosphorylcholine. Poster presentation. 14th Congress of Calcium Binding Proteins in Health and Disease, 2007, La Palma, Spain.

Kovacs E, Liliom K. Jelátviteli szfingolipidek sejten belüli kalcium felszabadításának lehetséges mechanizmusai: kalmodulin a hiányzó láncszem? Poszter előadás. A Magyar Biokémiai Egyesület Vándorgyűlése, 2007, Debrecen.

Kovacs E, Liliom K. Sphingosylphosphorylcholine as a novel calmodulin inhibitor. Poster presentation. FEBS Special Meeting "New concepts in lipidology: from lipidomics to disease", 2006, Noordwijkerhout, The Netherlands.

Kovacs E, Liliom K. Szfingolipidek kalmodulinnal való kölcsönhatásának jellemzése: a jelátvitelben betöltött szerepük kibővülhet. Poszter előadás. A Magyar Biokémiai Egyesület Vándorgyűlése, 2006, Pécs.

Kovacs E, Liliom K. Sphingolipids interact with calmodulin: new roles in signal transduction? Poster presentation. 31st FEBS Congress, 2006, Istanbul, Turkey.

Hodi Zs, Nemeth A, Kovacs E, Hetenyi Cs, Bodor A, Perczel A, Nyitray L. The dynein light chain binds to a non-coiled-coil tail domain of myosin-Va that includes an alternatively spliced exon coding for three amino acid residues. Poster presentation of Hodi Zs. 30th FEBS Congress, 2005, Budapest, Hungary.

10. REFERENCES

1 Downes, C. P., Gray, A. and Lucocq, J. M. (2005) Probing phosphoinositide functions in signaling and membrane trafficking. Trends Cell Biol. **15**, 259-268

2 Carlton, J. G. and Cullen, P. J. (2005) Coincidence detection in phosphoinositide signaling. Trends Cell Biol. **15**, 540-547

3 Krauss, M. and Haucke, V. (2007) Phosphoinositide-metabolizing enzymes at the interface between membrane traffic and cell signalling. EMBO Rep. **8**, 241-246

4 Smith, W. L. and Merrill, A. H., Jr. (2002) Sphingolipid metabolism and signaling minireview series. J Biol Chem. **277**, 25841-25842

5 Merrill, A. H., Jr. (2002) De novo sphingolipid biosynthesis: a necessary, but dangerous, pathway. J Biol Chem. **277**, 25843-25846

6 Hannun, Y. A. and Obeid, L. M. (2002) The Ceramide-centric universe of lipid-mediated cell regulation: stress encounters of the lipid kind. J Biol Chem. **277**, 25847-25850

7 Spiegel, S. and Milstien, S. (2002) Sphingosine 1-phosphate, a key cell signaling molecule. J Biol Chem. **277**, 25851-25854

8 van Meer, G. and Lisman, Q. (2002) Sphingolipid transport: rafts and translocators. J Biol Chem. **277**, 25855-25858

9 Birgbauer, E. and Chun, J. (2006) New developments in the biological functions of lysophospholipids. Cell Mol Life Sci. **63**, 2695-2701

10 Meyer zu Heringdorf, D. and Jakobs, K. H. (2007) Lysophospholipid receptors: signalling, pharmacology and regulation by lysophospholipid metabolism. Biochim Biophys Acta. **1768**, 923-940

11 Parrill, A. L. (2008) Lysophospholipid interactions with protein targets. Biochim Biophys Acta. **1781**, 540-546

12 Lemmon, M. A. (2008) Membrane recognition by phospholipid-binding domains. Nat Rev Mol Cell Biol. **9**, 99-111

13 van Meer, G., Voelker, D. R. and Feigenson, G. W. (2008) Membrane lipids: where they are and how they behave. Nat Rev Mol Cell Biol. **9**, 112-124

14 Ikonen, E. (2008) Cellular cholesterol trafficking and compartmentalization. Nat Rev Mol Cell Biol. **9**, 125-138

15 Hannun, Y. A. and Obeid, L. M. (2008) Principles of bioactive lipid signalling: lessons from sphingolipids. Nat Rev Mol Cell Biol. **9**, 139-150

16 Michell, R. H. (2008) Inositol derivatives: evolution and functions. Nat Rev Mol Cell Biol. **9**, 151-161

17 Wymann, M. P. and Schneiter, R. (2008) Lipid signalling in disease. Nat Rev Mol Cell Biol. **9**, 162-176

18 Snook, C. F., Jones, J. A. and Hannun, Y. A. (2006) Sphingolipid-binding proteins. Biochim Biophys Acta. **1761**, 927-946

19 Fantini, J. (2003) How sphingolipids bind and shape proteins: molecular basis of lipid-protein interactions in lipid shells, rafts and related biomembrane domains. Cell Mol Life Sci. **60**, 1027-1032

20 Spiegel, S. and Milstien, S. (2003) Sphingosine-1-phosphate: an enigmatic signalling lipid. Nat Rev Mol Cell Biol. **4**, 397-407

21 Meyer zu Heringdorf, D., Himmel, H. M. and Jakobs, K. H. (2002) Sphingosylphosphorylcholine-biological functions and mechanisms of action. Biochim Biophys Acta. **1582**, 178-189

22 Nixon, G. F., Mathieson, F. A. and Hunter, I. (2008) The multi-functional role of sphingosylphosphorylcholine. Prog Lipid Res. **47**, 62-75
23 Desai, N. N. and Spiegel, S. (1991) Sphingosylphosphorylcholine is a remarkably potent mitogen for a variety of cell lines. Biochem Biophys Res Commun. **181**, 361-366
24 Desai, N. N., Carlson, R. O., Mattie, M. E., Olivera, A., Buckley, N. E., Seki, T., Brooker, G. and Spiegel, S. (1993) Signaling pathways for sphingosylphosphorylcholine-mediated mitogenesis in Swiss 3T3 fibroblasts. J Cell Biol. **121**, 1385-1395
25 Tornquist, K. and Ekokoski, E. (1994) Effect of sphingosine derivatives on calcium fluxes in thyroid FRTL-5 cells. Biochem J. **299 (Pt 1)**, 213-218
26 Okajima, F. and Kondo, Y. (1995) Pertussis toxin inhibits phospholipase C activation and Ca2+ mobilization by sphingosylphosphorylcholine and galactosylsphingosine in HL60 leukemia cells. Implications of GTP-binding protein-coupled receptors for lysosphingolipids. J Biol Chem. **270**, 26332-26340
27 Meyer zu Heringdrof, D., van Koppen, C. J., Windorfer, B., Himmel, H. M. and Jakobs, K. H. (1996) Calcium signalling by G protein-coupled sphingolipid receptors in bovine aortic endothelial cells. Naunyn Schmiedebergs Arch Pharmacol. **354**, 397-403
28 Chen, P. F., Chin, T. Y. and Chueh, S. H. (1998) Ca2+ signaling induced by sphingosylphosphorylcholine and sphingosine 1-phosphate via distinct mechanisms in rat glomerular mesangial cells. Kidney Int. **54**, 1470-1483
29 Chin, T. Y. and Chueh, S. H. (1998) Sphingosylphosphorylcholine stimulates mitogen-activated protein kinase via a Ca2+-dependent pathway. Am J Physiol. **275**, C1255-1263
30 Orlati, S., Porcelli, A. M., Hrelia, S., Lorenzini, A. and Rugolo, M. (1998) Intracellular calcium mobilization and phospholipid degradation in sphingosylphosphorylcholine-stimulated human airway epithelial cells. Biochem J. **334 (Pt 3)**, 641-649
31 Seufferlein, T. and Rozengurt, E. (1995) Sphingosylphosphorylcholine activation of mitogen-activated protein kinase in Swiss 3T3 cells requires protein kinase C and a pertussis toxin-sensitive G protein. J Biol Chem. **270**, 24334-24342
32 Bunemann, M., Liliom, K., Brandts, B. K., Pott, L., Tseng, J. L., Desiderio, D. M., Sun, G., Miller, D. and Tigyi, G. (1996) A novel membrane receptor with high affinity for lysosphingomyelin and sphingosine 1-phosphate in atrial myocytes. EMBO J. **15**, 5527-5534
33 Boguslawski, G., Lyons, D., Harvey, K. A., Kovala, A. T. and English, D. (2000) Sphingosylphosphorylcholine induces endothelial cell migration and morphogenesis. Biochem Biophys Res Commun. **272**, 603-609
34 Xu, Y., Zhu, K., Hong, G., Wu, W., Baudhuin, L. M., Xiao, Y. and Damron, D. S. (2000) Sphingosylphosphorylcholine is a ligand for ovarian cancer G-protein-coupled receptor 1. Nat Cell Biol. **2**, 261-267
35 Zhu, K., Baudhuin, L. M., Hong, G., Williams, F. S., Cristina, K. L., Kabarowski, J. H., Witte, O. N. and Xu, Y. (2001) Sphingosylphosphorylcholine and lysophosphatidylcholine are ligands for the G protein-coupled receptor GPR4. J Biol Chem. **276**, 41325-41335
36 Ludwig, M. G., Vanek, M., Guerini, D., Gasser, J. A., Jones, C. E., Junker, U., Hofstetter, H., Wolf, R. M. and Seuwen, K. (2003) Proton-sensing G-protein-coupled receptors. Nature. **425**, 93-98

37 Xiao, Y. J., Schwartz, B., Washington, M., Kennedy, A., Webster, K., Belinson, J. and Xu, Y. (2001) Electrospray ionization mass spectrometry analysis of lysophospholipids in human ascitic fluids: comparison of the lysophospholipid contents in malignant vs nonmalignant ascitic fluids. Anal Biochem. **290**, 302-313
38 Liliom, K., Sun, G., Bunemann, M., Virag, T., Nusser, N., Baker, D. L., Wang, D. A., Fabian, M. J., Brandts, B., Bender, K., Eickel, A., Malik, K. U., Miller, D. D., Desiderio, D. M., Tigyi, G. and Pott, L. (2001) Sphingosylphosphocholine is a naturally occurring lipid mediator in blood plasma: a possible role in regulating cardiac function via sphingolipid receptors. Biochem J. **355**, 189-197
39 Nofer, J. R., Levkau, B., Wolinska, I., Junker, R., Fobker, M., von Eckardstein, A., Seedorf, U. and Assmann, G. (2001) Suppression of endothelial cell apoptosis by high density lipoproteins (HDL) and HDL-associated lysosphingolipids. J Biol Chem. **276**, 34480-34485
40 Betto, R., Teresi, A., Turcato, F., Salviati, G., Sabbadini, R. A., Krown, K., Glembotski, C. C., Kindman, L. A., Dettbarn, C., Pereon, Y., Yasui, K. and Palade, P. T. (1997) Sphingosylphosphocholine modulates the ryanodine receptor/calcium-release channel of cardiac sarcoplasmic reticulum membranes. Biochem J. **322 (Pt 1)**, 327-333
41 Rodriguez-Lafrasse, C. and Vanier, M. T. (1999) Sphingosylphosphorylcholine in Niemann-Pick disease brain: accumulation in type A but not in type B. Neurochem Res. **24**, 199-205
42 Okamoto, R., Arikawa, J., Ishibashi, M., Kawashima, M., Takagi, Y. and Imokawa, G. (2003) Sphingosylphosphorylcholine is upregulated in the stratum corneum of patients with atopic dermatitis. J Lipid Res. **44**, 93-102
43 Fujino, Y., Negishi, T. and Ito, S. (1968) Enzymic synthesis of sphingosylphosphorylcholine. Biochem J. **109**, 310-311
44 Higuchi, K., Hara, J., Okamoto, R., Kawashima, M. and Imokawa, G. (2000) The skin of atopic dermatitis patients contains a novel enzyme, glucosylceramide sphingomyelin deacylase, which cleaves the N-acyl linkage of sphingomyelin and glucosylceramide. Biochem J. **350 Pt 3**, 747-756
45 Sekiguchi, K., Yokoyama, T., Kurabayashi, M., Okajima, F. and Nagai, R. (1999) Sphingosylphosphorylcholine induces a hypertrophic growth response through the mitogen-activated protein kinase signaling cascade in rat neonatal cardiac myocytes. Circ Res. **85**, 1000-1008
46 Clair, T., Aoki, J., Koh, E., Bandle, R. W., Nam, S. W., Ptaszynska, M. M., Mills, G. B., Schiffmann, E., Liotta, L. A. and Stracke, M. L. (2003) Autotaxin hydrolyzes sphingosylphosphorylcholine to produce the regulator of migration, sphingosine-1-phosphate. Cancer Res. **63**, 5446-5453
47 Meyer Zu Heringdorf, D. (2004) Lysophospholipid receptor-dependent and -independent calcium signaling. J Cell Biochem. **92**, 937-948
48 Young, K. W. and Nahorski, S. R. (2001) Intracellular sphingosine 1-phosphate production: a novel pathway for Ca2+ release. Semin Cell Dev Biol. **12**, 19-25
49 Meyer zu Heringdorf, D., Niederdraing, N., Neumann, E., Frode, R., Lass, H., Van Koppen, C. J. and Jakobs, K. H. (1998) Discrimination between plasma membrane and intracellular target sites of sphingosylphosphorylcholine. Eur J Pharmacol. **354**, 113-122
50 Ghosh, T. K., Bian, J. and Gill, D. L. (1990) Intracellular calcium release mediated by sphingosine derivatives generated in cells. Science. **248**, 1653-1656

51 Ghosh, T. K., Bian, J. and Gill, D. L. (1994) Sphingosine 1-phosphate generated in the endoplasmic reticulum membrane activates release of stored calcium. J Biol Chem. **269**, 22628-22635
52 Kindman, L. A., Kim, S., McDonald, T. V. and Gardner, P. (1994) Characterization of a novel intracellular sphingolipid-gated Ca(2+)-permeable channel from rat basophilic leukemia cells. J Biol Chem. **269**, 13088-13091
53 Kim, S., Lakhani, V., Costa, D. J., Sharara, A. I., Fitz, J. G., Huang, L. W., Peters, K. G. and Kindman, L. A. (1995) Sphingolipid-gated Ca2+ release from intracellular stores of endothelial cells is mediated by a novel Ca(2+)-permeable channel. J Biol Chem. **270**, 5266-5269
54 Mao, C., Kim, S. H., Almenoff, J. S., Rudner, X. L., Kearney, D. M. and Kindman, L. A. (1996) Molecular cloning and characterization of SCaMPER, a sphingolipid Ca2+ release-mediating protein from endoplasmic reticulum. Proc Natl Acad Sci U S A. **93**, 1993-1996
55 Schnurbus, R., de Pietri Tonelli, D., Grohovaz, F. and Zacchetti, D. (2002) Re-evaluation of primary structure, topology, and localization of Scamper, a putative intracellular Ca2+ channel activated by sphingosylphosphocholine. Biochem J. **362**, 183-189
56 Dettbarn, C., Betto, R., Salviati, G., Sabbadini, R. and Palade, P. (1995) Involvement of ryanodine receptors in sphingosylphosphorylcholine-induced calcium release from brain microsomes. Brain Res. **669**, 79-85
57 Furuya, S., Kurono, S. and Hirabayashi, Y. (1996) Lysosphingomyelin-elicited Ca2+ mobilization from rat brain microsomes. J Lipid Mediat Cell Signal. **14**, 303-311
58 Balshaw, D. M., Yamaguchi, N. and Meissner, G. (2002) Modulation of intracellular calcium-release channels by calmodulin. J Membr Biol. **185**, 1-8
59 Balshaw, D. M., Xu, L., Yamaguchi, N., Pasek, D. A. and Meissner, G. (2001) Calmodulin binding and inhibition of cardiac muscle calcium release channel (ryanodine receptor). J Biol Chem. **276**, 20144-20153
60 Tripathy, A., Xu, L., Mann, G. and Meissner, G. (1995) Calmodulin activation and inhibition of skeletal muscle Ca2+ release channel (ryanodine receptor). Biophys J. **69**, 106-119
61 Uehara, A., Yasukochi, M., Imanaga, I. and Berlin, J. R. (1999) Effect of sphingosylphosphorylcholine on the single channel gating properties of the cardiac ryanodine receptor. FEBS Lett. **460**, 467-471
62 Yasukochi, M., Uehara, A., Kobayashi, S. and Berlin, J. R. (2003) Ca2+ and voltage dependence of cardiac ryanodine receptor channel block by sphingosylphosphorylcholine. Pflugers Arch. **445**, 665-673
63 Berridge, M. J., Bootman, M. D. and Roderick, H. L. (2003) Calcium signalling: dynamics, homeostasis and remodelling. Nat Rev Mol Cell Biol. **4**, 517-529
64 Carafoli, E. (2002) Calcium signaling: a tale for all seasons. Proc Natl Acad Sci U S A. **99**, 1115-1122
65 Clapham, D. E. (2007) Calcium signaling. Cell. **131**, 1047-1058
66 Chin, D. and Means, A. R. (2000) Calmodulin: a prototypical calcium sensor. Trends Cell Biol. **10**, 322-328
67 Hoeflich, K. P. and Ikura, M. (2002) Calmodulin in action: diversity in target recognition and activation mechanisms. Cell. **108**, 739-742
68 Vetter, S. W. and Leclerc, E. (2003) Novel aspects of calmodulin target recognition and activation. Eur J Biochem. **270**, 404-414
69 Gallay, J., Vincent, M., Li de la Sierra, I. M., Munier-Lehmann, H., Renouard, M., Sakamoto, H., Barzu, O. and Gilles, A. M. (2004) Insight into the activation

mechanism of Bordetella pertussis adenylate cyclase by calmodulin using fluorescence spectroscopy. Eur J Biochem. **271**, 821-833
70 Goraya, T. A. and Cooper, D. M. (2005) Ca2+-calmodulin-dependent phosphodiesterase (PDE1): current perspectives. Cell Signal. **17**, 789-797
71 Corcoran, E. E. and Means, A. R. (2001) Defining Ca2+/calmodulin-dependent protein kinase cascades in transcriptional regulation. J Biol Chem. **276**, 2975-2978
72 Soderling, T. R., Chang, B. and Brickey, D. (2001) Cellular signaling through multifunctional Ca2+/calmodulin-dependent protein kinase II. J Biol Chem. **276**, 3719-3722
73 Kamm, K. E. and Stull, J. T. (2001) Dedicated myosin light chain kinases with diverse cellular functions. J Biol Chem. **276**, 4527-4530
74 Klee, C. B., Ren, H. and Wang, X. (1998) Regulation of the calmodulin-stimulated protein phosphatase, calcineurin. J Biol Chem. **273**, 13367-13370
75 Carafoli, E. (1994) Biogenesis: plasma membrane calcium ATPase: 15 years of work on the purified enzyme. FASEB J. **8**, 993-1002
76 Taylor, C. W. and Laude, A. J. (2002) IP3 receptors and their regulation by calmodulin and cytosolic Ca2+. Cell Calcium. **32**, 321-334
77 Toutenhoofd, S. L. and Strehler, E. E. (2000) The calmodulin multigene family as a unique case of genetic redundancy: multiple levels of regulation to provide spatial and temporal control of calmodulin pools? Cell Calcium. **28**, 83-96
78 Persechini, A. and Stemmer, P. M. (2002) Calmodulin is a limiting factor in the cell. Trends Cardiovasc Med. **12**, 32-37
79 Kortvely, E. and Gulya, K. (2004) Calmodulin, and various ways to regulate its activity. Life Sci. **74**, 1065-1070
80 Harmat, V., Bocskei, Z., Naray-Szabo, G., Bata, I., Csutor, A. S., Hermecz, I., Aranyi, P., Szabo, B., Liliom, K., Vertessy, B. G. and Ovadi, J. (2000) A new potent calmodulin antagonist with arylalkylamine structure: crystallographic, spectroscopic and functional studies. J Mol Biol. **297**, 747-755
81 Osawa, M., Swindells, M. B., Tanikawa, J., Tanaka, T., Mase, T., Furuya, T. and Ikura, M. (1998) Solution structure of calmodulin-W-7 complex: the basis of diversity in molecular recognition. J Mol Biol. **276**, 165-176
82 Vandonselaar, M., Hickie, R. A., Quail, J. W. and Delbaere, L. T. (1994) Trifluoperazine-induced conformational change in Ca(2+)-calmodulin. Nat Struct Biol. **1**, 795-801
83 Martinez-Luis, S., Perez-Vasquez, A. and Mata, R. (2007) Natural products with calmodulin inhibitor properties. Phytochemistry. **68**, 1882-1903
84 Gopalakrishna, R. and Anderson, W. B. (1982) Ca2+-induced hydrophobic site on calmodulin: application for purification of calmodulin by phenyl-Sepharose affinity chromatography. Biochem Biophys Res Commun. **104**, 830-836
85 Kincaid, R. L., Vaughan, M., Osborne, J. C., Jr. and Tkachuk, V. A. (1982) Ca2+-dependent interaction of 5-dimethylaminonaphthalene-1-sulfonyl-calmodulin with cyclic nucleotide phosphodiesterase, calcineurin, and troponin I. J Biol Chem. **257**, 10638-10643
86 Abuin, E. B., Lissi, E. A., Aspee, A., Gonzalez, F. D. and Varas, J. M. (1997) Fluorescence of 8-Anilinonaphthalene-1-sulfonate and Properties of Sodium Dodecyl Sulfate Micelles in Water-Urea Mixtures. J Colloid Interface Sci. **186**, 332-338
87 Leslie, A. G. W. (1992) Recent changes to the MOSFLM package for processing film and image plate data. Joint CCP4 + ESF-EAMCB Newsletter on Protein Crystallography. **No. 26.**

88 Evans, P. (2005) Scaling and assessment of data quality. Acta Cryst. **D62**, 72-82
89 Vagin, A. and Teplyakov, A. (1997) MOLREP: an Automated Program for Molecular Replacement. J Appl Cryst. **30**, 1022-1025
90 Collaborative Computational Project, N. (1994) The CCP4 suite: programs for protein crystallography. Acta Cryst. **D50**, 760–763
91 Murshudov, G. N., Vagin, A. A. and Dodson, E. J. (1997) Refinement of macromolecular structures by the maximum-likelihood method. Acta Cryst. **D53**, 240-255
92 Emsley, P. and Cowtan, K. (2004) Coot: model-building tools for molecular graphics. Acta Cryst. **D60**, 2126-2132
93 Laskowski, R. A., MacArthur, M., Moss, D. S. and Thornton, J. M. (1993) PROCHECK: a program to check the stereochemical quality of protein structures. J Appl Cryst. **26**, 283–291
94 Bryan, R. K. (1990) In Maximum Entropy and Bayesian Methods (Fougere, P. F., ed.). pp. 221–232, Kluwer Academic Publishers, The Netherlands
95 Yoshii, N., Iwahashi, K. and Okazaki, S. (2006) A molecular dynamics study of free energy of micelle formation for sodium dodecyl sulfate in water and its size distribution. J Chem Phys. **124**, 184901
96 Kovacs, E., Toth, J., Vertessy, B. G. and Liliom, K. (2010) Dissociation of calmodulin - target peptide complexes by the lipid mediator sphingosylphosphorylcholine: implications in calcium signaling. J Biol Chem. **285**, 1799-1808
97 Mendes, P. (1997) Biochemistry by numbers: simulation of biochemical pathways with Gepasi 3. Trends Biochem Sci. **22**, 361-363
98 Rodney, G. G., Moore, C. P., Williams, B. Y., Zhang, J. Z., Krol, J., Pedersen, S. E. and Hamilton, S. L. (2001) Calcium binding to calmodulin leads to an N-terminal shift in its binding site on the ryanodine Receptor. J Biol Chem. **276**, 2069-2074
99 Sienaert, I., Nadif Kasri, N., Vanlingen, S., Parys, J. B., Callewaert, G., Missiaen, L. and de Smedt, H. (2002) Localization and function of a calmodulin-apocalmodulin-binding domain in the N-terminal part of the type 1 inositol 1,4,5-trisphosphate receptor. Biochem J. **365**, 269-277
100 Yamada, M., Miyawaki, A., Saito, K., Nakajima, T., Yamamoto-Hino, M., Ryo, Y., Furuichi, T. and Mikoshiba, K. (1995) The calmodulin-binding domain in the mouse type 1 inositol 1,4,5-trisphosphate receptor. Biochem J. **308 (Pt 1)**, 83-88
101 Enyedi, A., Vorherr, T., James, P., McCormick, D. J., Filoteo, A. G., Carafoli, E. and Penniston, J. T. (1989) The calmodulin binding domain of the plasma membrane Ca2+ pump interacts both with calmodulin and with another part of the pump. J Biol Chem. **264**, 12313-12321
102 Comte, M., Maulet, Y. and Cox, J. A. (1983) Ca2+-dependent high-affinity complex formation between calmodulin and melittin. Biochem J. **209**, 269-272
103 Xu, L., Tripathy, A., Pasek, D. A. and Meissner, G. (1999) Ruthenium red modifies the cardiac and skeletal muscle Ca(2+) release channels (ryanodine receptors) by multiple mechanisms. J Biol Chem. **274**, 32680-32691
104 Lee, H. B., Xu, L. and Meissner, G. (1994) Reconstitution of the skeletal muscle ryanodine receptor-Ca2+ release channel protein complex into proteoliposomes. J Biol Chem. **269**, 13305-13312
105 Volpe, P., Alderson-Lang, B. H. and Nickols, G. A. (1990) Regulation of inositol 1,4,5-trisphosphate-induced Ca2+ release. I. Effect of Mg2+. Am J Physiol. **258**, C1077-1085

106 Abe, Y., Saito, S., Hori, M., Ozaki, H., Fusetani, N. and Karaki, H. (1997) Stellettamide-A, a novel inhibitor of calmodulin, isolated from a marine sponge. Br J Pharmacol. **121**, 1309-1314
107 VanScyoc, W. S., Sorensen, B. R., Rusinova, E., Laws, W. R., Ross, J. B. and Shea, M. A. (2002) Calcium binding to calmodulin mutants monitored by domain-specific intrinsic phenylalanine and tyrosine fluorescence. Biophys J. **83**, 2767-2780
108 Lucas, J. L., Wang, D. and Sadee, W. (2006) Calmodulin binding to peptides derived from the i3 loop of muscarinic receptors. Pharm Res. **23**, 647-653
109 Turner, J. H. and Raymond, J. R. (2005) Interaction of calmodulin with the serotonin 5-hydroxytryptamine2A receptor. A putative regulator of G protein coupling and receptor phosphorylation by protein kinase C. J Biol Chem. **280**, 30741-30750
110 Kovacs, E. and Liliom, K. (2008) Sphingosylphosphorylcholine as a novel calmodulin inhibitor. Biochem J. **410**, 427-437
111 Kovacs, E., Harmat, V., Tóth, J., Vértessy, B. G., Módos, K., Kardos, J. and Liliom, K. (2010) Structure and mechanism of calmodulin binding to a signaling sphingolipid reveal new aspects of lipid-protein interactions. FASEB J. 2010 Jun 14. [Epub ahead of print]
112 Meador, W. E., Means, A. R. and Quiocho, F. A. (1992) Target enzyme recognition by calmodulin: 2.4 A structure of a calmodulin-peptide complex. Science. **257**, 1251-1255
113 Meador, W. E., Means, A. R. and Quiocho, F. A. (1993) Modulation of calmodulin plasticity in molecular recognition on the basis of x-ray structures. Science. **262**, 1718-1721
114 Persechini, A. and Kretsinger, R. H. (1988) The central helix of calmodulin functions as a flexible tether. J Biol Chem. **263**, 12175-12178
115 Andersen, K. K., Oliveira, C. L., Larsen, K. L., Poulsen, F. M., Callisen, T. H., Westh, P., Pedersen, J. S. and Otzen, D. (2009) The role of decorated SDS micelles in sub-CMC protein denaturation and association. J Mol Biol. **391**, 207-226
116 Pal-Gabor, H., Gombos, L., Micsonai, A., Kovacs, E., Petrik, E., Kovacs, J., Graf, L., Fidy, J., Naiki, H., Goto, Y., Liliom, K. and Kardos, J. (2009) Mechanism of lysophosphatidic acid-induced amyloid fibril formation of beta(2)-microglobulin in vitro under physiological conditions. Biochemistry. **48**, 5689-5699
117 Brokx, R. D., Lopez, M. M., Vogel, H. J. and Makhatadze, G. I. (2001) Energetics of target peptide binding by calmodulin reveals different modes of binding. J Biol Chem. **276**, 14083-14091
118 Papish, A. L., Tari, L. W. and Vogel, H. J. (2002) Dynamic light scattering study of calmodulin-target peptide complexes. Biophys J. **83**, 1455-1464
119 Brown, S. E., Martin, S. R. and Bayley, P. M. (1997) Kinetic control of the dissociation pathway of calmodulin-peptide complexes. J Biol Chem. **272**, 3389-3397
120 Murase, T. and Iio, T. (2002) Static and kinetic studies of complex formations between calmodulin and mastoparanX. Biochemistry. **41**, 1618-1629
121 Kovacs, E., Xu, L., Pasek, D. A., Liliom, K. and Meissner, G. (2010) Regulation of ryanodine receptors by sphingosylphosphorylcholine: involvement of both calmodulin-dependent and -independent mechanisms. Submitted to FEBS J.
122 Tripathy, A. and Meissner, G. (1996) Sarcoplasmic reticulum lumenal Ca2+ has access to cytosolic activation and inactivation sites of skeletal muscle Ca2+ release channel. Biophys J. **70**, 2600-2615

123 Colquhoun, D. and Sigworth, F. J. (1983) Fitting and statistical analysis of single-channel recording. In Single-channel recording (Sakmann, B. and Neher, E., eds.). pp. 191-263, Plenum Press, New York
124 Sutko, J. L., Airey, J. A., Welch, W. and Ruest, L. (1997) The pharmacology of ryanodine and related compounds. Pharmacol Rev. **49**, 53-98
125 LaPorte, D. C., Wierman, B. M. and Storm, D. R. (1980) Calcium-induced exposure of a hydrophobic surface on calmodulin. Biochemistry. **19**, 3814-3819
126 Jefferson, A. B. and Schulman, H. (1988) Sphingosine inhibits calmodulin-dependent enzymes. J Biol Chem. **263**, 15241-15244
127 Viani, P., Giussani, P., Riboni, L., Bassi, R. and Tettamanti, G. (1999) Sphingosine inhibits nitric oxide synthase from cerebellar granule cells differentiated in vitro. FEBS Lett. **454**, 321-324
128 Colina, C., Cervino, V. and Benaim, G. (2002) Ceramide and sphingosine have an antagonistic effect on the plasma-membrane Ca2+-ATPase from human erythrocytes. Biochem J. **362**, 247-251
129 Young, K. W., Willets, J. M., Parkinson, M. J., Bartlett, P., Spiegel, S., Nahorski, S. R. and Challiss, R. A. (2003) Ca2+/calmodulin-dependent translocation of sphingosine kinase: role in plasma membrane relocation but not activation. Cell Calcium. **33**, 119-128
130 Sutherland, C. M., Moretti, P. A., Hewitt, N. M., Bagley, C. J., Vadas, M. A. and Pitson, S. M. (2006) The calmodulin-binding site of sphingosine kinase and its role in agonist-dependent translocation of sphingosine kinase 1 to the plasma membrane. J Biol Chem. **281**, 11693-11701
131 Massom, L., Lee, H. and Jarrett, H. W. (1990) Trifluoperazine binding to porcine brain calmodulin and skeletal muscle troponin C. Biochemistry. **29**, 671-681
132 Brailoiu, E. and Dun, N. J. (2003) Extra- and intracellular sphingosylphosphorylcholine promote spontaneous transmitter release from frog motor nerve endings. Mol Pharmacol. **63**, 1430-1436
133 Di Leva, F., Domi, T., Fedrizzi, L., Lim, D. and Carafoli, E. (2008) The plasma membrane Ca2+ ATPase of animal cells: structure, function and regulation. Arch Biochem Biophys. **476**, 65-74
134 Furuichi, T., Furutama, D., Hakamata, Y., Nakai, J., Takeshima, H. and Mikoshiba, K. (1994) Multiple types of ryanodine receptor/Ca2+ release channels are differentially expressed in rabbit brain. J Neurosci. **14**, 4794-4805